Geosci 233: Physical Oceanography

Douglas R. MacAyeal

Department of Geophysical Sciences
University of Chicago
Chicago, Illinois

March 28, 2001

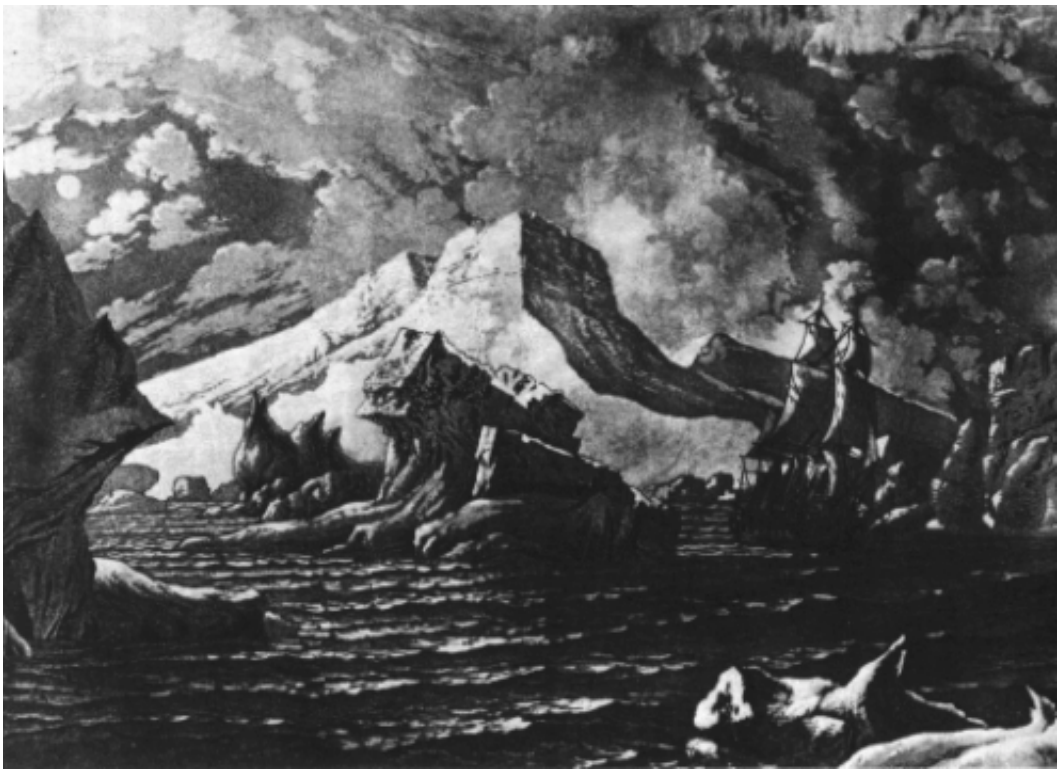

Figure 1: The *Atrevida* discovering the Aurora Islands.

Contents

Chapter 1

Maps

Maps provide a means to visually comprehend the ocean's temperature, salinity and circulation. Our first step in the study of oceanography will be to consider the mathematical and graphical tools which allow us to make maps.

It is easy to appreciate the main question of cartography: How is an essentially spherical body such as the earth represented on a two-dimensional map? It is impossible, for example, to peel a thin paper covering from a globe without tearing, stretching and distorting the paper. Thus, in making a map of the earth, the cartographer must accept various forms of distortion that are inherent in mapmaking. In some circumstances the cartographer will choose a map projection which minimizes or eliminates some forms of distortion (such as the magnification of area). In making such a choice, the cartographer will often be forced to compromise between various other forms of distortion (such as preservation of shape and direction).

1.1 Three Classes of Maps

Our goal is to understand the geometry of the three basic classes of map projections (cylindrical, conical and azimuthal). As shown in Fig. (1.2),

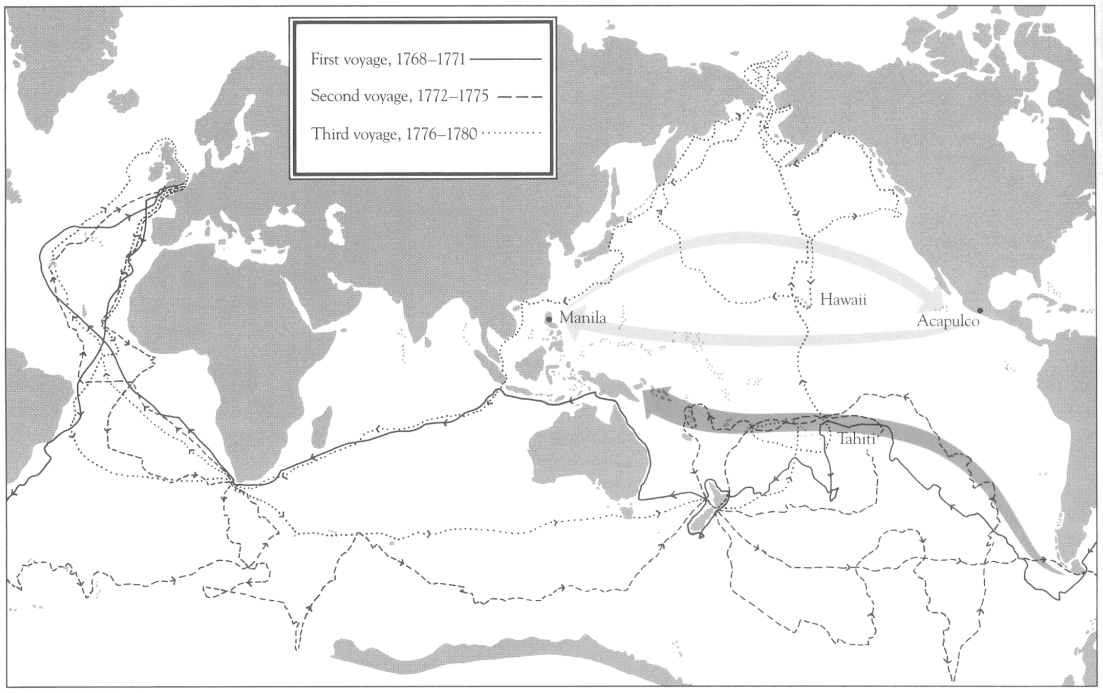

Figure 1.1: The voyages of Captain James Cook.

these classes are differentiated by the type of surface onto which the map of the earth is eventually to be drawn. These so-called developable surfaces are the cylynder, cone and plane. The cylinder and cone can be cut and unrolled into a flat map.

To make a map using one of the three classes of projections, we must transfer points from the surface of the earth to the surface of the map. This transformation, the map projection, can be done in one of two ways: mathematically, or physically (by plotting the location of shadows of points on the globe generated a small light source). While the physical map projections are easiest to comprehend, the most useful projections are often designed mathematically to produce maps with optimal distortion characteristics.

In the examples below, we shall consider three projections. The polar stereographic projection is an example of an azimuthal projection involving a physical transformation of points from the globe to the plane. The Lambert equal area projection is very similar to the polar stereographic projection, but is constructed mathematically to preserve the area of closed regions on the globe (but not their shape). The Mercator projection is an example of a cylindrical projection which involves a rather intricate mathematical construction designed to preserve compass headings for mariners (*i.e.,* is a loxodromic projection).

1.2 Spherical Coordinates

The natural coordinates for the representation of position on a spherical, or near-spherical, surface are the *spherical coordinates* (ϕ, λ, r). As shown in Fig. (1.3), specification of ϕ and λ alone are sufficient to uniquely describe the location of the point on a sphere of constant radius $r = R$. We refer to ϕ as the latitude, and it falls in the range $[\frac{\pi}{2}, \frac{\pi}{2}]$. Points in the Southern hemisphere are described by $\phi < 0$. The Equator is designated as the circle of points satisfying $\phi = 0$. We refer to λ as the longitude. It falls in the range $[-\pi, \pi]$. Points in the Western hemisphere (*e.g.,* here in Chicago), satisfy $\lambda < 0$. The Greenwich meridian is designated as the half-circle of points satisfying $\lambda = 0$.

Figure 1.2: The three classes of map projections.

Figure 1.3: Sphericalcoordinates.

The transformations between the (x, y, z)-coordinate system and the (ϕ, λ, r)-coordinate system involves simple trigonometry.

$$r = \sqrt{x^2 + y^2 + z^2} \tag{1.1}$$

$$\phi = \tan^{-1}\left(\frac{z}{\sqrt{x^2 + y^2}}\right) \tag{1.2}$$

$$\lambda = \tan^{-1}\left(\frac{y}{x}\right) \tag{1.3}$$

and,

$$x = r\cos(\phi)\cos(\lambda) \tag{1.4}$$

$$y = r\cos(\phi)\sin(\lambda) \tag{1.5}$$

$$z = r\sin(\phi) \tag{1.6}$$

In most of what follows, we will not make reference to the cartesian coordinates (x, y, z), or to the radial coordinate r. Our concern will principally involve the spherical coordinates (ϕ, λ), which we shall refer to as the *geographic coordinates*.

1.3 Map Projections

Even a modest scan of the reference literature on map projections (*e.g.,* Snyder and Boxland, 1989), reveals a vast variety of map projections. One can easily become overwhelmed by this variety. Our goal is to learn about just a few projections that will help us in our study of oceanography.

1.4 Polar Stereographic Projection

As shown in Fig. (1.4), the polar-stereographic map is an azimuthal projection that is constructed geometrically, i.e., using an imaginary point source of light to transfer points on the globe to points on the map. The simple

geometrical origin of the polar-stereographic projection has made it popular for representing the polar regions.

The mapping from (ϕ, λ) to (r, θ) is readily obtained by inspection of Fig. (1.4). First, we note that

$$\theta = \lambda \tag{1.7}$$

Next, we define the angle α which separates the rotational axis and the line segment passing through the South geographic pole and the (ϕ, λ)-point in question. The triangle which has the South pole, the center of the earth, and the (ϕ, λ)-point as vertices has two equal sides; thus, two of its angles are α. The other angle is $\frac{\pi}{2} + \phi$. The value of α is determined by the fact that the three angles of a triangle must sum to π

$$\alpha = \frac{\chi}{2} \tag{1.8}$$

The radial map coordinate is determined readily from the angle α

$$r = 2R \tan \alpha = 2R \tan \frac{\chi}{2} \tag{1.9}$$

The inverse map projection is determined easily from the above equations

$$\lambda = \theta = \tan^{-1}\left(\frac{y}{x}\right) \tag{1.10}$$

$$\chi = 2\tan^{-1}\left(\frac{r}{2R}\right) = 2\tan^{-1}\left(\frac{\sqrt{x^2+y^2}}{2R}\right) \tag{1.11}$$

1.4.1 Lambert Equal-Area Projection

The Lambert equal-area projection is an azimuthal projection constructed mathematically that is named after the great J. H. Lambert (1728-1777) who worked during the late eighteenth century on developing numerous maps for the British Admiralty. This projection is significant because it presents a polar image of the earth in which the area (or scaled area) of closed regions on the globe are preserved through the map transformation. Like its cousin, the polar stereographic projection discussed above, the Lambert equal-area projection is useful for presenting the polar regions.

As we shall see when we construct the Lambert equal-area projection in the lab, the shape of surface features such as continents is distored. This distortion is minimum for the polar region, thus features like Greenland or Antarctica can be represented without significant change from their image presented on a globe.

The transformation between the geographic coordinates (ϕ, λ) and the polar coordinates (r, θ) used to represent points on the flat (x, y)-plane of the Lambert equal-area map is derived by considering the area-preserving constraint. The Lambert equal-area projection is azimuthal, thus the longitude λ is mapped directly to the polar angle θ

$$\theta = \lambda \tag{1.12}$$

The relationship between r and the geographic coordinates is undetermined at this stage, however, we will insist that r depend only on the latitude. This restriction enforces the requirement that lines of constant latitude (*i.e.,* parallels) be circles centered on the origin of the map. In particular, we require

$$r = f(\chi) \tag{1.13}$$

where χ is the co-latitude, $\frac{\pi}{2} - \phi$.

Our goal is to find a function $f(\chi)$ such that the element of area on the sphere, $R^2 \sin(\chi) \mathrm{d}\chi \mathrm{d}\lambda$, where $R \approx 6380$ km is the radius of the earth, is equal to the area of the particular element's image on the map which, in cylindrical coordinates, is $r\mathrm{d}r\mathrm{d}\theta$. From elementary calculus, we have

$$\mathrm{d}r = f'(\chi)\mathrm{d}\chi \tag{1.14}$$

Thus, the equality of areas provides us with a constraint on the mathematical form of f. In particular, it provides us with a ordinary differential equation which we may integrate to determine the functional dependence of f on χ:

$$r\mathrm{d}r\mathrm{d}\theta = f f' \mathrm{d}\chi \mathrm{d}\lambda = R^2 \sin(\chi) \mathrm{d}\chi \mathrm{d}\lambda \tag{1.15}$$

Cancellation of $\mathrm{d}\chi\mathrm{d}\lambda$ from both sides of the above equation gives the ordinary differential equation for f

$$f' f = R^2 \sin(\chi) \tag{1.16}$$

or

$$\int f \mathrm{df} = \int \mathrm{R}^2 \sin(\chi) \mathrm{d}\chi \tag{1.17}$$

Integration yields

$$\frac{1}{2} f^2 + \text{constant} = -R^2 \cos(\chi) \tag{1.18}$$

The constant in the above equation will be evaluated in such a manner as to enforce the boundary condition $r = f = 0$ at $\chi = 0$ (*i.e.,* the North geographic pole). Making use of the trigonometric identity, $1 - \cos(\chi) = 2\sin^2\left(\frac{\chi}{2}\right)$, we obtain

$$f^2 = 2R^2 \left(2\sin^2 \frac{\chi}{2} - 1\right) + \text{constant} \tag{1.19}$$

We set constant$= 2R^2$ to satisfy the boundary condition, and are left with

$$r = f = 2R \sin\left(\frac{\chi}{2}\right) \tag{1.20}$$

In summary, the Lambert equal-area projection is represented by

$$\theta = \quad \lambda \tag{1.21}$$

$$r = \quad 2R \sin\left(\tfrac{\chi}{2}\right) \tag{1.22}$$

The inverse Lambert equal-area projection will also be of interest to us when we need to determine the latitude and longitude of a particular point on the map. It is readily shown that

$$\theta = \tan^{-1}\left(\frac{y}{x}\right) \tag{1.23}$$

$$r = \sqrt{x^2 + y^2} \tag{1.24}$$

$$\lambda = \theta \tag{1.25}$$

$$\phi = \frac{\pi}{2} - 2\sin^{-1}\left(\frac{r}{2R}\right) \tag{1.26}$$

1.4.2 Mercator's Projection

One of the difficulties of the Lambert equal-area map is that it presents a distorted picture of the equatorial region. In addition, it is not as convenient

for use by mariners who navigate by plotting lines of constant magnetic heading. The Mercator projection solves the navigation problem (i.e., is loxodromic), but still suffers from severe distortion of continental shape and the magnification of continental area.

The basic design of the Mercator projection is determined by considering a cylinder that is wrapped around the earth, and that touches the earth at the equator as shown in Fig. (1.2). The Mercator map is formed by projecting the points on the surface of the spherical earth onto the cylinder. The cylinder is then cut along a line parallel to its vertical axis (*i.e.,* the axis of rotation). The result is a flat planar map, when the cut cylinder is unwrapped.

The coordinates representing points on the Mercator map are cartesian. The horizontal coordinate on the Mercator map, x, describes the longitude of the particular point on the earth's surface

$$x = R\lambda \tag{1.27}$$

The vertical coordinate on the map, y, is determined by the requirement that the mapping be *conformal*, *i.e.,* that it preserve berings. To enforce this requirement, we ask that the degree to which the distance between two points on a parallel are stretched by the mapping be equal to the counterpart for two points on a meridian. Recalling that the distance between two points on a meridian and on a parallel are $R\mathrm{d}\phi$ and $R\cos\phi\mathrm{d}\lambda$, respectively, we may define the two stretching factors, h and k, as follows

$$h = \frac{\mathrm{dy}}{R\mathrm{d}\phi} \tag{1.28}$$

$$k = \frac{\mathrm{dx}}{R\cos\phi\mathrm{d}\lambda} = \frac{1}{\cos\phi} \tag{1.29}$$

By insisting $k = h$, we obtain

$$\mathrm{dy} = \mathrm{R}\frac{\mathrm{d}\phi}{\cos\phi} \tag{1.30}$$

Integrating,

$$y \;=\; R\int \sec\phi\mathrm{d}\phi$$

$$
\begin{aligned}
&= R \ln \tan\left(\frac{\pi}{4} + \frac{\phi}{2}\right) + \text{constant} \\
&= R \ln \tan\left(\frac{\pi}{4} + \frac{\phi}{2}\right) \qquad (1.31)
\end{aligned}
$$

The constant of integration in the above equation is zero because we require $y = 0$ on the equator.

As with the Lambert equal-area projection, we will have need to perform the inverse map projection to determine the latitude and longitude of points on the map. This inverse projection is easily determined

$$\phi = 2 \tan^{-1} e^{\frac{y}{R}} - \frac{\pi}{2} \qquad (1.32)$$

$$\lambda = \frac{x}{R} \qquad (1.33)$$

Digression: what is $\int \sec\phi \; d\phi$?

The integration represented in Eqn. (1.31) is particularly tedious, and some students will wish to see how it is managed. Here, I provide the details. First, we use a trigonometric identity

$$
\begin{aligned}
\cos\phi &= \cos^2\frac{\phi}{2} - \sin^2\frac{\phi}{2} \\
&= \cos^2\frac{\phi}{2}\left[1 - \tan^2\frac{\phi}{2}\right] \\
&= \cos^2\frac{\phi}{2}\left[1 - t^2\right] \qquad (1.34)
\end{aligned}
$$

where $t = \tan\frac{\phi}{2}$. We can change the variable of integration from ϕ to t by noting that

$$
\begin{aligned}
\frac{dt}{d\phi} &= \tfrac{d}{d\phi}\left(\tan\tfrac{\phi}{2}\right) \\
&= \tfrac{1}{2\cos^2\frac{\phi}{2}} \qquad (1.35)
\end{aligned}
$$

where we have made use of the derivative of the tangent function with respect to its argument,

$$\begin{aligned}
\tfrac{d}{dx}\tan x &= \frac{d}{dx}\frac{\sin x}{\cos x} \\
&= \frac{\cos x}{\cos x} + \frac{\sin^2 x}{\cos^2 x} \\
&= 1 + \tan^2 x \\
&= \frac{\cos^2 x + \sin^2 x}{\cos^2 x} \\
&= \frac{1}{\cos^2 x}
\end{aligned} \tag{1.36}$$

Thus, $d\phi = 2\cos^2\frac{\phi}{2}dt$. We can now write the integral of Eqn. (1.31) as follows

$$\begin{aligned}
y &= \int \sec\phi \; d\phi \\
&= \int \frac{2\cos^2\frac{\phi}{2}dt}{\cos^2\frac{\phi}{2}\left[1-t^2\right]} \\
&= \int \frac{2dt}{1-t^2}
\end{aligned} \tag{1.37}$$

We proceed further by rewriting the integrand as the product of two fractions

$$\begin{aligned}
y &= \int \frac{dt}{1-t} \; + \; \int \frac{dt}{1+t} \\
&= -\ln(1-t) + \ln(1+t) \\
&= \ln\left(\frac{1+t}{1-t}\right)
\end{aligned} \tag{1.38}$$

In the above equation, we have made use of the fact that the integral of $\frac{dx}{x}$ is equal to $\ln x$. At this point, we again return to our quiver of trigonometric identities, and consider how to simplify the argument of the log function. First, we write the tangent function in terms of sine and cosine

$$\frac{1+t}{1-t} = \frac{\cos\frac{\phi}{2} + \sin\frac{\phi}{2}}{\cos\frac{\phi}{2} - \sin\frac{\phi}{2}} \tag{1.39}$$

Next we multiply the result by 1, but we write 1 in a clever way, $1 = \frac{\frac{\sqrt{2}}{2}}{\frac{\sqrt{2}}{2}}$, and note that $\frac{\sqrt{2}}{2} = \sin\frac{\pi}{4} = \cos\frac{\pi}{4}$

$$\begin{aligned}
\frac{\left(\cos\frac{\phi}{2}+\sin\frac{\phi}{2}\right)}{\left(\cos\frac{\phi}{2}-\sin\frac{\phi}{2}\right)} &= \frac{\frac{\sqrt{2}}{2}\left(\cos\frac{\phi}{2}+\sin\frac{\phi}{2}\right)}{\frac{\sqrt{2}}{2}\left(\cos\frac{\phi}{2}-\sin\frac{\phi}{2}\right)} \\
&= \frac{\sin\frac{\pi}{4}\cos\frac{\phi}{2}+\cos\frac{\pi}{4}\sin\frac{\phi}{2}}{\cos\frac{\pi}{4}\cos\frac{\phi}{2}-\sin\frac{\pi}{4}\sin\frac{\phi}{2}} \\
&= \frac{\sin\left(\frac{\pi}{4}+\frac{\phi}{2}\right)}{\cos\left(\frac{\pi}{4}+\frac{\phi}{2}\right)} \\
&= \tan\left(\frac{\pi}{4}+\frac{\phi}{2}\right) \qquad (1.40)
\end{aligned}$$

That does it. We simply use the above identity as a substitute for $\left(\frac{1+t}{1-t}\right)$ to get the result $y = \ln\tan\left(\frac{\pi}{4}+\frac{\phi}{2}\right)$. Heck, I guess it would have been esier to have consulted a handbook of integrals on that one. Well, at least we can feel virtuous for the extra work we did on this one.

1.4.3 Hammer-Aitoff and Mollweide Projections

The Mercator projection is useful for its rendition of the equitorial regions of the earth. It is less useful for the polar regions because the areas of polar land masses is severely inflated. This is why school children often think of Alaska and Greenland as being vast lands which dwarf the continental United States. Here we shall introduce two projections that do not belong to any particular class (*i.e.,* are purely mathematical, are not cylindrical, conic or azimuthal), but which manage to preserve area and provide an equatorial view of the earth.

The area distortion of the Mercator map is eliminated by two map projections which also present an equitorial-view of the earth. The Hammer-Aitoff and Mollweide projections map the entire surface of the earth to the region contained within an ellipse centered on the origin of the map plane. These

maps thus produce pleasing pictures of the earth, and will be extremely useful in our study of oceanography. Unfortunately, both projections involve transendental functions in either their direct mapping from the geographic system to the map plane or their inverse mapping from the map plane back to the geographic system. (A transcendental function is one which cannot be easily inverted without use of approximation techniques.) We shall thus present each mapping in its most useful form: the Hammer-Aitoff for mapping known points on the globe to unknown positions on the map plane, and the Mollweide for mapping known points on the map plane to unknown points on the globe.

Hammer-Aitoff projection: mapping (ϕ, λ) to (x, y)

$$x = 2\sqrt{2}\left(\frac{\cos\phi \sin\frac{\lambda}{2}}{\sqrt{1+\cos\phi\cos\frac{\lambda}{2}}}\right) \tag{1.41}$$

$$y = \sqrt{2}\left(\frac{\sin\phi}{\sqrt{1+\cos\phi\cos\frac{\lambda}{2}}}\right) \tag{1.42}$$

Observe that the inverse mapping (taking a known (x, y) point and mapping it back to a (ϕ, λ) point) is impossible to express in closed analytic form.

Mollweide projection: mapping (x, y) to (ϕ, λ)

The forward mapping, from (ϕ, λ) to (x, y) is easy to express, but involves a transcendental function for the evaluation of an intermediate variable

$$x = \frac{\sqrt{8}\lambda}{\pi} R\cos\theta \tag{1.43}$$

$$y = \sqrt{2}R\sin\theta \tag{1.44}$$

where θ, the intermediate variable, is given by

$$\sin 2\theta + 2\theta = \pi \sin\phi \tag{1.45}$$

This equation cannot be readily evaluated for θ; thus, the direct mapping is used only when computer power is available to produce approximate solutions for θ.

If x and y are known, however, the geographical coordinates are easily determined. In this circumstance

$$\theta = \sin^{-1}\left(\frac{y}{\sqrt{2}R}\right) \tag{1.46}$$

$$\phi = \sin^{-1}\left(\frac{\sin 2\theta + 2\theta}{\pi}\right) \tag{1.47}$$

$$\lambda = \frac{\pi}{2}\frac{x}{\sqrt{2}R\cos\theta} \tag{1.48}$$

Assignment

Your first assignment is simple: create one example of each of the above described map projections, with the exception of the Mollweide projection (that one is too dificult, perhaps only advanced students will want to tackle that projection). For the Lambert equal-area map projection, create two maps of each hemisphere.

Print copies of your maps and copies of the MATLAB® scripts that created them. Save these print outs with your class notes for future reference.

Beginning a MATLAB® session

When you open a MATLAB® session on a MACINTOSH®, you will be presented with an interface to the mathematical, script-writing, and graphical capabilities of MATLAB®. The wake-up environment when you first begin MATLAB® consists of a *Command* window and a *Graph* window. The function bar at the top of the MACINTOSH® screen contains several options for manipulating files, loading data, exporting and saving data and command script files, and controling the Graph window. Of particular importance is the `help`-command interface. This can be invoked either by typing the command `help` at the prompt in the Command window, or by pulling down the menu under the *About* MATLAB® heading under the apple.

Your initial task for this assignment is to load the data set which contains the arrays `lat` and `lon`. These arrays are dimensioned 283×100, and contain the latitude and longitude of the sequence of points forming the continental and island outlines. The arrays have 283 rows. Each row represents one of the pen strokes of the map-making algorithm. Thus 283 strokes of the "graphical pen" yield the familiar map of the earth. The 100 columns of each row reporesent the individual points along each of the 283 pen strokes. Sometimes the pen strokes contain less than 100 points; thus, the columns after the last point actually plotted have zeros as their values. An additional vector `stroke` contains the 283 numbers which represent the column number of the last point in each of the 283 individual pen strokes.

To load the data into the MATLAB® environment, either execute the `load`

command at the prompt in the Command window, or use the pull-down menu. The file in which the data resides is called Assignment 1.mat, and will be located in the directory or folder designated by the Lab assignment.

Figure 1.4: Geometry of polar stereographic projection.

Chapter 2

Shape of the Ocean Basins

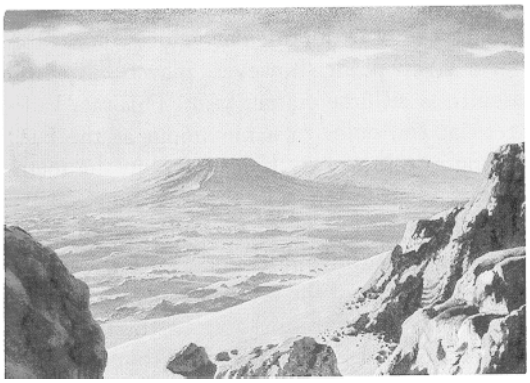

Figure 2.1: A painting by Chesley Bonestall.

In this chapter, we consider the shape of the ocean basins. There are many motivations for considering the bathymetry of the sea floor. The most important motivation concerns plate tectonics, one of the crucial paradigms of Earth sciences. Plate tectonics, also known as sea-floor spreading, was discovered as a result of the detailed examination of the depth and sediment-age relationship of the sea floor. Plate tectonics is responsible in large part for the chemistry and physical climate of the ocean and atmosphere. A physical

oceanographer must therefore be prepaired to recount the scientific history which led up to the discovery of sea-floor spreading.

A second motivation for our study of the sea-floor bathymetry is the fact that the bumps and ridges of the sea floor divide the deep ocean into many more separate parts than would be evident from looking at a simple map depicting the ocean surface. As we shall learn in the next chapters, much of the temperature, salinity, geochemical and circulation features of the ocean below 2000 m depth is affected by the geographic divisions associated with mid-ocean ridges. The goal of this chapter is to develop an appreciation for this geographic division that occurs at depth.

A third motivation for this chapter is that the problem of heat conduction in oceanic crust is a perfect, simple vehicle for learning additional mathematical techniques that are useful to a physical oceanographer. In particular, we shall learn how to solve a partial-differential equation describing the evolution of temperature in the cooling oceanic plate using finite differences (a numerical method that is conveniently implimented using MATLAB®). For the student who does not shy away from mathematical analysis, we will compare the finite-difference solution to the ocean-plate heat equation to an exact analytic solution derived using Laplace transforms and Fourier transforms.In addition to learning about finite-difference solutions to partial-differential equations, we will use this chapter as a vehicle for familiarization with the use of SPYGLASS® software, a graphics package for the MACINTOSH®.

2.1 Sea-Floor Spreading and Continental Drift

One of the crucial scientific discoveries in the twentieth century was the fact that the ocean floor moves horizontally across the surface of the globe like a great conveyor belt, carrying the continents with it. The importance of this movement is realized when one considers that it is responsible for most of the geochemical processes which, over the long term, are necessary for recycling the earth's crust and making the chemical composition of the ocean and atmosphere habitable. The effect of sea-floor spreading we shall consider here concerns only the ocean bathymetry. In particular, we want to know

why the ocean basins have a depth that appears to be minimum near their center and to increase with the square-root of the distance on either side. For a more complete discussion of sea-floor spreading and its effect on the earth, the reader should consult a text on geology.

A key step in the discovery of sea-floor spreading involved the analysis of the geologic age and depth of the ocean floor. As shown in Figs. (2.2) and (2.3), a typical transect across an ocean such as the North Atlantic shows a curious deepening and aging of the ocean floor away from the center of the ocean basin. The age vs. distance relationship suggests that ocean crust is created at the mid-ocean ridge, and moves away at a constant rate. The deepening can be explained by the thermal contraction of the oceanic crust as it cools with increasing ages. Recall that ocean crust is being constantly created by the solidification of hot, molten basalts in the seam of the mid-ocean ridges. Thus, as the oceanic crust moves away on either side of the ridge, it will progressively cool and sink deeper into the earth's mantle.

Several groups of marine geophysicists [Davis and Lister, 1974; Parsons and Sclater, 1977], realized that the depth of the sea-floor varied linearly with the square-root of its geologic age (at least for the portion of the sea floor that is younger than 70 million years). This relationship suggested that the cause of depth variation was thermal contraction associated with conductive cooling which, as will soon be shown, is a function of $\sqrt{t}$. This relationship is shown in Fig. (2.4), which displays typical depth values plotted as a function of the square-root of the age.

Several conductive-cooling models for the oceanic crust have been proposed to explain the relationship shown in Fig. (2.4). The simplest, proposed by Davis and Lister [1974], makes use of a solution Lord Kelvin [1864], the greatest physicist of the 19^{th} century, derived for the conductive cooling of the semi-infinite solid. This solution is derived below in the context of its original use by Kelvin, the estimation of the age of the earth as a solid planet from measurements of its geothermal properties. We will use Kelvin's solution, however, in a different context, that proposed by Davis and Lister [1974] to explain the depth of the ocean bottom.

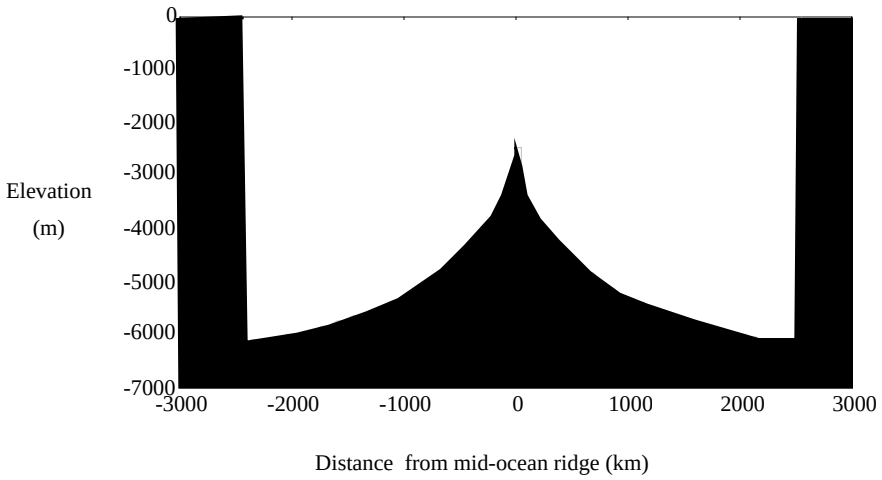

Figure 2.2: Ocean Bathymetry in typical cross section.

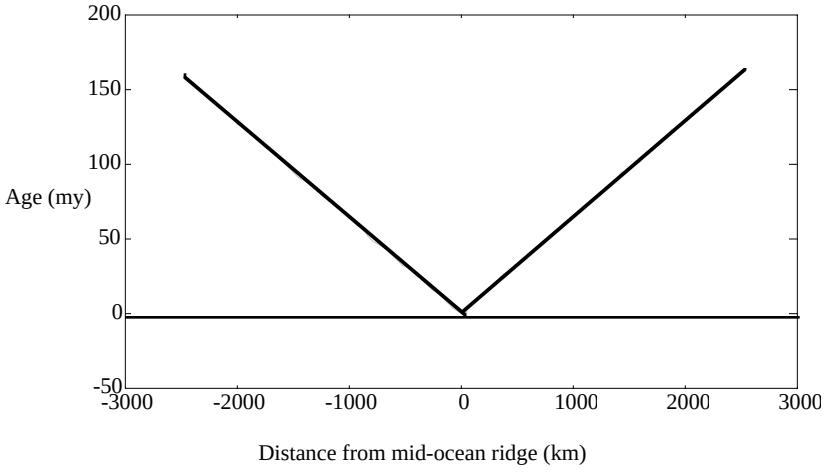

Figure 2.3: Schematic transect of the geological age of the ocean floor across a typical ocean basin. This age is determined typically by bio-stratigraphic analysis of the ocean sediments that are piled up atop the basaltic bedrock.

2.1.1 Kelvin's Solution for the Cooling of the Earth

In 1864, Lord Kelvin (Sir William Thompson) presented an estimate of the age of the Earth based on the geothermal temperature gradient measured in Scotland [Kelvin, 1864; see also Carslaw and Jeager, 1988, p. 85]. He assumed that the Earth was assembled in a molten state, and began to cool by conductive heat transfer. Using an estimate for the temperature of molten rock, the present-day geothermal gradient, and the solution to the conductive heat transfer equation, discussed below, he determined the time elapsed since the Earth was in a molten state. His estimate, 94 million years, contradicted the prevailing scientific view of his day that the Earth was many Billions of years old. We now know that the earth is over 4.5 billion years old. The error in Kelvin's estimate was due to the fact that he had not considered the effects of heat generated within the Earth by radioactive decay or of convection in the mantle. The story of Kelvin's work is interesting, nevertheless, and provides a valuable insight into the working of modern science [Richter, 1986]. I review Kelvin's work here because it provides a necessary result for the derivation of the bathymetric profiles of the ocean.

Kelvin [1864] treated the Earth as a semi-infinite solid occupying $z < 0$. Conductive heat transfer in this geometry is described by the following equations [Carslaw and Jeager, 1988]:

$$\theta_t = \kappa\theta_{zz} \tag{2.1}$$

$$\theta(0, z) = \theta_o \tag{2.2}$$

$$\theta(t, 0) = \theta_s = 0 \tag{2.3}$$

$$\theta_z(t, z \to -\infty) \to 0 \tag{2.4}$$

where θ is temperature, t is time, z is elevation with respect to the planar surface of the semi-infinite solid, and subscripts t and zz denote single and double partial differentiation with respect to the subscripted variable, respectively. The surface temperature θ_s is taken to be 0 C (roughly the atmospheric temperature in Scotland on a cold day).

There are several ways to solve (2.1) - (2.4) discussed in Carslaw and Jeager [1988]. We shall use the Laplace transform method [Arfken, 1970, p.

688]. First, a few words about the Laplace transform.

2.1.2 Laplace Transform

Let $\mathcal{L}(f(t)) = \tilde{f}(s)$ be the Laplace transform of $f(t)$. By definition,

$$\mathcal{L}(f(t)) = \int_0^\infty e^{-st} f(t) dt \tag{2.5}$$

One might wonder why the Laplace transform would be useful in solving a problem such as that defined by (2.1) - (2.4). The utility of the Laplace transform is appreciated when one considers how it transforms the time-derivative term in (2.1):

$$\begin{aligned}
\mathcal{L}(\theta_t) &= \int_0^\infty e^{-st} \frac{\partial \theta}{\partial t} dt \\
&= \int_0^\infty \frac{\partial}{\partial t} \left(e^{-st} \theta \right) dt + \int_0^\infty s e^{-st} \theta dt \\
&= -\theta_o + s\mathcal{L}(\theta) \\
&= -\theta_o + s\tilde{\theta}
\end{aligned} \tag{2.6}$$

We see that the advantage gained by applying the Laplace transform to (2.1) is that it eliminates the time-derivative term (thus, converting a partial differential equation into an ordinary differential equation where only derivatives with respect to z appear) and folds-in the initial condition at the same time. Taking the Laplace transform of (2.1) gives:

$$s\tilde{\theta} - \theta_o = \kappa \tilde{\theta}_{zz} \tag{2.7}$$

This equation is called the subsidiary equation. Notice that it is simply a second-order, non-homogeneous ordinary differential equation for the function $\tilde{\theta}(z)$.

The Laplace-transformed boundary conditions which go along with (2.7 are written

$$\tilde{\theta}(s, 0) \qquad = 0 \tag{2.8}$$

$$\tilde{\theta}_z(s, z \to -\infty) \quad \to 0 \tag{2.9}$$

2.1.3 Solution of the Subsidiary Equation

The general solution to the subsidiary equation may be written as the sum of two independent solutions of the homogeneous form of the subsidiary equation and a particular solution which satisfies the non-homogeneous form of the subsidiary equation:

$$\tilde{\theta}(s, z) = Ae^{\sqrt{\frac{s}{\kappa}}z} + Be^{-}\sqrt{\frac{s}{\kappa}}z + \frac{\theta_o}{s} \tag{2.10}$$

The boundary conditions imply $B = 0$ and $A = -\frac{\theta_o}{s}$, thus

$$\tilde{\theta}(s, z) = \frac{\theta_o}{s} - \frac{\theta_o e^{\sqrt{\frac{s}{\kappa}}z}}{s} \tag{2.11}$$

Now that we have $\tilde{\theta}(s, z)$, our problem becomes one of inverting the Laplace transform for $\theta(t, z)$.

2.1.4 Inverse Laplace Transform

The inverse Laplace transform is defined using the so-called Bromwich integral:

$$\mathcal{L}^{-1}(\tilde{f}(s)) = f(t) = \frac{1}{2\pi i} \int_{-i\infty+\gamma}^{i\infty+\gamma} \tilde{f}(s)e^{st}ds \tag{2.12}$$

where γ is a small positive real number and $i = \sqrt{-1}$. Clearly, the Bromwich integral represents a contour integration on the complex plain. Figure (2.5) displays the path of integration associated with the Bromwich integral.

To invert a Laplace transform, the first thing to try is a table of inverse Laplace transforms available in most mathematical handbooks. As a measure of last resort for the mathematically tolerant, the Bromwich integral can be assaulted in frontally. In an effort to demystify this tedious integration, we will choose the frontal assault.

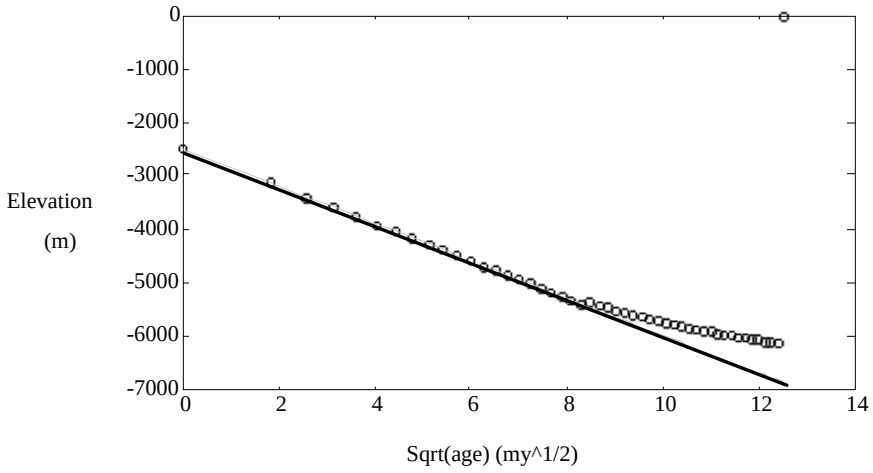

Figure 2.4: Schematic plot of depth (open circles) vs. the square-root of the geologic age. A linear relationship is demonstrated for the ocean floor that is younger than about 70-million years.

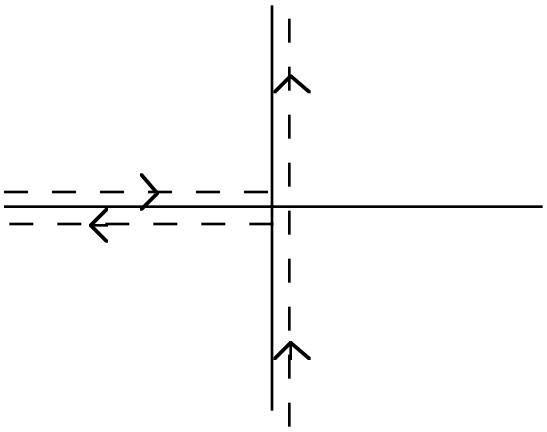

Figure 2.5: The contour required to invert the Laplace transform may, in the present problem, be deformed to the "keyhole" contour shown above.

2.1.5 Integrating the Bromwich Integral

Our goal is to evaluate

$$\theta(t,z) = \frac{\theta_o}{2\pi i}\int_{-i\infty+\gamma}^{i\infty+\gamma}\left(\frac{1}{s} - \frac{e^{\sqrt{\frac{s}{\kappa}}z}}{s}\right)e^{st}ds \tag{2.13}$$

One of the tricks of complex analysis at our disposal is Cauchy's integral theorem. Cauchy's theorem states that the integral of a function over any closed contour in the complex plain is identically zero when the function has no poles (singularities like $\frac{1}{s}$ as $s \to 0$) enclosed by the contour or branch cuts which cross the contour. The integrand of the above equation contains a pole at $s = 0$ and a branch cut along the negative part of the real axis. (The branch cut comes from the fact that we desire to make the function $\sqrt{s}$ single valued on the complex plain.) We may thus imagine a closed contour which contains, as one of its parts, the contour of the Bromwich integral and which avoids enclosing the poles or crossing the branch cut of the integrand in the above equation. A diagram showing this closed contour is shown in Fig. (2.5). Observe that Cauchy's integral theorem allows us to equate the above integral which represents half of the contour integration with -1 times the integral over the "keyhole" contour which excludes the branch cut along the negative real axis and the pole at $s = 0$. We find it easier to perform the integration along this keyhole contour. The inverse Laplace transform thus reduces to

$$\begin{aligned}\theta(t,z) &= \frac{-\theta_o}{2\pi i}\Big[\int_{\infty}^{0}\left(\frac{e^{-i\pi}}{r} - \frac{e^{-i\pi}}{r}e^{i\frac{\pi}{2}\frac{z\sqrt{r}}{\sqrt{\kappa}}}\right)e^{re^{i\pi}t}dr \\ &\quad + \int_{0}^{\infty}\left(\frac{e^{i\pi}}{r} - \frac{e^{i\pi}}{r}e^{-i\frac{\pi}{2}\frac{z\sqrt{r}}{\sqrt{\kappa}}}\right)e^{re^{-i\pi}t}dr \\ &\quad + \lim_{r\to 0}\int_{-\pi}^{\pi}\left(\frac{e^{-i\phi}}{r} - \frac{e^{-i\phi}}{r}e^{i\frac{\phi}{2}\frac{z\sqrt{r}}{\sqrt{\kappa}}}\right)e^{re^{i\phi}t}d\phi\Big]\end{aligned} \tag{2.14}$$

where we have made use of polar coordinates (r, ϕ) to represent s and $\sqrt{s}$:

$$s = re^{i\phi} \tag{2.15}$$

$$\sqrt{s} = \sqrt{r} e^{i\frac{\phi}{2}} \tag{2.16}$$

making note of the identities $e^{-i\pi} = -1$, $e^{-i\phi} = -1$, $e^{i\frac{\phi}{2}} = i$, and $e^{-i\frac{\phi}{2}} = -i$, the above integral over the keyhole contour is rewritten as

$$\begin{aligned}
\theta(t,z) &= \frac{-\theta_o}{2\pi i}\Big[\int_{\infty}^{0}\left(\frac{-1}{r} - \frac{-1}{r}e^{i\frac{z\sqrt{r}}{\sqrt{\kappa}}}\right)e^{-rt}dr \\
&\quad + \int_{0}^{\infty}\left(\frac{-1}{r} - \frac{-1}{r}e^{-i\frac{z\sqrt{r}}{\sqrt{\kappa}}}\right)e^{-rt}dr \\
&\quad + \lim_{r\to 0}\int_{-\pi}^{\pi}\left(\frac{e^{-i\phi}}{r} - \frac{e^{-i\phi}}{r}e^{i\frac{\phi}{2}\frac{z\sqrt{r}}{\sqrt{\kappa}}}\right)e^{re^{i\phi}t}d\phi\Big]
\end{aligned} \tag{2.17}$$

We observe that the third integral term on the right-hand side of the above equation is zero when the limit of $r \to 0$ is taken. We also observe that the limits of integration on the first integral term may be reversed to give

$$\begin{aligned}
\theta(t,z) &= \frac{-\theta_o}{2\pi i}\Big[\int_{0}^{\infty}\left(\frac{1}{r} - \frac{1}{r}e^{i\frac{z\sqrt{r}}{\sqrt{\kappa}}}\right)e^{-rt}dr \\
&\quad + \int_{0}^{\infty}\left(\frac{-1}{r} - \frac{-1}{r}e^{-i\frac{z\sqrt{r}}{\sqrt{\kappa}}}\right)e^{-rt}dr\Big] \\
&= \frac{\theta_o}{2\pi i}\Big[\int_{0}^{\infty}\left(\frac{e^{i\frac{z\sqrt{r}}{\sqrt{\kappa}}}}{r} - \frac{e^{-i\frac{z\sqrt{r}}{\sqrt{\kappa}}}}{r}\right)e^{-rt}dr\Big]
\end{aligned} \tag{2.18}$$

We again change coordinates using $\rho = \sqrt{r}$, $d\rho = \frac{dr}{2\sqrt{r}}$, and $dr = 2\rho d\rho$ to give

$$\begin{aligned}
\theta(t,z) &= \frac{\theta_o}{2\pi i}\int_{0}^{\infty}\left(\frac{e^{i\frac{z\rho}{\sqrt{\kappa}}}}{\rho^2} - \frac{e^{-i\frac{z\rho}{\sqrt{\kappa}}}}{\rho^2}\right)e^{-\rho^2 t}2\rho d\rho \\
&= \frac{\theta_o}{\pi i}\int_{0}^{\infty}\frac{1}{\rho}\left(e^{i\frac{z\rho}{\sqrt{\kappa}}-\rho^2 t} - e^{-i\frac{z\rho}{\sqrt{\kappa}}-\rho^2 t}\right)d\rho
\end{aligned} \tag{2.19}$$

The above integral is manupulated using the following identity

$$\int_0^\infty \frac{1}{\rho} e^{\frac{-i\rho z}{\sqrt{\kappa}} - \rho^2 t} d\rho = \int_{-\infty}^0 \frac{-1}{\rho} e^{\frac{i\rho z}{\sqrt{\kappa}} - \rho^2 t} d\rho \tag{2.20}$$

to give

$$\theta(t,z) = \frac{\theta_o}{\pi i} \int_{-\infty}^\infty \frac{1}{\rho} e^{i\frac{z\rho}{\sqrt{\kappa}} - \rho^2 t} d\rho \tag{2.21}$$

We now define $\zeta = \frac{z}{\sqrt{4\kappa t}}$ and $x = \sqrt{t}\rho$. With these new variables, the argument of the exponential function in the integrand of the above equation becomes

$$\begin{aligned} \frac{iz\rho}{\sqrt{\kappa}} - t\rho^2 &= 2i\zeta\sqrt{t}\rho - t\rho^2 \\ &= 2i\zeta x - x^2 \\ &= 2i\zeta x - x^2 - \zeta^2 + \zeta^2 \\ &= (\zeta + ix)^2 - \zeta^2 \end{aligned} \tag{2.22}$$

We also note that

$$\frac{d\rho}{\rho} = \frac{dx}{x} \tag{2.23}$$

Thus, the integral we are evaluating becomes

$$\theta(t,z) = \frac{\theta_o}{\pi i} \int_{-\infty}^\infty e^{(\zeta+ix)^2 - \zeta^2} \frac{dx}{x} \tag{2.24}$$

This integral is too difficult to evaluate as it stands, but we can make progress towards its evaluation by considering the ζ-derivative of $\theta(t,z)$:

$$\begin{aligned} \frac{\partial\theta(t,z)}{\partial\zeta} &= \frac{\theta_o}{\pi i} \int_{-\infty}^\infty \left(2(\zeta+ix) - 2\zeta\right) e^{(\zeta+ix)^2 - \zeta^2} \frac{dx}{x} \\ &= \frac{2\theta_o}{\pi i} \int_{-\infty}^\infty ix e^{(\zeta+ix)^2 - \zeta^2} \frac{dx}{x} \\ &= \frac{2\theta_o}{\pi} e^{-\zeta^2} \int_{-\infty}^\infty e^{(\zeta+ix)^2} dx \end{aligned} \tag{2.25}$$

We find that this integral for the ζ-derivative of $\theta(t,z)$ is easy to evaluate if we define two variables, u and v, such that

$$u^2 = -(\zeta + ix)^2 \tag{2.26}$$

and

$$v^2 = u^2 \tag{2.27}$$

with $du = dv = -dx$. With this change of variables, and with the identity $Y = \sqrt{YY}$, the integral for the ζ-derivative of $\theta(t,z)$ becomes

$$\begin{aligned}
\tfrac{\partial\theta(t,z)}{\partial\zeta} &= \frac{-2\theta_o}{\pi} e^{-\zeta^2} \int_{-\infty}^{\infty} e^{-u^2} dx \\
&= \frac{-2\theta_o}{\pi} e^{-\zeta^2} \sqrt{\int_{-\infty}^{\infty} e^{-u^2} du \int_{-\infty}^{\infty} e^{-v^2} dv} \\
&= \frac{-2\theta_o}{\pi} e^{-\zeta^2} \sqrt{\int_{-\infty}^{\infty} \int_{-\infty}^{\infty} e^{-(u^2+v^2)} du\ dv} \\
&= \frac{-2\theta_o}{\pi} e^{-\zeta^2} \sqrt{\int_{0}^{\infty} \int_{0}^{2\pi} e^{-r^2} r d\phi\ dr} \\
&= \frac{-2\theta_o}{\pi} e^{-\zeta^2} \sqrt{2\pi \int_{0}^{\infty} \frac{-1}{2} \frac{\partial}{\partial r} \left(e^{-r^2}\right) dr} \\
&= \frac{-2\theta_o}{\pi} e^{-\zeta^2} \sqrt{\pi}
\end{aligned} \tag{2.28}$$

We now know the ζ-derivative of $\theta(t,z)$, so it is an easy matter to determine $\theta(t,z)$ (here, we make use of the definition of the error function):

$$\begin{aligned}
\theta(t,z) &= \frac{-2\theta_o}{\sqrt{\pi}} \int_{0}^{-\zeta} e^{-\xi^2} d\xi \\
&= \theta_o \mathrm{erf}(-\zeta) \\
&= \theta_o \mathrm{erf}\left(\frac{-z}{\sqrt{4\kappa t}}\right)
\end{aligned} \tag{2.29}$$

Observe that the error function is antisymmetric about the $z = 0$ level.

The error function, $\mathrm{erf}(x)$, is a well-known special function that is tabulated in various mathematical handbooks [Abramowitz and Stegun, 1964; Press *et al.*, 1989]. In particular, the student will find that it is implimented as a function in MATLAB®.

2.1.6 Geothermal Gradient

For interest's sake, we compute the geothermal gradient at $z = 0$ associated with the above solution because this is the formula Kelvin used to date the age of the earth. The geothermal gradient is given by the derivative of (2.29) with respect to z

$$\begin{aligned} \theta_z(t,0) &= \frac{\partial}{\partial z}\left(\frac{2\theta_o}{\sqrt{\pi}}\int_0^{\frac{z}{\sqrt{4\kappa t}}} e^{-\xi^2}\,d\xi\right)\Big|_{z=0} \\ &= -\frac{\theta_o}{\sqrt{\pi\kappa t}} \end{aligned} \tag{2.30}$$

The cooling history of the upper 100 km of a semi-infinite solid with a diffusivity of $\kappa = 1.18 \times 10^{-6}$ m^2 s^{-1} occupying the region $z < 0$ is displayed in Fig. (2.6). Each curve represents $\theta(t, z)$ at 10-million year intervals starting with an initial temperature of $\theta_o(z) = 3871$ C. (The values for κ, θ_s and θ_o are taken from Kelvin's [1864] analysis.) The surface temperature is assumed constant at 0 C for the entire cooling history. Note that significant deviation from the initial temperature profile occurs in a relatively thin upper crust of the Earth, according to this model. This suggests that the cooling half-space model may be adequate for describing the early stages of a more complicated Earth model such as the model of the oceanic crust we will discuss below.

2.1.7 Kelvin's Edinburgh Calculation

Kelvin [1864] used (2.30) to estimate the age of the Earth, T_e, from measurements of the geothermal gradient made near Edinburgh, Scotland:

$$T_e = \frac{-1}{\pi\kappa}\left(\frac{\theta_o}{\theta_z(T_e, z=0)}\right)^2 \tag{2.31}$$

Using measurements to evaluate the right-hand side of (2.31), in particular $\theta_z(T_e, z=0) = -1/27$ C m^{-1}, Kelving determined that $T_e \approx 94 \times 10^6$ years. A plot of $\theta_z(t, z)$ for the first 100-million years of the cooling history of the semi-infinite solid shown in Fig. (2.6) is displayed in Fig. (2.7).

Kelvin's [1864] analysis was flawed for two reasons. He did not account for the generation of heat within the earth due to the decay of radioactive elements, and he was unaware of convective cooling processes associated with mantle convection. Radioactivity and mantle convection were not discovered until the next century, so Kelvin had no way of knowing about these flaws. As suggested by Richter [1986], Kelvin's method, despite its flaws, was important because it represented the first time the laws of physics were applied to something so large and seemingly inscrutible as the Earth.

2.2 Theory of Sea-Floor Subsidence

Having finished with the interesting story of Lord Kelvin, we are now ready to get back to buisness and develop a theory which explains the bathymetry of the ocean. Following Davis and Lister [1974], we adopt (2.29) as a satisfactory approximation to the temperature profile of a column of oceanic crust as it cools from its initial molten state. We assume that subsidence $\Delta d(t)$ of the sea floor from its initial elevation at the mid-ocean ridge $d(t=0)$ is determined by two processes: thermal contraction, and isostatic depression due to increasing water load above the subsiding sea floor.

Thermal contraction $\Delta h(t)$ is related to $\theta(t, z)$ by the thermal expansion

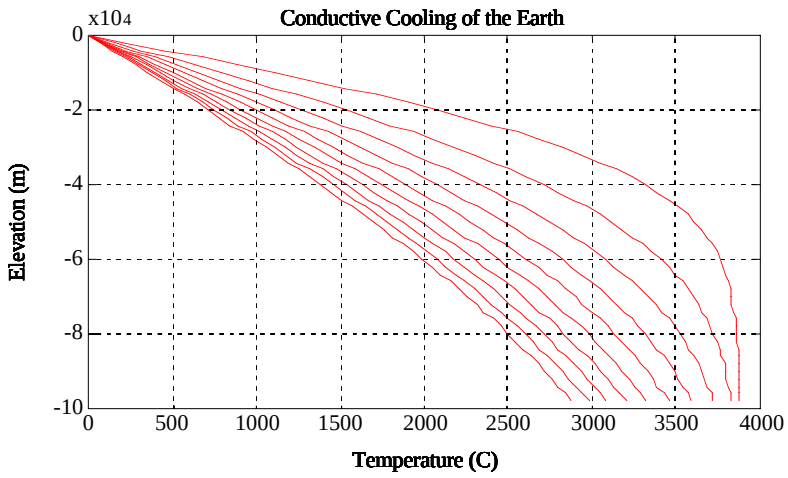

Figure 2.6: Conductive cooling of a semi-infinite solid occupying $z < 0$.

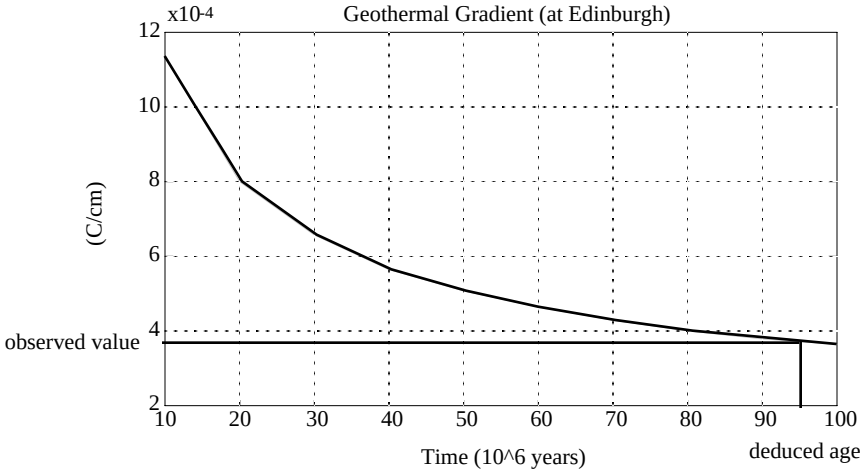

Figure 2.7: History of geothermal gradient at $z = 0$ for a semi-infinite solid occupying $z < 0$. Values of $\theta_z(T_e, z = 0)$ and T_e described by Kelvin [1864] in his determination of the age of the Earth are indicated by the lines.

coefficient α

$$\Delta h(t) = -\alpha\theta_o \int_{-\infty}^{0} \left(1 - \mathrm{erf}(\frac{-z}{2\sqrt{\kappa t}})\right) \mathrm{d}z \tag{2.32}$$

Here the role of the integral is to sum the temperature change over what we take to be the infinite depth of the oceanic crust. We know, of course, that the oceanic crust is of limited thickness. The minus sign appears in (2.32) due to the fact that the temperature of the oceanic crust is cooling with time, and is thus contracting vertically. We use the expression for an infinitely thick crust here because we know that during the brief time interval oceanic crust actually resides on the surface of the earth (up to about 200 million years), there is little difference between the heat lost from a plate and that lost from a semi-infinite solid. We thus avoid the complexity of dealing with finite thickness by taking $-\infty$ as the lower limit on the integral of (2.32). Before evaluating this integral, we consider the effect of isostatic depression.

Isostatic depression due to sea-water loading, $\Delta g(t)$, is determined from $\Delta d(t)$ (to be determined later) by assuming that deep below the Earth's surface there exists a horizontal *compensation level* that is parallel to the sea-surface (*i.e.,* the geoid). Gravitational equilibrium requires that the the total mass of water *and* oceanic crust above is a constant that is independent of location. In other words,

$$\rho_m \Delta g(t) = \rho_w \Delta d(t) \tag{2.33}$$

where ρ_w and ρ_m are the densities of seawater and mantle material, respectively, and $\rho_w \Delta d(t)$ is the extra load caused by sea-water filling the void caused by the thermal contraction of the oceanic crust. The net change in ocean depth $\Delta d(t)$ is the sum of $\Delta h(t)$ and $\Delta g(t)$. This gives

$$\Delta d(t) = \frac{1}{1 - \rho_w/\rho_m} \Delta h(t) \tag{2.34}$$

We are now ready to determine $\Delta d(t)$ by evaluating the integral in (2.32). This is somewhat tricky and is done as follows. First, change the variable of

integration from z to $x = -z/(2\sqrt{\kappa t})$

$$\begin{aligned}\int_{-\infty}^{0} \left(1 - \operatorname{erf}\left(\tfrac{-z}{\sqrt{4\kappa t}}\right)\right) dz &= -2\sqrt{\kappa t} \int_{\infty}^{0} (1 - \operatorname{erf}(x))\, dx \\ &= 2\sqrt{\kappa t} \int_{0}^{\infty} (1 - \operatorname{erf}(x))\, dx \end{aligned} \tag{2.35}$$

We next make use of the definition of the complementary error function ($\operatorname{erfc}(x) = \frac{2}{\sqrt{\pi}} \int_{x}^{\infty} e^{-\xi^2} d\xi$)

$$\begin{aligned} 2\sqrt{\kappa t} \int_{0}^{\infty} (1 - \operatorname{erf}(x))\, dx &= 2\sqrt{\kappa t} \int_{0}^{\infty} \operatorname{erfc}(x) dx \\ &= \frac{4\sqrt{\kappa t}}{\sqrt{\pi}} \int_{0}^{\infty} \int_{x}^{\infty} e^{-\xi^2} d\xi\ dx \end{aligned} \tag{2.36}$$

We recognize that the domain of integration in the above double integral is the wedge contained within the region of the first quadrant of the (ξ, x)-plain enclosed by the positive ξ axis and the line $x = \xi$. We can reverse the order of integration, without changing this domain of integration, to obtain a simplification:

$$\begin{aligned} \tfrac{4\sqrt{\kappa t}}{\sqrt{\pi}} \int_{0}^{\infty} \int_{x}^{\infty} e^{-\xi^2} d\xi\ dx &= \frac{4\sqrt{\kappa t}}{\sqrt{\pi}} \int_{0}^{t} \int_{0}^{\infty} e^{-\xi^2} d\xi\ dx \\ &= \frac{4\sqrt{\kappa t}}{\sqrt{\pi}} \int_{0}^{\infty} \xi e^{-\xi^2} d\xi \\ &= \frac{4\sqrt{\kappa t}}{\sqrt{\pi}} \int_{0}^{\infty} \frac{-1}{2} \frac{\partial}{\partial \xi} \left(e^{-\xi^2}\right) d\xi \\ &= \frac{-2\sqrt{\kappa t}}{\sqrt{\pi}} e^{-\xi^2} \Big|_{0}^{\infty} \\ &= \frac{2\sqrt{\kappa t}}{\sqrt{\pi}} \end{aligned} \tag{2.37}$$

We thus achieve the following expression for $\Delta d(t)$:

$$\Delta d(t) = \frac{-2\rho_m \alpha \theta_o \sqrt{\kappa t}}{\sqrt{\pi}(\rho_m - \rho_w)} \tag{2.38}$$

where $\Delta d(t) < 0$ denotes *increasing* depth. Assuming a mid-ocean ridge depth of d_m, the depth function $d(t)$ can be written

$$d(t) = d_m + \frac{-2\rho_m \alpha \theta_o \sqrt{\kappa t}}{\sqrt{\pi}(\rho_m - \rho_w)} \tag{2.39}$$

(Again, remember that depths are intended to be negative numbers, thus $d_m < 0$ and $d(t)$ will become increasingly negative as $t \to \infty$. This is Davis and Lister's [1974] solution, and it proved to be a good first step towards understanding the physical mechanism which determines the shape of the ocean floor.

2.3 A Plate Model of Oceanic Crust

The conductive cooling model presented in the previous section describes the ocean bathymetry for young (less than 70 million years) oceanic crust with reasonable accuracy (see Fig. 2.4). For older crust, the actual ocean depth is more shallow than that predicted by Eqn. (2.39). This inaccuracy is a consequence of a thermal-cooling model that is too simple. Parsons and Sclater [1977] proposed that the oceanic crust should be modeled as a plate of fixed thickness, and that it should sit above an astheonsphere that has fixed temperature due to vigorous mantle convection. The advantage of Parsons and Sclater's model is that it captures the asymptotic behavior of ocean depth as the age becomes very large without sacrificing the ability to explain the depth of young oceanic crust.

Parsons and Sclater [1977] were concerned primarily with the asymptotic behavior of the ocean crust after it has cooled for a very long time. They thus considered the oceanic crust to be a plate of fixed final thickness a_o to be reached as $t \to \infty$. The geometry of this plate is summarized in Fig. (2.8).

The equations which govern the conductive cooling of this plate are

$$\theta_t = \kappa\theta_{zz} \qquad -a(t) < z < 0 \tag{2.40}$$

$$\theta(0,z) = \theta_o \qquad -a(t) < z < 0 \tag{2.41}$$

$$\theta(t,0) = \theta_s = 0 \tag{2.42}$$

$$\theta(t,-a(t)) = \theta_o \tag{2.43}$$

where $a(t)$ is the plate thickness. To account for the changing thickness of the plate, it is convenient to adopt a stretched vertical coordinate $\zeta = z/a(t)$ so that the domain of Eqns. (2.40) - (2.43) can be treated as the fixed interval $0 > \zeta > -1$. To perform this coordinate transformation on the governing equations, we note that

$$\frac{\partial}{\partial t} \rightarrow \frac{\partial}{\partial t} - \frac{\dot{a}\zeta}{a}\frac{\partial}{\partial \zeta} \tag{2.44}$$

and

$$\frac{\partial^2}{\partial z^2} \rightarrow \frac{1}{a^2}\frac{\partial^2}{\partial \zeta^2} \tag{2.45}$$

where $\dot{a}$ is the time derivative of a. To simplify the above equations, we adopt a non-dimensional time variable

$$t \rightarrow \frac{a^2}{\kappa}t \tag{2.46}$$

$$\theta \rightarrow \theta_o\theta \tag{2.47}$$

and note that $\frac{\dot{a}}{a} << \frac{\kappa}{a^2}$ for our problem. These simplifications allow us to rewrite (2.40) - (2.43) as

$$\theta_t = \theta_{\zeta\zeta} \qquad -1 < \zeta < 0 \tag{2.48}$$

$$\theta(0,\zeta) = 1 \qquad -1 < \zeta < 0 \tag{2.49}$$

$$\theta(t,0) = 0 \tag{2.50}$$

$$\theta(t,-1) = 1 \tag{2.51}$$

Equations (2.48) - (2.51) are readily solved by the separation of variables method. First we note that the asymptotic solution when $t \rightarrow \infty$ is $\theta \rightarrow$

$-\zeta$. The full solution can be written as the sum of this asymptotic, steady-state solution and a transient solution, $\tilde{\theta}$ which satisfies homogenous (=0) boundary conditions and a slightly different initial condition ($=1+\zeta$)

$$\tilde{\theta} = T(t)Z(\zeta) \tag{2.52}$$

Equation (2.48) becomes

$$\frac{T'}{T} - \frac{Z''}{Z} = 0 \tag{2.53}$$

where primes denote differentiation. Noting that (2.53) requires that a function of t only (T'/T) cancel a function of ζ only (Z''/Z), we must conclude that both terms in (2.53) must be scalar quantities. In other words,

$$\frac{T'}{T} = \lambda = \frac{Z''}{Z} \tag{2.54}$$

Solutions Z_n which satisfy the homogeneous boundary conditions are of the form

$$Z_n(\zeta) = b_n \sin(n\pi\zeta) \qquad n = 1, \ldots, \infty \tag{2.55}$$

Corresponding solutions T_n are of the form

$$T_n(t) = e^{-(n\pi)^2 t} \qquad n = 1, \ldots, \infty \tag{2.56}$$

The full solution may be written as linear combinations of the $T_n(t) \cdot Z_n(\zeta)$'s:

$$\theta(t, \zeta) = -\zeta + \sum_{n=1}^{\infty} b_n e^{-(n\pi)^2 t} \sin(n\pi\zeta) \tag{2.57}$$

The constants $\{b_n, n = 1, \ldots, \infty\}$ may be evaluated by enforcing the initial condition $\theta(0, \zeta) = 1$, which implies that

$$\begin{aligned} \tilde{\theta}(0, \zeta) = &\quad 1 + \zeta \\ = &\quad \sum_{n=1}^{\infty} b_n \sin(n\pi\zeta) \qquad -1 < \zeta < 0 \end{aligned} \tag{2.58}$$

The b_n's are evaluated by standard Fourier series techniques. First, we note that

$$b_n = 2 \int_{-1}^{0} (1 + \zeta) \sin(n\pi\zeta) \mathrm{d}\zeta \tag{2.59}$$

The integrand may be broken into two terms which are readily integrated:

$$\begin{aligned} 2\int_{-1}^{0}\sin(n\pi\zeta)\mathrm{d}\zeta = & \quad \frac{-2}{n\pi}\cos(n\pi\zeta)|_{-1}^{0} \\ & = \quad \frac{-2}{n\pi}(1-(-1)^n) \\ & = \quad \begin{cases} \frac{-4}{n\pi} & \text{if n is odd} \\ 0 & \text{if n is even} \end{cases} \end{aligned} \tag{2.60}$$

for $n = 1, \ldots, \infty$. Also,

$$\begin{aligned} & 2\int_{-1}^{0}\zeta\sin(n\pi\zeta)\mathrm{d}\zeta \\ & = \quad 2\int_{-1}^{0}\mathrm{d}\left(\frac{-\zeta\cos(n\pi\zeta)}{n\pi}\right) - 2\int_{-1}^{0}\frac{-\cos(n\pi\zeta)}{n\pi}\mathrm{d}\zeta \\ & = \quad \frac{-2}{n\pi}(\zeta\cos(n\pi\zeta))|_{-1}^{0} - \frac{-2}{(n\pi)^2}\sin(n\pi\zeta)|_{-1}^{0} \\ & = \quad \begin{cases} \frac{2}{n\pi} & \text{if n is odd} \\ \frac{-2}{n\pi} & \text{if n is even} \end{cases} \end{aligned} \tag{2.61}$$

Combining the intermediate results presented in (2.60) and (2.61) we find that

$$b_n = \frac{-2}{n\pi} \qquad n = 1, \ldots, \infty \tag{2.62}$$

Thus the complete solution to the plate model is

$$\theta(t,\zeta) = -\zeta + \sum_{n=1}^{\infty}\frac{-2}{n\pi}e^{-(n\pi)^2 t}\sin(n\pi\zeta) \tag{2.63}$$

In dimensional form (recall (2.46) and (2.47)), this expression is

$$\theta(t,\zeta) = \theta_o\left(-\frac{z}{a} + \sum_{n=1}^{\infty}\frac{-2}{n\pi}e^{\frac{-(n\pi)^2\kappa t}{a^2}}\sin(\frac{n\pi z}{a})\right) \tag{2.64}$$

The geothermal heat flux at $z = 0$, $q(t,0)$, is readily determined by taking the z-derivative of $\theta(t,z)$

$$q(t,0) = -k\theta_o\left(-\frac{1}{a} + \sum_{n=1}^{\infty}\frac{-2}{a}e^{\frac{-(n\pi)^2\kappa t}{a^2}}\right) \tag{2.65}$$

where k is the thermal conductivity of the oceanic crust.

The thermal subsidence is again determined by summing a thermal contraction contribution and an isostatic depression contribution.

$$\Delta h(t) = \alpha\theta_o \int_{-a}^{0} \left(1 + \frac{z}{a} - \sum_{n=1}^{\infty} \frac{-2}{n\pi} e^{\frac{-(n\pi)^2\kappa t}{a^2}} \sin(\frac{n\pi z}{a})\right) \mathrm{d}z \tag{2.66}$$

This expression is easily evaluated by noting that

$$\int_{-a}^{0} \left(1 + \frac{z}{a}\right) \mathrm{d}z = \frac{a}{2} \tag{2.67}$$

and

$$\int_{-a}^{0} \frac{-2}{n\pi} \sin(\frac{n\pi z}{a}) \mathrm{d}z = \begin{cases} 0 & \text{if n is even} \\ \frac{4a}{(n\pi)^2} & \text{if n is odd} \end{cases} \tag{2.68}$$

The result is

$$\Delta h(t) = \frac{\alpha\theta_o a}{2} \left(1 - \sum_{n \text{ odd}} \frac{8}{(n\pi)^2} e^{\frac{-(n\pi)^2\kappa t}{a^2}}\right) \tag{2.69}$$

Making use of (2.34), we derive the depth anomaly

$$\Delta d(t) = \frac{\alpha\rho_m\theta_o a}{2(\rho_m - \rho_w)} \left(1 - \sum_{n \text{ odd}} \frac{8}{(n\pi)^2} e^{\frac{-(n\pi)^2\kappa t}{a^2}}\right) \tag{2.70}$$

We note that the asymptotic subsidence at $t \to \infty$ is given by (this is the result when all the exponential terms in the sum have decayed to zero)

$$\Delta d_s = \frac{\alpha\rho_m\theta_o a}{2(\rho_m - \rho_w)} \tag{2.71}$$

Thus,

$$d(t) = d_m + \Delta d_s \left(1 - \sum_{n \text{ odd}} \frac{8}{(n\pi)^2} e^{\frac{-(n\pi)^2\kappa t}{a^2}}\right) \tag{2.72}$$

We note as a reminder that (2.72) is approximate in the sense that we did not account for the fact that a changes with time. This change, as argued

previously, is so small compared to the size of a (typically 100 km or so), that the approximation is satisfactory for practical application

Parsons and Sclater [1977] demonstrated that the plate model for ocean crust subsidence was superior to the semi-infinite solid model derived by Davis and Lister [1974] because it captured the otherwise anomalous behavior of the ocean floor at large geologic ages shown in Fig. (2.4) without losing the satisfactory attributes of the $\sqrt{t}$-dependence for young ages. The advantage of the plate model is reflected in the fact that as the ocean crust ages, it becomes less like a semi-infinite body and more like a plate with a finite amount of heat to be dissipated. Eventually, the plate is able to attain a steady-state temperature depth profile (the linear term in (2.64)). Thus at great age, the plate reaches a constant asymptotic elevation, and this is in agreement with the very old ocean crust in Fig. (2.4).

Parsons and Sclater [1977] suggested that two simple empirical formulae could be derived from the solution (2.72)

$$d(t) = 2500 + 350\sqrt{t} \quad \text{m} \qquad \text{for } 0 < t < 70\text{m.y.} \tag{2.73}$$

and

$$d(t) = 6400 - 3200\ e^{\frac{-t}{62.8}} \quad \text{m} \qquad \text{for } t > 70\text{m.y.} \tag{2.74}$$

These results perform reletively well in explaining the depth/age relationships for the ocean floor around the Earth. Recent revisions of the Parsons and Sclater model [Stein and Stein, 1992] suggest that improvements to the Parsos and Sclater model can be made by using inverse methods (what is taught in GeoSci 235) to fit the above expressions for thermal subsidence and geothermal heat flow in Eqns. (2.72) and (2.65) to the observations from the world ocean. Parameters to be fit include θ_o, α, and a.

2.4 Numerical Methods

The above-derived solution for the sea-floor bathymetry can be developed using what is called a numerical method to solve Eqns. (2.40) - (2.43). For

many scientists, numerical methods are easier to understand and apply than the tedious mathematical analysis, such as that presented above, needed to develop exact solutions for partial-differential equations. Here we shall develop a finite-difference solution for the Parsons and Sclater cooling-plate model using MATLAB®.

We begin by restating the equations which govern the cooling of a column of oceanic plate as it moves away from the mid-ocean spreading center:

$$\theta_t = \kappa\theta_{zz} \qquad -a < z < 0 \tag{2.75}$$

$$\theta(0, z) = \theta_o \qquad -a < z < 0 \tag{2.76}$$

$$\theta(t, 0) = \theta_s = 0 \tag{2.77}$$

$$\theta(t, -a(t)) = \theta_o \tag{2.78}$$

where a is the plate thickness which we now take to be constant (for the purpose of describing the thermal-evolution). The finite-difference approach begins with a discretization of the interval $[-a < z < 0]$ into $N-1$ discrete intervals with N grid points as shown in Fig. (2.9). The distance between grid point i and grid point $i+1$ is $\Delta z = \frac{a}{N-1}$. The time interval $t > 0$ is also discretized into an indefinite number of intervals and time steps (the indefinite number can be defined by how long we wish to compute the solution). The n'th time step corresponds to $t = (n-1)\Delta t$ where Δt is the length of each time step.

The temperature θ is discretized in space and time. The values of θ at grid point i and at time step n are denoted by subscript i and superscript n, *e.g.*, θ_i^n. We find it convenient to define the N-dimensional column vector $\underline{\theta}^n$ to be the finite-difference solution at time step n:

$$\underline{\theta}^n = \begin{bmatrix} \theta_1^n \\ \theta_2^n \\ \vdots \\ \theta_N^n \end{bmatrix} \tag{2.79}$$

The initial condition and two boundary conditions expressed in Eqns. (2.76)

- (2.78) are written in the following finite-difference form:

$$\underline{\theta}^1 = \begin{bmatrix} \theta_o \\ \theta_o \\ \vdots \\ \theta_o \end{bmatrix} \tag{2.80}$$

$$\theta_1^n = 0 \qquad \text{for } n \geq 1 \tag{2.81}$$

$$\theta_N^n = \theta_o \qquad \text{for } n \geq 1 \tag{2.82}$$

where θ_o is the melting temperature of rock. The partial-differential equation, Eqn. (2.75), is converted to finite-difference form by using the following expressions for derivatives of θ:

$$\frac{\partial \theta}{\partial t} \rightarrow \frac{\theta_i^{n+1} - \theta_i^n}{\Delta t} \tag{2.83}$$

$$\frac{\partial^2 \theta}{\partial z^2} \rightarrow \frac{\theta_{i+1}^n + \theta_{i-1}^n - 2\theta_i^n}{\Delta z^2} \tag{2.84}$$

The finite-difference version of Eqn. (2.75) is constructed by using the conversion formulae shown in Eqns. (2.83) and (2.84). One choice must be made in constructing the equation, however. This choice concerns the time at which the $\frac{\partial^2 \theta}{\partial z^2}$ term is evaluated.

There are two basic conventions to the above choice, the *explicit* time step and the *implicit* time step. (For a more complete description of available choices, consult a numerical methods text.) They differ in the following manner:

Explicit time step

$$\frac{\theta_i^{n+1} - \theta_i^n}{\Delta t} = \kappa \frac{\theta_{i+1}^n + \theta_{i-1}^n - 2\theta_i^n}{\Delta z^2} \tag{2.85}$$

Implicit time step

$$\frac{\theta_i^{n+1} - \theta_i^n}{\Delta t} = \kappa \frac{\theta_{i+1}^{n+1} + \theta_{i-1}^{n+1} - 2\theta_i^{n+1}}{\Delta z^2} \tag{2.86}$$

It is readily seen that the difference between the two conventions is whether the second-derivative of θ with respect to z is evaluated at the *beginning* or at the *end* of the time step. There are important technical reasons for choosing the *implicit* time stepping convention over the *explicit* convention that have to do with what is called numerical stability. We shall choose the implicit convention in what follows because of its attribute of being unconditionally stable.

2.4.1 Finite-Difference Solution as a Matrix Algebra Problem

The finite-difference version of the plate-cooling problem is conveniently set-up as a matrix-algebra problem. If we define the $N \times N$ matrix $\mathbf{A}$ as follows:

$$\mathbf{A} = \begin{bmatrix} 1 & 0 & 0 & 0 & 0 & \cdots \\ \frac{-\kappa\Delta t}{\Delta z^2} & 1 + \frac{2\kappa\Delta t}{\Delta z^2} & \frac{-\kappa\Delta t}{\Delta z^2} & 0 & 0 & \cdots \\ 0 & \frac{-\kappa\Delta t}{\Delta z^2} & 1 + \frac{2\kappa\Delta t}{\Delta z^2} & \frac{-\kappa\Delta t}{\Delta z^2} & 0 & \cdots \\ & & & \ddots & & \\ & & & \cdots & 0 & 1 \end{bmatrix} \tag{2.87}$$

and define the column vector $\mathbf{R}$:

$$\mathbf{R} = \begin{bmatrix} 0 \\ \theta_2^n \\ \theta_3^n \\ \vdots \\ \theta_{N-1}^n \\ \theta_o \end{bmatrix} \tag{2.88}$$

then the implicit finite-difference time-stepping scheme (Eqn. 2.86) may be written as follows:

$$\mathbf{A}\underline{\theta}^{n+1} = \mathbf{R} \tag{2.89}$$

We regard Eqn. (2.89) as the formula which advances the finite-difference solution vector $\underline{\theta}$ forward through one time step. We must thus solve Eqn. (2.89) over and over again to advance the solution through the desired number of time steps.

The solution of this matrix algebra equation involves inverting or factoring the matrix $\mathbf{A}$. This can be a lot of work. (Some savings in computational difficulty can be gained by exploiting the fact that the matrix $\mathbf{A}$ is of tridiagonal form.) Fortunately, for our situation, the matrix $\mathbf{A}$ does not change from time-step to time-step, thus we may invert it or factor it once (depending on our solution proceedure), and then use the result to perform the all of the desired number of time steps. This solution algorithm will be explained in greater detail in class.

2.5 Hypsometry

One of the critical skills in the analysis of the ocean is the ability to determine distribution functions of its various properties. In this chapter, we will begin with a determination of the distribution of the earth's surface elevation with respect to sea level. In other words, we wish to determine the *hypsometry* of the earth's surface. Our interest is to be able to describe how much of the earth's total surface area possesses a surface elevation within a particular range. For example, we might wish to note that only 0.003 percent of the earth's surface has an elevation larger than 8000 m.

There are many ways to approach the problem of deriving a distribution function for a given parameter. Let $\mathfrak{A}(p)$ denote the distribution function for property p (which we leave as undefined for now, but it could be surface elevation, or surface salinity, etc.). The physical meaning of $\mathfrak{A}(p)$ is defined as follows. For a specific value of p, say p_o, $\mathfrak{A}(p_o)$ denotes the fraction (on a scale from 0 to 1) of *total* surface area of the earth which has p_o as its value of

p. (Note, in the future, we might wish to define other distribution functions where the total surface area of the ocean alone replaces the total area of the earth.) It is convienent to define another function $\Phi(p)$ such that

$$\Phi = \int_{p_{min}}^{p} \mathfrak{A}(p')dp' \tag{2.90}$$

In this circumstance,

$$\mathfrak{A}(p) = \frac{d\Phi}{dp} \tag{2.91}$$

One way to derive $\mathfrak{A}$ from measurements of surface elevation is to first derive the function Φ, and then to take its derivative. This is the approach we shall take in the following assignment.

To determine Φ for the surface-elevation of the earth, we will have to perform the integration in (2.90) using a discrete, finite-element representation of the earth's spherical surface. The data we are provided comes in the form of a 180 by 360 rectilinear grid. The column label of each grid point referrs to a discrete longitude, beginning at the international date line (-180 degrees) and extending to one-degree west of the prime meridian. The row label of each grid point referrs to a discrete latitude, beginning at 89.5 degrees north and extending to 89.5 degrees south. Excluding the small polar caps which lie at latitudes poleward of 89.5 north and south latitudes (this introduces a small error which we shall ignore), the entire earth surface is represented by a 179 by 359 array of segments of a spherical shell. The area of each segment, $A_{i,j}$, corresponding to the ith latitude and the jth longitude of the array, varies with the latitude according to the following rule

$$A_{ij} = R_e^2 \left(\frac{\pi}{359}\right)^2 \cos(\frac{\pi(89-j)}{180}) \tag{2.92}$$

where R_e is the radius of the earth (6380 km). The total area of the earth (minus the two polar caps, which we ignore) is thus

$$\begin{aligned} A_e &= \int_{-\pi/2}^{\pi/2} \int_0^{2\pi} R_e^2 cos(\phi) d\lambda d\phi \\ &= 4\pi R_e^2 \\ &\approx \sum_{i=1}^{179} \sum_{j=1}^{359} A_{ij} \end{aligned} \tag{2.93}$$

Notice that the double integral over latitude and longitude has been broken into a double sum over the range of the i and j indices of the array of spherical shell segments.

To determine the hypsometry of the earth, we compute $\mathbf{\Phi}$, a discrete version of the continuous function Φ. Our interest is in determining the relative surface area of the earth in discrete categories starting at -10,000 m and going up to 10,000 m in 1,000 m intervals. We define the vector $\mathbf{\Phi}$ as follows

$$\mathbf{\Phi} = (\Phi_1 \Phi_2 \cdots \Phi_{19})$$

where each component, Φ_i, represents the relative area of the earth with surface elevation less than E_i, where

$$\mathbf{E} = (-9000 - 8000 \cdots 0 \cdots 1000 \cdots 10000)$$

To evaluate $\mathbf{\Phi}$, the following summation must be performed for each component i

$$\Phi_i = \sum_{l=1}^{179} \sum_{k=1}^{359} \gamma_{lk} \frac{A_{lk}}{A_e} dE \tag{2.94}$$

where γ_{lk} is defined to be 1 if the average surface elevation in the l, kth segment of the discretized earth's surface is less than E_i, and 0 otherwise; and $dE = 1000$ is the interval of elevation used to discretize the hypsometry.

The discretized distribution function $\mathfrak{A}_\mathbf{i}$ is defined by

$$\mathfrak{A}_\mathbf{i} = (\mathfrak{A}_1 \mathfrak{A}_2 \cdots \mathfrak{A}_1 8)$$

where,

$$\mathfrak{A}_i = \Phi_{i+1} - \Phi_i \tag{2.95}$$

The discretized distribution function, once determined, can be plotted to see if there are any special patterns to the planetary surface. In the following exercises, you will notice that the earth's distribution functions displays a curious bi-modal pattern. This pattern reflects the fact that there are two kinds of crust, oceanic and continental. One of the interesting projects underway today is the mapping of the planet Venus using a radar altimeter aboard a satellite called Magellan. The data from this project suggests that Venus does not have two kinds of crust.

2.6 Assignment: Analysis of Ocean Bathymetry

In the MATLAB® file called `ocean_depth_data`, you will find data for 83 measurements of depth and age made in the Pacific Ocean near the Darwin Rise (a region geophysicists have had difficulty explaining in terms of simple crustal cooling theories). This data is provided by a couple of Chicago scientists Stein and Stein [1992] (Seth is at Northwestern University and Carol is at University of Illinois at Chicago).

1. Plot the depth as a function of age.

2. Using the following physical properties of oceanic basalt:

$$\begin{aligned} \kappa &= 8.047 \times 10^{-7} \text{m}^2 \text{ s}^{-1} \\ \rho_m &= 3330 \text{kg m}^{-3} \\ \theta_o &= 1333 \text{C} \\ d_m &= 2895.6 \text{m} \\ \rho_w &\approx 1035 \text{kg m}^3 \end{aligned} \tag{2.96}$$

   find a value of $\alpha \approx 3 \times 10^{-5}$ C^{-1}, the thermal contraction coefficient, which best fits the depth data. Use trial and error as a technique to search through all possible values of α to determine the best value.

3. Display the result of the above determination by plotting your predicted values of depth $\tilde{d}$ against the measured values of depth d as a function of age. Use the MATLAB® errorbar routine to indicate the confidence interval of the data.

4. Now, we are ready to confront the bathymetry of the entire ocean. In the MATLAB® file called `world_elevation_data`, you will fine an 180×360 array of data which represents the earth's surface elevation (with respect to sea level) for a 1-degree by 1-degree rectilinear grid of the earth's surface. Contour this data using the MATLAB® contouring commands.

5. Create another contour of the earth's surface elevation, but this time "mask out" any regions that are above sea level by artificially setting

all elevations greater than zero to be equal to zero. The continental land masses will thus appear as regions of very shallow depth.

6. Open the same 1-degree by 1-degree data set in SPYGLASS®. Create an image using the SPYGLASS® imaging utility. Also create a contour map of the same data using the SPYGLASS® contouring utility. On the contour map, place contour labels. Finally, create a histogram of the data using the color table utility.)

7. In SPYGLASS®, create Mercator, Lambert equal-area and Mollweide maps of the ocean bathymetry using the SPYGLASS® notebook functions that are provided in the external notebook function library called `map_projections.lib`. In MATLAB®, create a map of the continental outlines for the Mercator and Lambert equal-area maps, and overlay them on the SPYGLASS® maps. Do this with the clipboard of the MACINTOSH®. Note that the maximum latitude which appears on the SPYGLASS® version of the Mercator map is 74.5854 degrees (north and south). In addition, the "window" on the Lambert equal-area map has a width of 16,000 kilometers. You will need these two points of information to make the MATLAB® versions of the continental outline maps for your overlays.

8. In SPYGLASS®, create a surface image of the world elevation data.

2.6.1 Assignment: Hypsometry of the Earth

You will again refer to the data in the MATLAB® file called `world_elevation_data` to perform an analysis of the earth's surface and, in particular, the ocean basins.

1. Determine $\mathbf{\Phi}$ and $\mathfrak{A}$ for the earth using the discrete levels contained in the vector $\mathbf{E}$ defined above. Plot both $\mathbf{\Phi}$ and $\mathfrak{A}$ as a function of the elevation cut off or elevation range they represent.

2. Determine $\mathbf{\Phi}$ and $\mathfrak{A}$ for the ocean basins only using the discrete levels contained in the vector (-10000, -9000, -8000, $\cdots$, 0). Remember to

replace the area of the earth with the area of ocean in this exercise. Again, plot your results.

3. Using the formula (2.39) derived in the previous section, determine the distribution of age of the ocean basins using the results of the previous problem. From your results, suggest a time scale for all geological processes which affect the ocean floor.

2.6.2 Assignment: Finite-difference model of cooling plate

1. Construct a finite-difference solution (using $N = 25$ and a $\Delta t = 10^6$ years) of the Parsons and Slater cooling-plate problem. Compute from the finite-difference solution the net contraction Δh of the cooling plate as a function of time for a history of 100 million years.

2. Compute the sea floor depth anomaly (with respect to the depth at the mid-ocean ridge) Δd associated with the Δh computed above. Compare your finite-difference prediction of Δd with that predicted by Parsons and Slater.

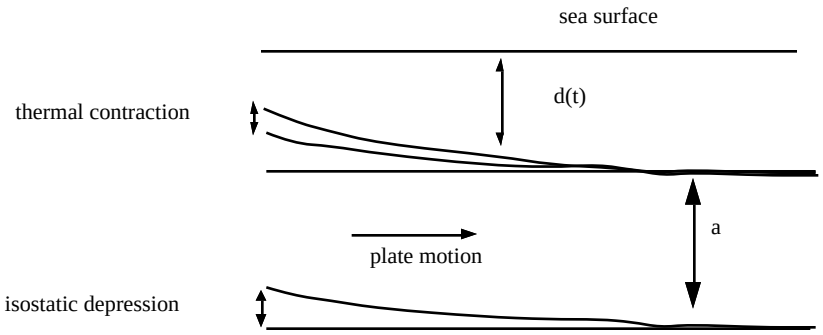

Figure 2.8: Schematic plot of Parsons and Sclater's [1977] oceanic plate geometry.

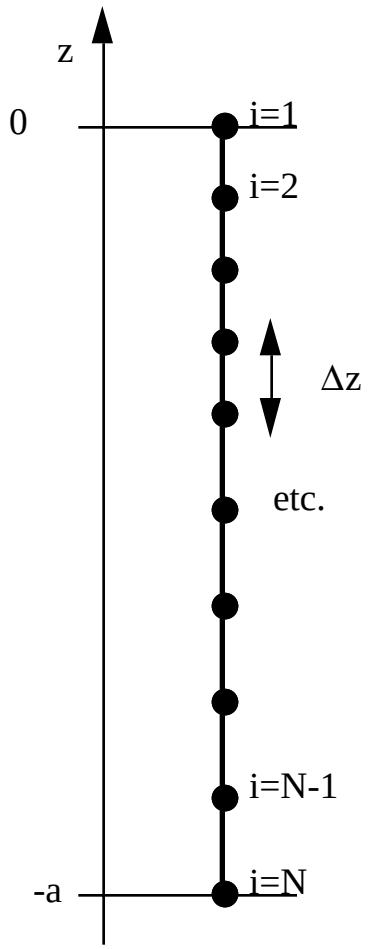

Figure 2.9: Finite-difference grid used to construct a numerical solution of Parsons and Sclater's [1977] model of oceanic plate cooling.

Chapter 3

Hydrography I

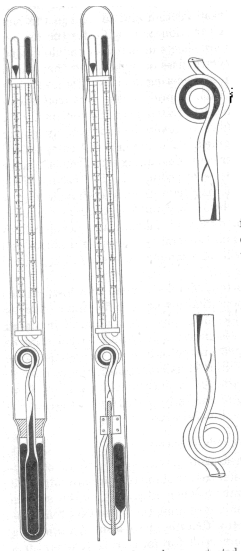

Figure 3.1: Reversing thermometers (protected and unprotected).

In the previous chapters, we developed an understanding of the shape of a container called the ocean basins. In the present chapter, we shall begin the process of filling the container with seawater. Of primary concern in this chapter and the next is the physical and chemical composition of the seawater. Our interest in the hydrographic structure of the ocean is motivated by the fact that measurements of temperature, salinity and other attributes are extremely useful as tracers of the flow and mixing that goes on in the ocean.

Temperature and salinity measurements help us understand the way in which watermasses of different origin intermingle within the deep ocean. Our understanding of ocean circulation thus stems in large part from our view of the temperature and salinity patterns derived from numerous oceanographic research expeditions. Temperature and salinity are also important in a determining the density of seawater. Thus the oceanic circulation is driven in part by the density differences between watermasses of different temperature and salinity.

Our investigation of the earth's hydrographic structure will be spread across several chapters. In this chapter, we shall consider the basic definitions of temperature, salinity, density, and other physical properties. We will use these definitions to investigate the nature of the ocean surface, the upper "skin" of the ocean. In the next chapter, we will see how the aspects of the ocean surface we find here relate to the properties of the ocean at depth.

3.1 Temperature

The temperature of seawater, T, is a measure of how much thermal heat is contained in the water. Generally speaking, people have an intuitive "feel" for what T stands for despite the fact that its strict definition involves some fairly difficult thermodynamic concepts. In addition to temperature, oceanographers sometimes need to know the *potential temperature*, θ, which is defined to be the temperature the water would have if it were to be adiabatically (without exchanging heat with its surroundings) moved to a chamber of constant reference pressure (say, atmospheric pressure). We will not concern ourselves in this course with the potential temperature, but a complete discussion of it may be found in Gill [1982].

The temperature in the ocean obeys the *advective-diffusion equation*, which may be written

$$\frac{\partial T}{\partial t} + \mathbf{u} \cdot \nabla T = \kappa_T \nabla^2 T \tag{3.1}$$

The second term on the left-hand side of the above equation represents the

effect of fluid motion of the ocean. In this course, we will not have the occasion to use (3.1) other than in a conceptual sense when we consider the problem of *double diffusion* described in the next chapter. The main thing to remember is that the thermal diffusivity of seawater, κ_T, is much greater than the diffusivity of salt in seawater, κ_S. This difference gives rise to interesting micro-scale phenomena as we shall see in the next chapter.

Temperature Measurement

One of the most impressive engineering feats in oceanography was the development of thermometers capable of measuring T at great depths. The difficulty of this measurement is appreciated when one thinks about the great length of time required to lower cable over the side of an oceanic research vessel. To measure the temperature at the depth of 10,000 m in the Mariana Trench, for example, it might take several hours for the thermometer to be winched back aboard the ship before it could be read. Clearly, if a temperature measurement is to be made, the thermometer must somehow be protected from the thermal conditions it encounters along its journey back to the ship.

Engineers of the last century devised an ingenious means of "reading" the temperature measurement of the thermometer at depth. In essence, they found a way to "break" the thermometer at the instant when they wanted to take the reading, so that subsequent temperature changes encountered by the thermometer would not effect its reading. (This reminds me of the detective in the movie *Chinatown* who put cheap pocket watches below the tires of parked cars. He could return to the parking site at a later time, and determine from the position of the clock hands on the smashed face of the watch when the car was moved.) The thermometers devised for oceanographic study are called *reversing thermometers* (both protected, for measuring temperature, and unprotected, for measuring depth in the days before sonic depth finders).

A diagram displaying the design of reversing thermometers is provided in Fig. (3.1). The key features to be noted are: mercury bulbs at both ends, the thin capillary tube that connects the bulbs, and the loop and "appendix" in the center of the capillary tube. The purpose of the appendix

in the capillary tube is to break the mercury column at that point when the thermometer is reversed (surface tension keeps the mercury in the upper end of the capillary tube from running down into the lower). The basic technique for measurement was to lower many such reversing thermometers on a long cable into the ocean. A weight, or messenger, was then sent sliding down the cable. As it encountered the first thermometer, it would trigger a reversal, and this, in turn, would trigger the release of a second messenger that would slide on down the cable to trigger the next thermometer.

3.2 Sea Surface Temperature

The sea surface temperature (SST) varies throughout the year, but is relatively constant compared to the variation of surface temperature on land. An animation showing the month-by-month progression of surface temperature derived from satellite data will be viewed in the Lab assignment using the SPYGLASS® utility VIEW®. A single frame from this animation is displayed in Fig. (3.2).

Several structures in the sea-surface temperatures of Fig. (3.2) strike the eye. First, there is a curious lineation of cold water aligned with the equator in the Pacific. Second, two broad patches of cold water appear to hug the Western coasts of the Equatorial Americas. Third, there is a curious stream of warm water that appears along the Eastern coast of North America. These features, of course, reflect the circulation of the ocean; and we shall discuss them later. For now, however it is interesting to note that the first and second features mentioned above relate to the famous *El Niño* events.

3.2.1 Freezing Point of Seawater

As will be readily appreciated in the exercises associated with this chapter, much of the ocean surface is at the freezing point. Both the Arctic and Antarctic waters are ice-covered for much, if not all, of the year. It is thus important to note the experimental determination of the temperature (in C)

at which sea water of salinity S and pressure p freezes [Millero, 1978]:

$$T_f(S,p) = -0.0575S + 1.710523 \times 10^{-3} S^{\frac{3}{2}} - 2.154996 \times 10^{-4} S^2 - 7.53 \times 10^{-3} p \tag{3.2}$$

This formula is accurate to approximately 0.004 C.

The key points to remember when considering the formation and melting of ice in the ocean is that salinity and pressure both depress the freezing point. Sea water temperatures as low as -1.8 C, for example, are possible at the ocean surface. At depth where the pressure is high, below the great ice shelves of Antarctica, for example, water temperature as low as -2.5 C has been measured.

3.3 Salinity

Ocean water is full of organic and inorganic impurities, and disolved gasses. The inorganic impurities are referred to collectively as "salt" . Salinity, S, refers to the mass of disolved inorganic materials divided per mass unit of sea water. We express S in units of parts per thousand ($^\circ/_{\circ\circ}$); thus, a salinity of 35 $^\circ/_{\circ\circ}$ denotes a concentration of 35 g of disolved inorganic material in 1 kg of sea water.

The composition of ocean salt is generally quite uniform throughout the ocean. The majority of ocean salt is composed of Clorine (CL), Sodium (Na), Sulphate (SO_4), Magnesium (Mg) and Potassium (K). Many trace elements also exist, and are quite important in the grand scheme of things. The concentration of calcium carbonate ions, for example, has an important bearing on the properties of ocean-bottom sediments and on the ability of ocean water to absorb atmospheric CO_2. One cannot belittle the role of various nutrients in the ocean either.

In the early days of ocean exploration, it was very difficult to make accurate measurements of salinity. This was because the compositions of the several inorganic ions had to be determined by tedious chemical titration. Silver nitrate, for example is used as a titration solution to determine the

concentration of Cl. During the H. M. S. *Challenger* expedition, salinity of 77 water samples was determined through painstaking titration procedures. Today, modern ocean research vessels can measure salinity at thousands of points per second using electrical conductivity sensors.

The great uniformity of ocean salt chemical composition is due to the fact that disolved inorganic elements have a very long residence time in the ocean compared with the mixing timescale of ocean circulation. Salt is introduced to the ocean by groundwater circulation through the mid-ocean ridge basalts, and by river fluxes into the ocean containing the by-products of rock weathering. Salt leaves the ocean by precipitation, such as in the Great Bonneville salt flats of Utah, and by biological productivity, such as the creation of limestone reefs by coral polyps.

As with temperature, the distribution of salinity satisfies the advective-diffusion equation

$$\frac{\partial S}{\partial t} + \mathbf{u} \cdot \nabla S = \kappa_S \nabla^2 S \tag{3.3}$$

where $\kappa_S \approx 1.5 \times 10^{-9} \mathrm{m}^2 \mathrm{s}^{-1}$, the diffusivity of salt, is much less than the diffusivity of heat, $\kappa_S < \kappa_T$. For the most part, we will regard ocean salinity to be a *conserved tracer*. That is to say salinity of water parcels are conserved within the ocean except when the water parcels are at or near the sea surface (or the base of ice shelves and icebergs) where salts can be concentrated or diluted by the process of atmospheric evaporation and precipitation, and by sea-ice formation and melting.

In the assignment associated with this chapter, we will investigate the relationship between the surface salinity, $S(z = 0)$, and the patterns of net atmospheric precipitation, P. We will find that the latitudes of the *subtropical high pressure cells* of the atmosphere will have the greatest salinity due to the fact that evaporation dominates over precipitation in those areas.

3.4 Density

The most important physical property of sea water from the standpoint of ocean circulation is its density, $\rho(S,T,p)$, which is a function of S, T and the pressure, p. The empirical formula for determining $\rho(S,T,p)$ is a polynomial of impressive complexity. It has 41 coefficients multiplying the various powers of S, T and p. We will not attempt to describe the polynomial here (the interested student may consult Appendix 3 of [Gill, 1982]). A MATLAB® function will be provided to assist the student in the calculation of $\rho(S,T,p)$ when needed.

The key feature of the density function to remember is that *both* temperature and salinity are important in determining the density of sea water. Today, polar waters are denser than equatorial waters because they are so cold. The equatorial waters are more saline, however, so only a small degree of polar warming is required to make the equatorial waters denser than the polar waters, thereby reversing the pole-to-equator gradient in surface density.

Pressure has an important effect on density due to the fact that water is compressible. The effect is non-linear, and this can lead to some interesting results (referred to as "cabaling" after what witches do). One water parcel may be denser than another if both parcels are at one particular depth in the ocean where the pressure is low, whereas, the other parcel may be denser if both parcels are taken down to a greater depth where the pressure is high. This interesting possiblility leads to very intersting and difficult problems of convection in the ocean.

Oceanographers commonly use a secondary variable σ_t as a proxy for density. This variable is defined using the conventional wisdom that density is nearly always very close to 1000 kg/m^3

$$\sigma_t = 1000 \left(\frac{\rho(S,T,0)}{\rho(0,0,0)} - 1 \right) \tag{3.4}$$

We will often use σ_t as a short-hand variable as a quick means to appreciate the density structure of the ocean.

3.5 Assignment

In the following exercises, you will manipulate MATLAB® and SPYGLASS® data files provided by the instructor. These data represent the annual average properties of the ocean surface, and are derived from averages of many thousands of individual measurements. All data files contain information relating to the ocean surface only, and have the same 1-degree by 1-degree resolution.

1. Create Lambert equal-area (both North and South), Mollweide and straight rectilinear maps of the surface salinity, temperature and precipitiation minus evaporation using SPYGLASS®. Take note of the important features that you see in these maps, number them, and create a caption which lists these features and provides a brief, qualitative description of why they caught your eye.

2. Using MATLAB®, determine the zonal average properties for the ocean for each latitude. In other words, determine $\bar{S}^\lambda$, $\bar{T}^\lambda$ and $\bar{P}^\lambda$ defined by integrals of the following nature

$$\bar{S}^\lambda(\phi) = \frac{\int_{-\pi}^{\pi} S(\phi,\lambda)\gamma(\phi,\lambda)d\lambda}{\bar{\gamma}^\lambda(\phi)} \tag{3.5}$$

   where γ is a variable that is 1 where there is ocean and 0 where there is land, and

$$\bar{\gamma}^\lambda = \int_{-\pi}^{\pi} \gamma(\phi,\lambda)d\lambda \tag{3.6}$$

   Plot line graphs of these zonal average properties and describe the relationship between that of the salinity and that of the net precipitation. Some caution must be applied in dealing with the extreme southern latitudes where there is no ocean at any longitude.

3. Determine and plot $\bar{\rho}^\lambda(S,T,0)$. At what latitudes is the density greatest?

4. Make SPYGLASS® maps (straight rectilinear, Mollweide and Lambert equal-area in both hemispheres) of the salinity and temperature anoma-

lies defined by

$$\tilde{S}(\phi,\lambda) = \quad S(\phi,\lambda) - \bar{S}^{\lambda}(\phi) \tag{3.7}$$

$$\tilde{T}(\phi,\lambda) = \quad T(\phi,\lambda) - \bar{T}^{\lambda}(\phi) \tag{3.8}$$

Make an informal catalogue of features, number them and list them with brief descriptions in a caption.

5. The instructor will provide an animation of a 10-year record of satellite derived sea-surface temperatures. Please watch the animation using SPYGLASS® utility VIEW®. Describe briefly the most important features you noticed in the animation. Print single "frames" of the movie in addition to the description to illustrate the features you see.

6. The instructor will provide access to the JEdI CD-ROM. On this file volume, you will find an application program called *image*. Run this application (using a color monitor set to 256 colors), and click on the "Special" macro called "SMMRmacro" . This will give you two images of the sea-ice which surrounds Antarctica at two times during the year when it is either at maximum or minimum extend. Inspect this data (the variable plotted is sea-ice concentration in percent of ocean surface covered by sea ice) and describe any interesting features you find. Provide an annotated figure with your description.

7. On another CD-ROM called ADI, you will find a Hypercard stack called "SSMR Main" . Open this stack, read the description on the two cards, then click on the movie icon (it looks like a piece of 35 mm film and has the word DATA written on it) to see three years of Arctic sea-ice concentration data. Examine this data by clicking from year to year and from month to month. Provide a description of key features you find interesting. Provide maps and figures to illustrate your description.

Figure 3.2: Sea-surface temperature (relative scale) in January of 1979. Cold water appears darker than warm water.

Chapter 4

Hydrography II

In the previous chapter we considered the distribution of temperature, salinity and density over the surface of the ocean. Here we consider the variation of these properties with depth. In particular, we will learn about the basic watermass composition of the ocean as a preparation for investigating its circulation and its impact on climate. We will also develop an empirically based concept of how ocean circulation distributes various special watermasses such as the famous North Atlantic Deep Water (NADW).

In addition to developing an understanding of the distribution of water properties, we will discuss the rammifications of density stratification. In particular, we will learn about internal gravity waves and how they propagate through the density structure of the ocean.

4.1 Stratification

Analysis of various vertical profiles of S and T in the ocean reveals the fact that density virtually always increases downward. This feature reflects the fact that the ocean is a fluid having variable density, and that gravitational potential energy is reduced when the fluid is arranged in a manner to have

density always increasing downward. This aspect of the density structure will be demonstrated through the analysis of hydrographic station data in the exercises associated with this chapter. The importance of stratification will be reinforced by considering its role in determining the gravitational potential energy stored within the water column and in determining the propagation of internal gravity waves. There is one other important aspect of oceanography that stems from stratification: it allows vertical gradients in horizontal geostrophic flows. We will postpone an analysis of this last point until we begin a formal discussion of geostrophic balance.

4.1.1 Available Potential Energy

Consider the water column shown in Fig. (4.1), the gravitational potential energy E per unit area of the ocean is defined as the following integral quantity:

$$E = \int_0^H \rho(z) g z dz \tag{4.1}$$

where H is the water depth and the vertical coordinate z is positive upward, with $z = 0$ the ocean bottom. If the density field has a linear variation with z (*e.g.,* a particularly simple density stratification),

$$\rho = \rho_o + \frac{d\rho}{dz} \cdot z \tag{4.2}$$

then E becomes

$$E = \frac{1}{2}\rho_o g H^2 + \frac{1}{3}\frac{d\rho}{dz} g H^3 \tag{4.3}$$

If $\frac{d\rho}{dz} < 0$, *i.e.,* the water column is stratified with the densest water at the bottom, then the total potential energy is reduced over what it would be if the density were uniform at ρ_o. If $\frac{d\rho}{dz} > 0$, *i.e.,* unstable stratification, then the total potential energy is *increased*.

The natural state of rest for the ocean requires that E be minimized. Thus, stable stratification is what we expect to observe in most circumstances. In the few opportunities oceanographers have had to observe neutral

or unstable stratification, vigorous currents are also observed. This reflects the fact that *convection* is not easily supressed in the ocean.

4.1.2 Buoyancy

Another important concept associated with density stratification is *buoyancy*, the force felt by objects or water-parcels immersed in the ocean. Buoyancy is the restoring force which drives convection when density gradients are unstable and which allows internal gravity waves to propagate. Before introducing buoyancy as a concept, I introduce the notion of a *hydrostatic pressure field*, *i.e.,* a pressure field which has a vertical gradient given by

$$\frac{dp}{dz} = -\rho g \tag{4.4}$$

Hydrostatic Pressure

Pressure is defined to be a force that is exerted by the material on one side of a surface of unit area to the material on the other side of the same surface. The magnitude of this force, by definition, does not depend on the orientation of the surface. The direction of this force is, by definition, always perpendicular to the plane of the surface, regardless of the surface orientation.

Air pressure inside the tires of an automobile, for example, exerts a force on the surface of the inside of the rubber tire which conterbalances the weight of the automobile. Likewise, water pressure at the bottom of the ocean exerts a force on the seafloor that counterbalances the net force of gravity acting on the water column above.

Hydrostatic pressure is the pressure that water possesses when it is at rest in a gravitational field. The magnitude of the pressure at any level z in the water column must counterbalance the weight of the water that lies above that level. Thus, a hydrostatic pressure field depends only on z (where z is the vertical coordinate). When the density field is constant,

$$p(z) = \rho g(z_s - z) \qquad \text{for } z < z_s \tag{4.5}$$

where ρ is a constant density (if it is a function of z, then we must broaden our definition of the hydrostatic pressure to define it using an integral), g is the acceleration of gravity at the earth's surface (9.81 m s^{-2}), and $(z_s - z)$ is the distance below the surface z_s of the ocean (which we take to be the origin of our vertical coordinate system). When the density field is variable, *i.e.*, $\rho = \rho(z)$, then

$$p(z) = \int_z^{z_s} \rho(z')g dz' \qquad \text{for } z < z_s \tag{4.6}$$

By taking the z-derivative for either of the above two definitions of hydrostatic pressure, we arrive at the important relation

$$\frac{dp}{dz} = -\rho g \tag{4.7}$$

Except when considering the propagation of sound waves in the ocean, the above relation represents a very good approximation to the vertical derivative of the actual pressure field in the ocean at any point. The predominance of hydrostatic pressure in the ocean is one of its basic characteristics. As we shall see, this predominance also allows us to simplify the very complicated description of force balance in the ocean when deriving notions of what drives ocean circulation.

Most large-scale motions in the ocean are not sufficiently strong to disturb or alter the basic hydrostatic pressure field (small-scale motions, such as sound waves, are not of interest at this juncture). Objects immersed in the ocean thus "feel" a vertical force which is equal to the difference between their weight and the weight of the water displaced by the object. This is the buoyancy force.

To see how the buoyancy force arises from a hydrostatic pressure field, I display the definition of the "skin force" F (the force a pressure field exerts on the skin of an object), and use a version of the divergence theorem to convert an integral over a surface to the volume integral over the contained volume

$$F = -\int\int p\mathbf{n}\, da \tag{4.8}$$

$$= -\int\int\int \nabla p \; dv \tag{4.9}$$

$$= \int\int\int \rho g \mathbf{n}_z \; dv \tag{4.10}$$

the last term on the right-hand side is nothing more than the net weight of the displaced water times a unit vector, $\mathbf{n}_z$, directed vertically. The above equations may also be interpreted as a statement of Archimedes' principle. The difference between the weight of an object and the force due to the water it displaces is defined to be the buoyancy.

4.2 A Bouncing Beachball

We may use the above concept of buoyancy to understand the motions of a beachball of unit radius filled with water of density ρ_o when it is is gently perturbed from its level of neutral buoyancy z_o where ρ_o is equal to the ambient density in a stratified water column. We define the density field to be a simple linear function of z:

$$\rho(z) = \rho_o + \gamma(z - z_o) \tag{4.11}$$

where z is positive upward and $\gamma = \frac{d\rho}{dz}$ is the density gradient (assumed constant for simplicity). We define $\Delta z = z - z_o$, so that

$$\rho(z) = \rho_o + \gamma \Delta z \tag{4.12}$$

Newton's law says that force equal mass times acceleration. Thus, if we wish to specify the accelerations of the beachball in the water column, we must sum the forces that act on the beachball. There are two forces which act on the beachball, the force of gravity and the force transmitted by pressure through the outer skin of the beachball. The force of gravity acting on the mass of water contained inside the beachball is found by integration:

$$F_g = \int_0^1 \int_{\frac{-\pi}{2}}^{\frac{\pi}{2}} \int_0^{2\pi} -\rho_o g \mathbf{n}_z r^2 \cos\phi d\lambda d\phi dr \tag{4.13}$$

where $\mathbf{n}_z$ is a unit vector that points upward along the vertical axis. This integral is easily evaluated to give

$$F_g = -\rho_o g \frac{4\pi}{3} \mathbf{n}_z \tag{4.14}$$

The force of pressure acting on the skin of the beachball F_p is a bit more difficult to calculate. The first step is to determine the pressure field at all points on the skin of the beachball. To do this, we make use of the hydrostatic relation. To avoid complication encountered later, we shall express the pressure at z as the sum of its value at the level z_o, P_o, with a correction term Δp accounting for the difference between the weight of water above level z and that above level z_o :

$$p(z) = P_o + \Delta p = P_o - \int_0^{\Delta z} (\rho_o + \gamma \Delta z) g d(\Delta z) \tag{4.15}$$

Integrating the above expression gives

$$p(z) = P_o - \rho_o g \Delta z - \gamma g \frac{1}{2} \Delta z^2 \tag{4.16}$$

If we define ζ to be the vertical displacement of the center of the beachball from z_o (ζ is positive for upward displacements), then $\Delta z = \zeta + \sin\phi$. The pressure at points (ϕ, λ) on the surface of the beachball, where ϕ and λ are the usual spherical coordinates, is thus

$$p(z_b, \phi) = P_o - \rho_o g(\zeta + \sin\phi) - \frac{1}{2}\gamma g(\zeta + \sin\phi)^2 \tag{4.17}$$

The origin of the $\sin\phi$ terms in the above expression is due to the use of trigonometry to determine the vertical displacement of a given patch of surface area at angle ϕ from the level of the center of the beachball.

To compute F_p we integrate $p(\zeta, \phi)$ over the surface of the beachball. The x-, y- and z-components of the vector F_p are determined, by definition of pressure, by the orientation of the unit normal $\mathbf{n}(\phi, \lambda)$. This orientation is determined as follows,

$$\mathbf{n} \cdot \mathbf{n}_x = -\cos\phi\cos\lambda \tag{4.18}$$

$$\mathbf{n} \cdot \mathbf{n}_y = -\cos\phi\sin\lambda \tag{4.19}$$

$$\mathbf{n} \cdot \mathbf{n}_z = -\sin\phi \tag{4.20}$$

The x-, y- and z-components of F_p are thus:

$$(F_p)_x = -\int_{\frac{-\pi}{2}}^{\frac{\pi}{2}} \int_0 2\pi p(\zeta, \phi) \cos^2 \phi \cos \lambda d\lambda d\phi \tag{4.21}$$

$$(F_p)_y = -\int_{\frac{-\pi}{2}}^{\frac{\pi}{2}} \int_0 2\pi p(\zeta, \phi) \cos^2 \phi \sin \lambda d\lambda d\phi \tag{4.22}$$

and

$$(F_p)_z = -\int_{\frac{-\pi}{2}}^{\frac{\pi}{2}} \int_0 2\pi p(\zeta, \phi) \sin \phi \cos \phi d\lambda d\phi \tag{4.23}$$

These integral expressions look daunting, but we can make immediate progress by noting that

$$\int_0^{2\pi} \sin \lambda d\lambda = \int_0^{2\pi} \cos \lambda d\lambda = 0 \tag{4.24}$$

Thus,

$$(F_p)_x = 0 \tag{4.25}$$

$$(F_p)_y = 0 \tag{4.26}$$

The vertical component of F_p is found by carefully integrating the many terms that arise in the expression for the pressure. To perform these integrations, we make use of the formulae:

$$\int_{\frac{-\pi}{2}}^{\frac{\pi}{2}} \sin^2 \phi \cos \phi d\phi = \int_{\frac{-\pi}{2}}^{\frac{\pi}{2}} \sin^2 \phi d(\sin \phi) = \frac{2}{3} \tag{4.27}$$

$$\int_{\frac{-\pi}{2}}^{\frac{\pi}{2}} \sin \phi \cos \phi d\phi = 0 \tag{4.28}$$

and

$$\int_{\frac{-\pi}{2}}^{\frac{\pi}{2}} \sin^3 \phi \cos \phi d\phi = 0 \tag{4.29}$$

With the above identities, only two terms in the complicated expression for $p(\zeta, \phi)$ contribute to a non-zero integral:

$$(F_p)_z = 2\pi \int_{\frac{-\pi}{2}}^{\frac{\pi}{2}} (\rho_o + \gamma\zeta) g \sin^2\phi \cos\phi d\phi \tag{4.30}$$

Using the integral formula given above, we obtain

$$(F_p)_z = \frac{4\pi}{3}(\rho_o g + \gamma\zeta) \tag{4.31}$$

or

$$F_p = \frac{4\pi}{3}(\rho_o g + \gamma\zeta)\mathbf{n}_z \tag{4.32}$$

Summing the two net forces acting on the beachball, gives the mass times the acceleration $\mathbf{a}$ of the beachball, according to Newton's law:

$$\frac{4\pi}{3}\rho_o \mathbf{a} = F_g + F_p = \frac{4\pi}{3}\gamma g \zeta \mathbf{n}_z \tag{4.33}$$

where we have made use of the formula for the volume of a sphere to obtain the mass of the beachball. By defining $\mathbf{a} = \ddot{\zeta}\mathbf{n}_z$, we obtain a second order differential equation for ζ:

$$\ddot{\zeta} = \frac{\gamma g}{\rho_o}\zeta \tag{4.34}$$

The solution to the above equation can be of two forms depending on the sign of $\gamma = \frac{d\rho}{dz}$:

$$\zeta(t) = A \sin \omega t \tag{4.35}$$

if $\gamma < 0$, *i.e.,* the water column is *stably* stratified, or

$$\zeta(t) = Ae^{\omega t} \tag{4.36}$$

if $\gamma > 0$, *i.e.,* the water column is *unstably* stratified. In the above expressions, A is an arbitrary constant (determined by initial conditions, which are unspecified here), and the buoyancy frequency ω is defined by

$$\omega = \sqrt{\frac{-\gamma g}{\rho_o}} \tag{4.37}$$

From the form of the above solutions, we see that the beachball will undergo buoyancy oscillations about it's position of rest (neutral stability) in the case of stable stratification, and will drift away exponentially with time in the case of unstable stratification. This behavior gives us insight into the notions of convection and internal wave propagation. In unstable waters, water parcels (whether they are covered by plastic beachball skin or not) will drift away; this suggests that massive, chaotic convection is possible. In stable waters, water parcels will bob up and down with a specific frequency of bobbing (that is independent of the amplitude of the motion).

The simple analysis presented above suggests that one effect of the ocean's stratification is to introduce a "restoring force" to vertical displacements of water parcels. We can exploit this concept to develop a notion of internal gravity wave mechanics.

4.2.1 Internal Gravity Waves

Let's investigate the hydrodynamic equations of motion to see if there are "wave-like" solutions. Since the object of the course is to introduce basic physical concepts associated with physical oceanography, I will not belabor the derivation of these hydrodynamic equations. Instead, I will simply use them (or simplified versions of them) and refer the interested student to the literature for their derivation.

Consider a situation where all particle motions are confined to the x, z-plane (*e.g.,* the earth's rotation is disregarded for the time being) as shown in Fig. (4.2). The principles of fluid dynamics which govern these motions are listed as follows: all motion is incompressible (a simplification which excludes sound waves in the ocean), the horizontal and vertical accelerations of water parcels are in balance with the gravitational force and the forces which arise because of pressure, and density variations are caused by displacements of the basic density layers (again, an approximation which simplifies the problem). The equations which represent these principles are

$$\nabla \cdot \mathbf{u} \quad = 0 \tag{4.38}$$

$$u_t = \frac{-1}{\rho} p_x \tag{4.39}$$

$$w_t = \frac{-1}{\rho} p_z - g \tag{4.40}$$

$$\rho_t = -\mathbf{u} \cdot \nabla \rho \tag{4.41}$$

where $\mathbf{u} = (\mathbf{u}, \mathbf{w})$ is the velocity field of the water, ρ is the density, p is the pressure, $g = 9.81$ m s^{-2} is the acceleration of gravity (at the earth surface), $\nabla = (\frac{\partial}{\partial x}, \frac{\partial}{\partial z})$ denotes the gradient operator, and $\nabla\cdot$ denotes the divergence operator, *i.e.,*

$$\nabla \mathbf{u} = \frac{\partial \mathbf{u}}{\partial \mathbf{x}} + \frac{\partial \mathbf{w}}{\partial \mathbf{z}} \tag{4.42}$$

These equations are too difficult to work with because they are *non-linear.* One way to make them linear, is to consider the density to be the sum of a basic stratified density profile, $\rho_o(z)$, and a minute perturbation, $\rho'(x, z, t) \ll \rho_o$. In this circumstance, we may write

$$\rho = \rho_o \cdot \left(1 + \frac{\rho'}{\rho_o}\right) \tag{4.43}$$

and

$$\frac{1}{\rho} \approx \frac{1}{\rho_o} \left(1 - \frac{\rho'}{\rho_o}\right) \tag{4.44}$$

We may also consider the pressure, p, to be composed of a hydrostatic pressure plus a small perturbation pressure that results from the motions we are interested in (*i.e.,* we assume small amplitude to the waves we seek to describe)

$$p = \Pi + p' \tag{4.45}$$

where

$$\Pi_z = -\rho_o g \tag{4.46}$$

$$\Pi_x = 0 \tag{4.47}$$

Using these new defninitions, we can rewrite Eqns. (4.38 - 4.41) in a manner which neglects non-linear terms, *e.g.,* we perform the following simplification

$$\tfrac{-1}{\rho} p_x = \frac{-1}{\rho_o} \left(1 - \frac{\rho'}{\rho_o}\right) (\Pi_x + p'_x) \tag{4.48}$$

$$\approx \frac{-1}{\rho_o} p'_x \tag{4.49}$$

The linearized equations are

$$\nabla \cdot \mathbf{u} = 0 \tag{4.50}$$

$$u_t = \frac{-1}{\rho_o} p'_x \tag{4.51}$$

$$w_t = \frac{-1}{\rho_o} p'_z - \frac{g\rho'}{\rho_o} \tag{4.52}$$

$$\rho'_t = -w(\rho_o)_z \tag{4.53}$$

The last term on the right-hand side of Eqn. (4.52) represents the buoyancy force introduced by stratification. Note that the hydrostatic pressure term has also been eliminated, along with the non-linear terms.

The question of how to analyze Eqns. (4.50 - 4.53) is somewhat difficult. Experience with this sort of wave-propagation problem suggests that the equations may be combined in such a manner as to eliminate all but one variable. When this is accomplished, wave-like solutions to the resulting equation can be attempted. If one is found, the other variables can then be determined by stepping backwards through the steps needed to eliminate the other variables. We proceed with this analysis as follows.

First, we take the time derivative of Eqn. (4.52) and use Eqn. (4.53) to eliminate reference to perturbation density. This gives:

$$\left(\partial_x^2 - \frac{g(\rho_o)_z}{\rho_o}\right) w = \frac{-1}{\rho_o} p'_{zt} \tag{4.54}$$

The x-derivative of the above equation is next combined with Eqn. (4.51) to yield the second result which eliminates pressure

$$\left(\partial_x^2 - \frac{g(\rho_o)_z}{\rho_o}\right) w_x = u_{ztt} \tag{4.55}$$

Taking another x-derivative, and using Eqn. (4.50) gives

$$\left(\partial_x^2 - \frac{g(\rho_o)_z}{\rho_o}\right) w_{xx} = -w_{ttzz} \tag{4.56}$$

which may be re-written as,

$$\nabla^2 w_{tt} + N^2 w_{xx} = 0 \tag{4.57}$$

A wave-like solution to Eqn. (4.57) can be formulated using a convention which presumes w to be a complex-valued function (the physical meaning is that we take the real part of the function as the actual vertical velocity)

$$w = Ae^{i(\omega t - kx - lz)} \tag{4.58}$$

where A is an undetermined amplitude (which we are not particularly interested in). This is a plane wave (lines of constant phase are parallel; if the lines were concentric spheres, the wave would be a spherical wave radiating from a point source) that propagates upward and to the left. (The way to see this is to ask what change to x and z must be made to "ride a crest" of the wave as time increases.) What interests us is whether or not the above equation will satisfy Eqn. (4.57). To make this check, we substitute the plane-wave solution into Eqn. (4.57), eliminate terms, and derive a *dispersion relation* that specifies the relation between the frequency of the wave, ω, and the wave numbers k and l. Recall that $\omega = \frac{2\pi}{T_p}$, where T_p is the period of oscillation (the time it takes successive crests to pass a particlar point); and, $\mathbf{k} = (\mathbf{k}, \mathbf{l})$ is the wave vector which determines the direction of propagation. The wave vector is related to the wavelength, λ, by $\|\mathbf{k}\| = \frac{\mathbf{2\pi}}{\lambda}$. The dispersion relation for internal waves is

$$\omega^2 = \frac{N^2 k^2}{k^2 + l^2} = N^2 \cos^2 \alpha \tag{4.59}$$

where we have noted the fact that

$$\frac{k^2}{k^2 + l^2} = cos^2 \alpha \tag{4.60}$$

where α is the direction the wave vector makes with the x-axis (*i.e.,* the angle of wave propagation with respect to the horizontal).

Observe that water-parcel displacements are all confined to be linear along lines that are $\perp$ to $\mathbf{k}$, *i.e.,* perpendicular to the direction of propagation. This can be shown by using the incompressiblility condition, Eqn. (4.50), to write u in terms of w, and then replacing w with the plane-wave solution

$$u = \frac{-l}{k} Ae^{i(\omega t - kx - lz)} \tag{4.61}$$

So,

$$\mathbf{u} = \left(\frac{-\mathbf{l}}{\mathbf{k}}, \mathbf{1}\right) \mathbf{A}\mathbf{e}^{\mathbf{i}(\omega \mathbf{t} - \mathbf{k}\mathbf{x} - \mathbf{l}\mathbf{z})} = \mathbf{A}(-\tan\alpha, \mathbf{1}) \tag{4.62}$$

It is thus readily demonstrated that,

$$\mathbf{u} \cdot \mathbf{k} = \frac{-\mathbf{l}}{\mathbf{k}}\mathbf{k} + \mathbf{l} = \mathbf{0} \tag{4.63}$$

which is proof that the water-parcel displacements are $\perp$ to the direction of propagation.

We can use this result to understand the dispersion relation. When $\alpha = 0$, *i.e.,* the wave propagates horizontally and the water-parcel motions are purely vertical, the dispersion relation gives $\omega = N$, which was the result derived in §(4.2). This corresponds to the circumstance when the highest frequency of oscillation is achieved ($0 < \cos^2 \alpha < 1$ for all non-zero α) because the motion is perpendicular to the lines of constant density. In this circumstance, the buoyancy force exerts its strongest influence on the water parcels. When $\alpha = \frac{\pi}{2}$, *i.e.,* vertical propagation, the parcel motions are horizontal, thus they feel no buoyancy effects. In this circumstance $\omega = 0$, *i.e.,* the waves have infinite period (they cease to propagate).

The phase and group velocity of the internal gravity wave, $\mathbf{c}$ and $\mathbf{c_g}$, respectively, are defined as follows:

$$\mathbf{c} = \frac{\omega}{\mathbf{k} \cdot \mathbf{k}}\ \mathbf{k} \tag{4.64}$$

$$\mathbf{c_g} = \nabla_{\mathbf{k}}\ \omega \tag{4.65}$$

$$= \left(\frac{\partial \omega}{\partial k}, \frac{\partial \omega}{\partial l} \right) \tag{4.66}$$

Note that

$$\|\mathbf{c}\| = \mathbf{N} \sin \alpha \tag{4.67}$$

and the direction of $\mathbf{c}$ is the same as $\mathbf{k}$. The direction of $\mathbf{c_g}$ can be evaluated by either a tedious differentiation as above or by considering a contour plot of ω in (k, l) space. As shown in Fig. (4.3), the contour plot shows that $\mathbf{c_g}$ is directed $\perp$ to $\mathbf{k}$; and is downward when $\mathbf{k}$ is upward, and upward when $\mathbf{k}$ is downward. Internal gravity waves are thus very strange. Energy is propagated at right angles to the direction that crests travel. Furthermore, as demonstrated by the dispersion relation, waves excited at a particular frequency (such as the semidiurnal tidal frequency) can only propagate in one of four possible directions, *i.e.,* they must maintain a constant α.

4.3 Temperature and Salinity Diagrams

One of the first things oceanographers do when they occupy a hydrographic station and determine the temperature and salinity profiles is plot the $(T(z), S(z))$ points on a graph which has S and T as the axes. Often, the graph paper will have contours of $\rho(S, T, 0$ or σ_t pre-printed on it so that the data can be checked for unstable stratification (usually taken to be a sign of error). The value of a (T, S) plot is that it allows one to see the fact that the various vertical layers of the water column have different "points of origin" at the ocean surface. This gives an appreciation for the fact that the ocean is a mobile, circulating mass of fluid.

The "classic" (T, S)-diagram to be used as an example comes from the Atlantic near the equator. The (T, S) plot shown in Fig. (4.4) shows an interesting S-shaped structure. This S-shaped structure represents the superposition of 4 watermasses: Surface Water (SW), Antarctic Intermediate Water (AIW), North Atlantic Deep Water (NADW), and Antarctic Bottom Water (ABW). The two polar Antarctic watermasses lie atop and below the polar Arctic watermass (NADW) because of the happenstance of their densities. It is important to point out that NADW may be the leading watermass in causing climate fluctuations over the great ice age.

4.3.1 Mixing

One of the utilities of the (T, S)-diagram is the fact that it allows us to appreciate and identify the mixing of two distinct watermass types in the ocean. When two watermasses of constant but distinct temperature and salinity mix, the result is an array of watermasses that lie on a straight line in the (T, S)-diagram. This can be shown by considering the conservation of mass, salt and heat during the mixing process:

Suppose two volumes V_1 and V_2 of two separate watermasses of properties (T_1, S_1) and (T_2, S_2), respectively, are mixed together to form a third watermass of volume V_3 with properties (T_3, S_3). Conservation of mass, salt and

heat (temperature) are described by the following equations:

$$V_3 = V_1 + V_2 \tag{4.68}$$
$$S_3V_3 = S_1V_1 + S_2V_2 \tag{4.69}$$
$$T_3V_3 = T_1V_1 + T_2V_2 \tag{4.70}$$

The last of the above equations may be modified as follows

$$T_3 = \frac{V_1}{V_3}T_1 + \frac{V_2}{V_3}T_2 \tag{4.71}$$

Making use of Eqn. (4.68), the above equation becomes

$$T_3 = \gamma T_1 + (1-\gamma)T_2 \tag{4.72}$$

where γ is a "mixture" parameter defined by

$$\gamma = \frac{V_1}{V_3} \tag{4.73}$$

The expression for S_3 is the same

$$S_3 = \gamma S_1 + (1-\gamma)S_2 \tag{4.74}$$

The point (T_3, S_3) must therefore lie on a line which connects (T_1, S_1) and (T_2, S_2). Mixing of watermasses is thus identified by groups of (T, S) measurements arrayed on a straight line.

4.4 Bulk Ocean Properties

The mean salinity and temperature of the world ocean (1320.5×10^6 km^3) are 34.57 $^\circ/_{\circ\circ}$ and 3.13 C, respectively. A census of the water masses of the world ocean reveals that approximately 50 % of all ocean water lies in the narrow range of temperature (-1.9 C to 3 C) and salinity (34.5 $^\circ/_{\circ\circ}$ - 35.0 $^\circ/_{\circ\circ}$) that is seen at the surface of the ocean only in the polar regions. This spectacular domination of the world ocean by cold polar waters is direct evidence of the thermohaline circulation of the ocean: a gentle meridional overturning that accompanys sinking polar waters and upwelling equatorial waters.

One of the curious features of the world ocean is that the distribution function of water mass properties is Y-shaped (see Fig. (4.5)). This reflects the fact that NADW is very much more salty than the rest of the polar waters. We will see in a later chapter that the circulation of NADW is intimately tied to the salt budget of the North Atlantic, and it's interuption at times when fresh water is dumped into the North Atlantic brings on very cold, glacial climates.

4.5 Exercises

In the following exercises, you will manipulate SPYGLASS® data files provided by the instructor. These data represent the annual average properties of the ocean as a whole, and are derived from averages of many thousands of individual measurements [Levitus, 19]. All data files have the same 1-degree by 1-degree resolution in the horizontal. There are 33 vertical levels in the data corresponding to the surface, -10M -20M -30M -50M -75M -100M -125M -150M -200M -250M -300M -400M -500M -600M -700M -800M -900M -1000M -1100M -1200M -1300M -1400M -1500M -1750M -2000M -2500M, and -3000M. Unfortunately, at the present time, this assignment is not completely formlated, thus the students will be given only a few *token* problems to work on. The variable vertical resolution of the data will not be treated accurately.

1. Open the global ocean salinity data (the file S.HDF) in SPYGLASS® DICER®. Create and print separate slices in the data sets to display the following hydrographic cross sections (and slices): (1) up the middle of the Atlantic, (2) across the equatorial Pacific, (3) a horizontal slice at mid-depths in the ocean to display the Mediteranian outflow. Create a caption that enumerates and identifies the features you notice in the data set.

2. Create similar cross sections (and slices) for the temperature field found in the file T.HDF.

3. In SPYGLASS® TRANSFORM® create a Lambert equal area map of the Northern Hemisphere region where water having the average temper-

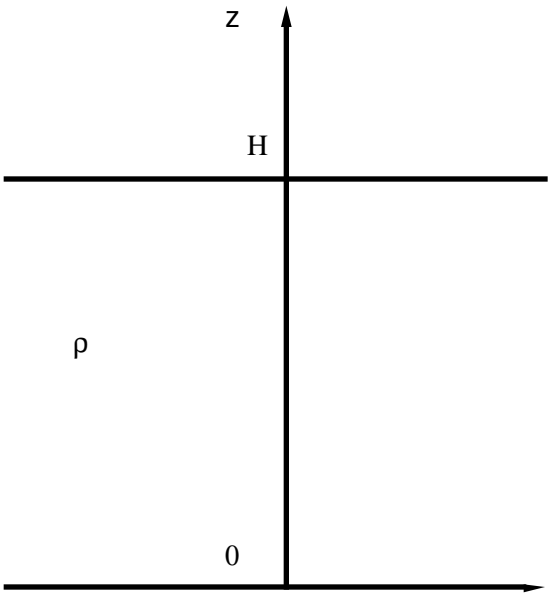

Figure 4.1: Water-column geometry.

ature and density of the world ocean outcrops at the earth's surface. Estimate the fraction of total ocean area this outcrop represents.

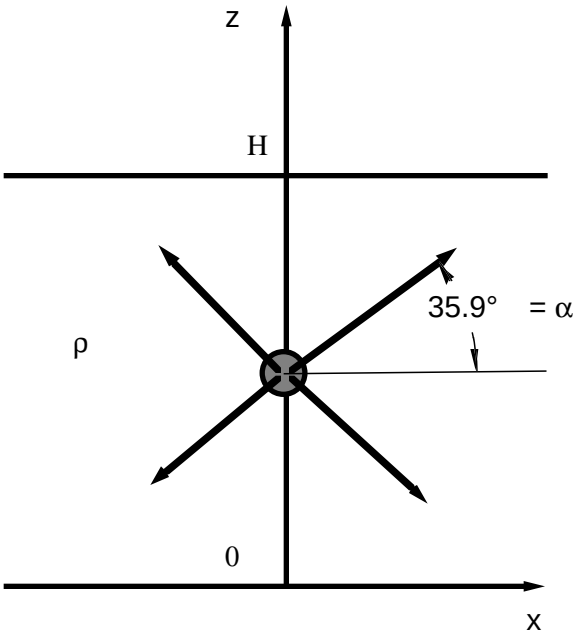

Figure 4.2: Water-column geometry for internal wave propagation.

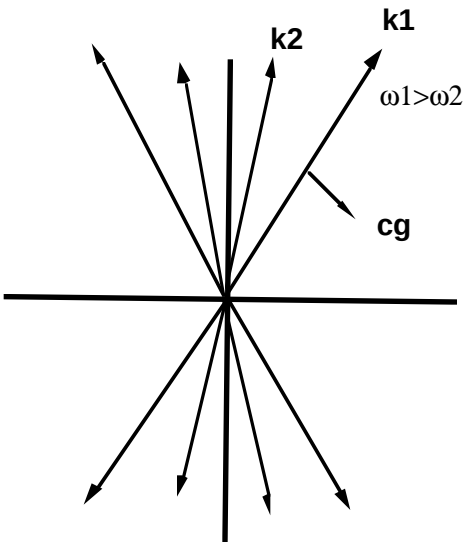

Figure 4.3: Graphical determination of group velocity.

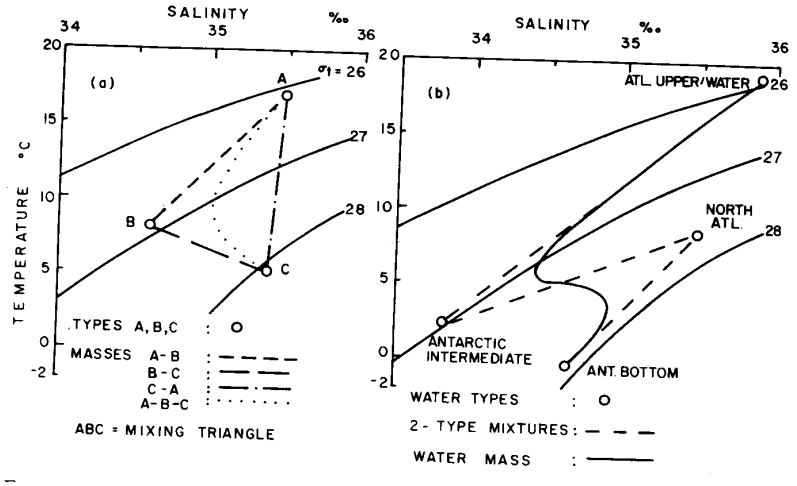

Figure 4.4: Schematic temperature vs. salinity plot.

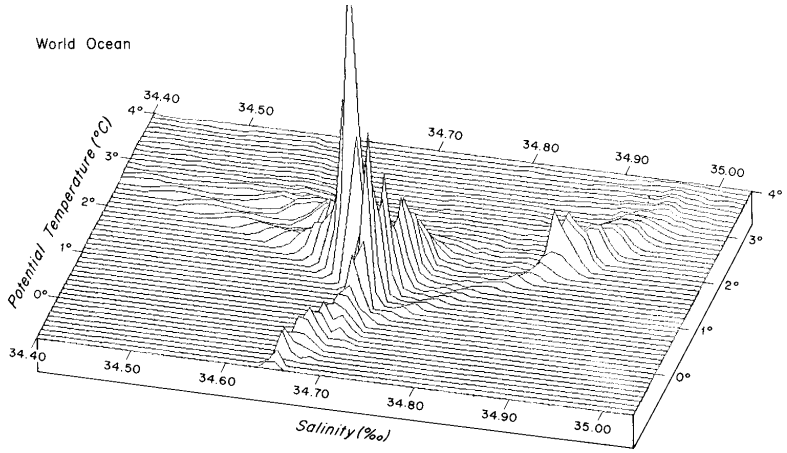

Figure 4.5: World water masses.

Chapter 5

Bogus Forces

We have seen that the ocean exibits great spatial variation that can only be attributed to the effects of circulation. In this chapter, we begin the arduous, but productive, task of describing the physical equations which govern ocean circulation. One of the things that makes this task difficult is the need to describe "bogus" forces which in a reference frame which rotates with the earth (*i.e.,* the centrifugal and Coriolis forces).

To an observer in the rotating reference frame, two bogus forces are needed to describe motion. One force is called the *centrifugal force*. This is the force that deflects plumb bobs and causes the earth's surface to bulge more at the equator than at the poles. The second force is called the *Coriolis force* (after the great teacher Gaspard Gustave de Coriolis, 1792-1843, see Fig. (5.1)). This is the force which causes the Foucault pendulum to precess once a day and which plays against the pressure gradient force in establishing the all-important geostrophic balance in ocean circulation.

It was not easy to discover the Coriolis force. It was first noted by Laplace in 1790 in the context of describing the oceanic tides. Coriolis derived the formal mathematical description of the force which bears his name in 1836, but didn't apply the description to any notable atmospheric or oceanic problem. Foucault used the Coriolis force to explain the pendulum in 1895. In 1911, Arther Holly Compton (former chairman of the Department of Physics

GASPARD GUSTAVE de CORIOLIS
1792–1843

Figure 5.1:

at the University of Chicago and Nobel Prize winner) wrote his first student paper on the subject of the Coriolis force. [1] In the 1950's the Coriolis force was finally "tamed" and put to rest in the form of a *quasigeostrophic theory* of the atmosphere by Joule Charney and Arnt Eliassen.

There are many ways to approach the derivation of the Coriolis force. We will adopt an exceedingly simple, and perhaps un-elegant, approach here. The goal is to develop a familiarity with why the Coriolis force arise. Once this familiarity has been developed, we will move on to the next chapter where we will use the Coriolis force to understand ocean circulation. In particular, we will examine its role in two fundamental styles of flow: the Eckman boundary layer (where friction acts on ocean circulation) and the geostrophic balance (how pressure gradients are maintained by ocean circulation).

[1] Compton's paper contained a famous factor of two error. This goes to show how difficult the material is!

5.1 The Rotating Plane

Consider two reference frames which describe points on a plane (Fig. 5.2). The (x, y) plane describes the coordinate system for an observer which rotates about the z axis at a rotation rate of $\Omega = \frac{2\pi}{T_d}$, where T_d is the length of day. The (ζ, η) plane describes the inertial coordinate system within which Newton's laws are described. Suppose that at an instant in time, a vector $\mathbf{B}$ described by the rotating observer has the same coordinates in the (x, y) system as it does in the (ζ, η) coordinate system. In this circumstance,

$$\left(\frac{d\mathbf{B}}{dt}\right)_f = \frac{d}{dt}\left(B_\zeta \hat{e}_\zeta + B_\eta \hat{e}_\eta\right) \tag{5.1}$$

where $\hat{e}_\zeta$ and $\hat{e}_\eta$ are unit vectors pointing along the ζ and η axes of the inertial coordinate system, B_ζ and B_η are the components of $\mathbf{B}$ in the inertial reference frame, and the subscript f on the time derivative on the left-hand side of the above equation denotes the time-rate-of-change of $\mathbf{B}$ in the inertial (or "fixed") coordinate system. The vector is also observed in the rotating reference frame, and it's coordinates are B_x and B_y. We can thus rewrite the above equation as follows:

$$\begin{aligned}
\left(\tfrac{d\mathbf{B}}{dt}\right)_f &= \frac{d}{dt}\left(B_x \hat{n}_x + B_y \hat{n}_y\right) && (5.2)\\
&= \left(\frac{dB_x}{dt}\right)_r \hat{n}_x + B_x \left(\frac{d\hat{n}_x}{dt}\right)_f + \left(\frac{dB_y}{dt}\right)_r \hat{n}_y + B_y \left(\frac{d\hat{n}_y}{dt}\right)_f && (5.3)\\
&= \left(\frac{d\mathbf{B}}{dt}\right)_r + B_x \Omega \hat{n}_y - B_y \Omega \hat{n}_x && (5.4)\\
&= \left(\frac{d\mathbf{B}}{dt}\right)_r + \boldsymbol{\Omega} \times \mathbf{B} && (5.5)
\end{aligned}$$

where $\hat{n}_x$ and $\hat{n}_y$ are the unit vectors pointing along the x and y axes of the rotating coordinate system. In deriving the above expressions, we have made use of the fact that the two coordinate systems align instantaneously at the time at which the vector $\mathbf{B}$ is described, and

$$\begin{aligned}
\left(\tfrac{d\hat{n}_x}{dt}\right)_f &= |\hat{n}_x| \Omega \hat{e}_\eta = 1 \cdot \Omega \hat{n}_y && (5.6)\\
\left(\tfrac{d\hat{n}_y}{dt}\right)_f &= -|\hat{n}_y| \Omega \hat{e}_\zeta = -1 \cdot \Omega \hat{n}_x && (5.7)
\end{aligned}$$

and,

$$\mathbf{\Omega} \times \mathbf{B} = \begin{vmatrix} \hat{n}_x & \hat{n}_y & \hat{n}_z \\ 0 & 0 & \Omega \\ B_x & B_y & 0 \end{vmatrix} = -\hat{n}_x \Omega B_y + \hat{n}_y \Omega B_x \tag{5.8}$$

where $\mathbf{\Omega}$ is the rotation vector which aligns with the z axis (perpendicular to the plane in which all vectors we are interested in reside). Eqn. (5.5) can be used to describe the time-rate-of-change of a position vector, *i.e.,* the velocity $\mathbf{u_f}$ of a point mass moving through an inertial reference frame

$$\mathbf{u_f} = \mathbf{u_r} + \mathbf{\Omega} \times \mathbf{B} \tag{5.9}$$

where $\mathbf{u_r}$ is the velocity of the same particle measured by the rotating observer, and $\mathbf{B}$ is taken to be the instantaneous position vector of the point mass. The same proceedure used to derive the relation between the velocity in the inertial and rotating reference frames can be used to derive the acceleration $\mathbf{a}$ of the point particle

$$\mathbf{a} = \left(\frac{d}{dt}(\mathbf{u_r} + \mathbf{\Omega} \times \mathbf{B}) \right)_r + \mathbf{\Omega} \times [\mathbf{u_r} + \mathbf{\Omega} \times \mathbf{B}] \tag{5.10}$$

$$= \left(\frac{d\mathbf{u}_r}{dt} \right)_r + 2\mathbf{\Omega} \times \mathbf{u}_r + \mathbf{\Omega} \times \mathbf{\Omega} \times \mathbf{B} \tag{5.11}$$

We can use Eqn. (5.11) to express Newton's law as seen by an observer in a rotating reference frame:

$$\frac{\mathbf{F}}{M} = \dot{\mathbf{u}}_r + 2\mathbf{\Omega} \times \mathbf{u}_r + \mathbf{\Omega} \times \mathbf{\Omega} \times \mathbf{B} \tag{5.12}$$

where $\mathbf{F}$ is the force that acts on the particle and M is the mass of the particle. The last two terms on the right-hand side of Eqn. (5.12) are "bogus" forces. The first is the Coriolis force and the second is the centrifugal force. Observe that the Coriolis force always acts at right angles to the velocity vector, and its magnitude scales with the velocity magnitude. If the rotation of the plane is counter-clockwise when viewed in the inertial reference frame (as in the Northern Hemisphere), particles with a velocity $\mathbf{u}_r$ will appear to be deflected to the right.

In component notation, where $\mathbf{u}_r = (u, v)$, Eqn. (5.12) may be written

$$\dot{u} = 2\Omega v - \Omega^2 B_x + \frac{F_x}{M} \tag{5.13}$$

$$\tag{5.14}$$

$$\dot{v} = -2\Omega u - \Omega^2 B_y + \frac{F_y}{M} \tag{5.15}$$

Observe that the centrifugal force depends only on position relative to the origin of the rotating plane. This feature allows experimentalists to build slightly parabolic "platforms" on the rotating plane which will counterbalance the centrifugal force.

A Rotating Skating Rink

Consider a "skating rink" platform built on the rotating plane with a non-uniform floor elevation $Z(x, y)$. (Let's see the next Winter Olympics conduct figure skating and ice hockey competitions on a rotating ice rink!) The gravitational pull on a skater in the rink is assumed to point along the $-z$ axis, which, if Z is non-uniform, means that the skater feels a component of gravitational force that tends to cause their (x, y) position to change. The slope of the rink can be designed to counter balance the centrifugal force if

$$-g\nabla Z = (-\Omega^2 x, -\Omega^2 y) \tag{5.16}$$

The above differential equation suggests that a skating rink with a floor constructed so that

$$Z(x, y) = \frac{\Omega^2}{2g}(x^2 + y^2) \tag{5.17}$$

will negate the effects of the centrifugal force. The above equation indicates that the skating rink must have a parabolic shape to "shield" skaters from the centrifugal force.

5.1.1 Assignment - Inertial oscillations

1. Determine the path of a skater with initial velocity $\mathbf{u}_r = (U, 0)$. Assume that the skating rink is constructed to eliminate the effects of the

centrifugal acceleration and that the ice is frictionless (ask a glaciologist if that is true!). Discuss the relationship between the time taken to complete the orbital motion of the skater and the length of day ($2\pi/\Omega$). Why is there a discrepancy?

2. Determine the elevation Z of the skating rink at a distance from the origin that is equal to the radius of the earth. How does this compare with the equatorial bulge of the earth?

5.2 Foucault Pendulum

We next describe the famous Foucault pendulum experiment. This experiment was conducted by Foucault in 1895 as a demonstration of the Coriolis force and of the effects of the earth's rotation on motions in an inertial reference frame. Consider the diagram in Fig. (5.3) which shows the Foucault pendulum at a time when its swing is confined to the (x, z) plane. The net force acting on the pendulum, $\mathbf{F}$, is equal to the sum of the components of gravity, the components of string tension, and the centrifugal forces. Designating θ as the deflection angle of the string,

$$\mathbf{F} = (M\Omega^2 x - Mg\sin\theta\cos\theta)\hat{n}_x + (-Mg + Mg\cos^2\theta)\hat{n}_z \tag{5.18}$$

where x is the x-coordinate of the mass M on the end of the pendulum string.

For small amplitude oscillations,

$$\theta \approx \tan\theta = \frac{x}{L} \tag{5.19}$$

$$\sin\theta \approx \theta \tag{5.20}$$

$$\cos\theta \approx 1 \tag{5.21}$$

where L is the length of the pendulum string. In this circumstance,

$$F_x = M\ddot{x} = -\left(\frac{Mg}{L} - M\Omega^2\right)x = -\frac{Mg'}{L}x \tag{5.22}$$

where $g' = g - \Omega^2 L$ is designated as the effective gravitational acceleration which accounts for the component of centrifugal force which acts to modify

the swing of the pendulum. (Observe that, as $\Omega \to \infty$, $g' \to 0$ and the pendulum stops swinging.) An equation for $\ddot{y}$ is determined following the same procedure as for determining the equation for $\ddot{x}$. The complete description of the pendulum's motion is thus obtained

$$\ddot{x} = 2\Omega\dot{y} - \frac{g'x}{L} \tag{5.23}$$

$$\ddot{y} = -2\Omega\dot{x} - \frac{g'y}{L} \tag{5.24}$$

Observe that a rather subtle trick has been applied in the derivation of the above equations. The force analysis leading to the determination of F_x was done at the specific time when $\dot{y} = 0$, *i.e.,* the pendulum was confined to swing along the x axis. In this circumstance, the pendulum's restoring force, and the effect of the centrifugal force, were derived without need to consider the Coriolis force. The above equations are derived by simply adding in the Coriolis force, in the case of the expression for $\ddot{x}$, or by analogy with the x eqation, in the case of the expression for $\ddot{y}$.

A solution of the above equations is

$$x = A\cos\left(\sqrt{\frac{g'}{L}}t\right)\sin\Omega t \tag{5.25}$$

$$y = A\cos\left(\sqrt{\frac{g'}{L}}t\right)\cos\Omega t \tag{5.26}$$

The motion of the Foucault pendulum given by Eqns. (5.25) - (5.26) is thus very peculiar. Two oscillations are superimposed. One oscillation has a very high frequency, $\sqrt{\frac{g'}{L}}$, and has a period lasting only a few seconds (depending on the length of the string). The other oscillation has a very low frequency, Ω, and has a period equal to the length of time taken for the the reference frame to rotate (a day). The Foucault pendulum thus describes an oscillatory back-and-forth motion that slowly rotates in direction once a rotation period.

5.2.1 Assignment - Foucault pendulum

1. Demonstrate that the expressions given above in Eqns. (5.25) - (5.26)

satisfy the equations of motion in a rotating reference frame.

5.3 Description of Motion at the Earth's Surface

The bogus forces derived above for the description of motion on a rotating plane are now generalized to describe motion on the surface of the earth. Consider the coordinate system shown in Fig. (5.4). The time derivatives of unit vectors which describe an (x, y, z) coordinate system fixed at the earth's surface (where x is the East coordinate, y is the North coordinate and z is the Vertical coordinate) are readily determined from the geometry of of the sphere and the circles or cones swept out by the individual vectors during one day.

$$\left(\frac{d\hat{n}_x}{dt}\right)_f = \Omega \sin\phi \hat{n}_y - \Omega \cos\phi \hat{n}_z \tag{5.27}$$

$$\left(\frac{d\hat{n}_y}{dt}\right)_f = -\Omega \sin\phi \hat{n}_x \tag{5.28}$$

$$\tag{5.29}$$

$$\left(\frac{d\hat{n}_z}{dt}\right)_f = \Omega \cos\phi \hat{n}_x \tag{5.30}$$

where subscript f denotes the fact that the time derivative is taken in the inertial frame, as before, and ϕ is the latitude. Following the conventions of the previous section, we immediately deduce the relation between the velocity $\mathbf{u}_r = (u_r, v_r, w_r)$ in the rotating frame and that in the inertial frame $\mathbf{u}_f$

$$\left(\frac{dx}{dt}\right)_f = u_r - y\Omega \sin\phi + z\Omega \cos\phi + R_e\Omega \cos\phi \tag{5.31}$$

$$\left(\frac{dy}{dt}\right)_f = v_r + x\Omega \sin\phi \tag{5.32}$$

$$\left(\frac{dz}{dt}\right)_f = w_r - x\Omega \cos\phi \tag{5.33}$$

where $R_e \approx 6280$ km is the radius of the earth. The last term in Eqn. (5.31) represents the "extra" velocity due to the fact that the origin of the rotating reference frame is itself orbiting around the rotation axis of the earth. (This

extra velocity does not affect the expressions which describe the time rate of change of the unit vectors.)

The acceleration in the inertial reference frame is determined by subjecting the above equations to another time differentiation. The result is

$$\left(\frac{d^2x}{dt^2}\right)_f = \dot{u}_r - 2\Omega \sin\phi v_r + 2\Omega \cos\phi w_r - \Omega^2 x \tag{5.34}$$

$$\left(\frac{d^2y}{dt^2}\right)_f = \dot{v}_r + 2\Omega \sin\phi u_r + R\Omega^2 \sin\phi \tag{5.35}$$

$$\left(\frac{d^2z}{dt^2}\right)_f = \dot{w}_r - 2\Omega \cos\phi u_r - R\Omega^2 \sin\phi \tag{5.36}$$

where

$$R = R_e \cos\phi - y \sin\phi + z \cos\phi \tag{5.37}$$

represents the net distance between the point (x, y, z) and the earth's rotational axis.

As with the rotating plane, two Bogus forces arise. The Coriolis force is seen to vary in strength with the latitude ϕ. The quantity

$$f = 2\Omega \sin\phi \tag{5.38}$$

is referred to as the Coriolis parameter. It represents the component of the *planetary vorticity* (something that you will learn about in graduate-level courses) that is perpendicular to the tangent plane of the earth's surface at any given location.

5.3.1 Assignment – Rotating earth coordinates.

1. Describe the motion of the Foucault pendulums that are located in the following positions: Quito, Havana, Chicago and Thule (Greenland). Why do the pendulums differ in their motions?

2. Determine the "figure" of the earth required to eliminate forces in the tangent plane of the surface of the earth that would otherwise act on stationary objects. (*i.e.,* Determine the equatorial bulge that is required to counterbalance the centrifugal force due to the rotation of the earth.) Hint: first determine the angle of deflection of a plumb bob as a function of latitude.

3. Determine the deflection of an object that is allowed to fall from the leaning Tower of Pisa (about 50 m tall) due to the earth's rotation. Does the object's mass have anything to do with the deflection? Assume the earth to be spherical.

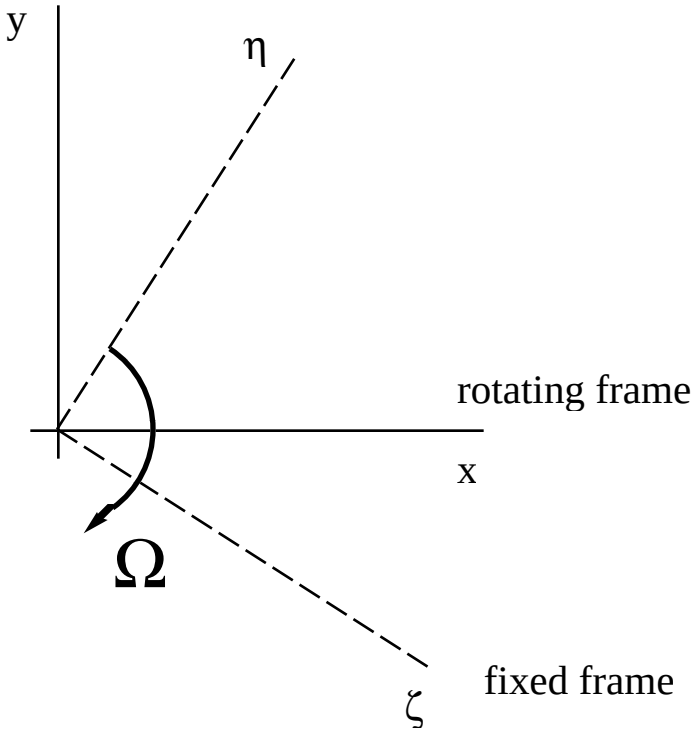

Figure 5.2: Rotating and fixed reference frame for the f-plane.

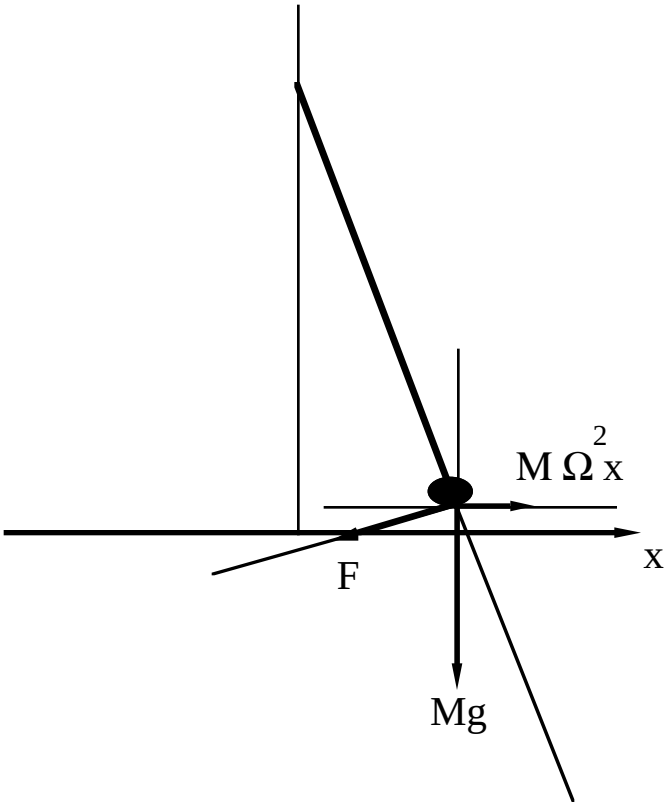

Figure 5.3: Force balance of a Foucault pendulum on an f-plane.

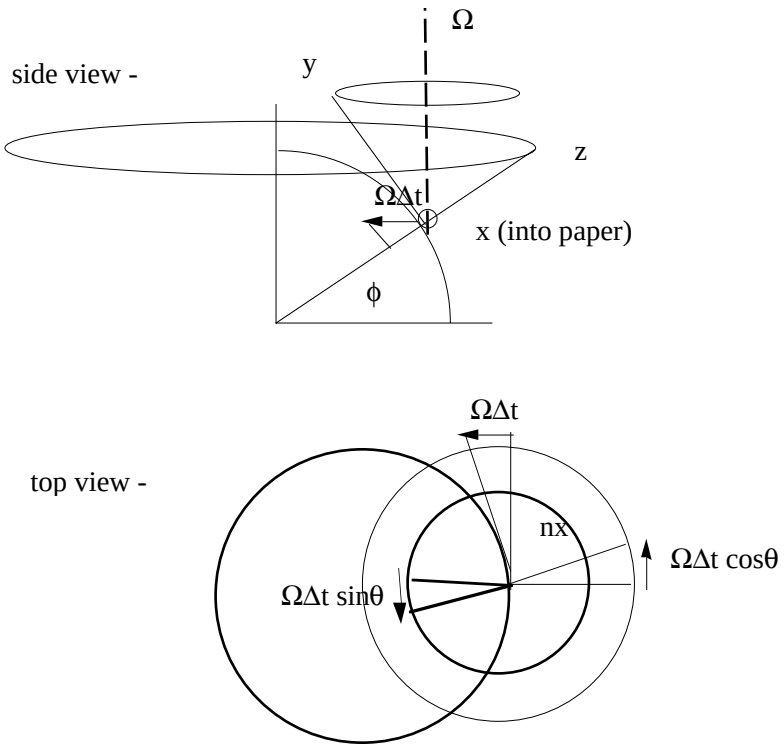

Figure 5.4: Rotation of unit vectors which describe a reference frame fixed to the surface of the earth.

Chapter 6

Geostrophy

The purpose of this chapter is to further-define the notion of the geostrophic balance between pressure gradient forces and Coriolis forces. In the accompanying laboratory exercises, we apply the geostrophic balance towards developing an understanding of the mean (time average) circulation of the ocean.

6.1 Equations Governing Horizontal Motion

To derive the equations which govern horizontal flow in the ocean (viewed as an inviscid, frictionless fluid), we consider the small cube of seawater depicted in Figure (6.1). Newton's law says that the net acceleration of this small cube is equal to the mass times the sum of forces which act on it. The acceleration in the x-direction is $\frac{\partial u}{\partial t}$. The mass of the cube is $\rho \Delta x \Delta y \Delta z$, where Δx, etc., are the length of the sides of the cube.

There are two forces that have components in the x-direction: the pressure-gradient force and the Coriolis force. The pressure-gradient force acting in the x-direction is equal to the net difference between the pressures acting on the two faces that are perpendicular to the x-axis. The magnitude of the pressure force on each side is equal to the average pressure on the side times

the area of the side. The direction of the pressure force on one side is opposite the direction of the pressure force on the other. With these considerations, the pressure-gradient force is

$$\left(p(x, y+\frac{\Delta y}{2}, z+\frac{\Delta z}{2}) - p(x+\Delta x, y+\frac{\Delta y}{2}, z+\frac{\Delta z}{2})\right)\Delta y \Delta z \qquad (6.1)$$

The Coriolis force is equal to the Coriolis acceleration in the x-direction times the mass of the fluid contained within the cube. The Coriolis acceleration in the x-direction is just $f = 2\Omega \sin\phi$ (the Coriolis parameter for latitude ϕ) times v, the horizontal velocity of the fluid in the cube in the y-direction. Thus, the Coriolis force in the x-direction may be written

$$fv\rho\Delta x\Delta y\Delta z \qquad (6.2)$$

Newton's law may now be written as follows:

$$\begin{aligned}\rho\Delta x\Delta y\Delta z\frac{\partial u}{\partial t} &= \left(p(x, y+\frac{\Delta y}{2}, z+\frac{\Delta z}{2}) - p(x+\Delta x, y+\frac{\Delta y}{2}, z+\frac{\Delta z}{2})\right)\Delta y\Delta z \\ &\quad + fv\rho\Delta x\Delta y\Delta z \end{aligned} \qquad (6.3)$$

If we divide both sides of the above equation by $\rho\Delta x\Delta y\Delta z$, and switch the order of terms appearing in the pressure-gradient force, we obtain:

$$\frac{\partial u}{\partial t} = \frac{-1}{\rho}\frac{p(x+\Delta x, y+\frac{\Delta y}{2}, z+\frac{\Delta z}{2}) - p(x, y+\frac{\Delta y}{2}, z+\frac{\Delta z}{2})}{\Delta x} + fv \qquad (6.4)$$

We realize that the expression for the pressure-gradient force gives the x-derivative of the pressure in the limit that $\Delta x \to 0$; thus,

$$\frac{\partial u}{\partial t} = \frac{-1}{\rho}\frac{\partial p}{\partial x} + fv \qquad (6.5)$$

The equation for the balance of forces in the y-direction follows from the same considerations and is written

$$\frac{\partial v}{\partial t} = \frac{-1}{\rho}\frac{\partial p}{\partial y} - fu \qquad (6.6)$$

Notice the sign change that appears before the Coriolis term.

6.2 The Geostrophic Balance

In simple terms, the geostrophic balance is described as follows:

$$v_g = \frac{1}{\rho f}\frac{\partial p}{\partial x} \tag{6.7}$$

$$u_g = -\frac{1}{\rho f}\frac{\partial p}{\partial y} \tag{6.8}$$

in Cartesian coordinates, and

$$v_g = \frac{1}{\rho f R\cos\phi}\frac{\partial p}{\partial \lambda} \tag{6.9}$$

$$u_g = -\frac{1}{\rho f R}\frac{\partial p}{\partial \phi} \tag{6.10}$$

in spherical coordinates (where v_g is the meridional component of the geostrophic velocity and u_g is the zonal component of the geostrophic velocity).

6.2.1 "Thermal-wind" relationship

A corollary associated with the geostrophic balance is called the *thermal-wind* relationship, and is derived by taking the z-derivative of Eqns. (6.7) and (6.8) and then using the hydrostatic balance, $p_z = -\rho g$:

$$\frac{\partial v_g}{\partial z} \approx \frac{-g}{\rho f}\frac{\partial \rho}{\partial x} \tag{6.11}$$

$$\frac{\partial u_g}{\partial z} \approx \frac{g}{\rho f}\frac{\partial \rho}{\partial y} \tag{6.12}$$

where terms $\frac{\rho_z}{f\rho^2}\frac{\partial p}{\partial x}$ and $\frac{\rho_z}{f\rho^2}\frac{\partial p}{\partial y}$ have been neglected because they are much smaller in magnitude than the other terms appearing in Eqns. (6.11) and (6.12).

The import of the thermal-wind equations is that they tell us that vertical gradients in the geostrophic velocity can be expected when there are

horizontal gradients in the density structure of the ocean. In the absence of horizontal density gradients, the geostrophic flow is independent of z. This z-independence is sometimes referred to as the Taylor-Proudman theorem.

6.3 Dynamic Topography

Perhaps the most important opportunity available to oceanographers is the ability to use the geostrophic balance to compute the *relative* geostrophic flow using temperature and salinity measurements distributed throughout the ocean. The word *relative* is important in describing the computation of geostrophic flow because of the fact that there is an underdetermined quality to the computation: oceanographers, so far, have been unable to measure the geostrophic component of the free-surface elevation of the ocean. The relative geostrophic currents computed using just the temperature and salinity structure of the ocean (i.e., the density structure) are thus the currents at depth z relative to the currents at the surface $z = 0$.

Often, oceanographers like to think in terms of an arbitrary "level of no motion", $z = z_{NM}$, that exists deep below the surface, and which defines a dynamic topography η_g that counter-balances the pressure gradients at $z = z_{NM}$ caused by internal density structure. With this concept in mind, the pressure field at an arbitrary depth z is approximated by integrating the hydrostatic balance from the "undisturbed" free-surface of the ocean ($z = 0$) and applying a correction due to the dynamic topography of the ocean

$$p(z) = \int_z^0 \rho(z')g dz' + \rho_o g \eta_g \tag{6.13}$$

where η_g is determined by the requirement that

$$\rho_o g \eta_g = -\int_{z_{NM}}^0 \rho(z')g dz' + \bar{p}^{x,y} \tag{6.14}$$

where $\bar{p}^{x,y}$ is the area-average pressure on the level of no motion. The definition of η_g allows us to insist that the pressure on the level of no motion is uniform at the average value. In this circumstance, there will be no horizontal pressure gradients at the level of no motion.

6.4 Assignment

On *Jeeves* you will find two cross sections of the ocean in a MATLAB®-native file called *Chap8:geostrophy*. The zonal cross section of temperature and salinity, Tz and Sz, represents conditions at 35N, and is designed to show the North Atlantic and North Pacific gyres. The meridional cross section of temperature and salinity, Tm and Sm, represents conditions at 60W, and is designed to show the North Atlantic gyre and the Antarctic circumpolar current near the Drake Passage. The depths of each of the 33-levels in the two cross sections are contained in the vector z.

1. Determine the density field in each cross section. Export the density field to SPYGLASS® (*i.e.,* use the `save filename densityzonal` command to create a file containing the density field, then open it with SPYGLASS® using the MATLAB® check box in the data open menu) and produce a contour map of σ_t (recall $\sigma_t = \rho - 1000$). For simplicity, evaluate the density at all levels in the ocean using $p = 0$ (sea-surface pressure) in the density function $\rho(T, S, p)$.

2. Draw a sketch map of the geostrophic currents you expect from the two density cross sections produced above. Assume that the sea-surface elevation is perfectly flat.

3. Compute the geostrophic currents associated with the density structures in the two cross sections. Again, assume that the sea-surface elevation is flat.

4. Select a level of no motion (your guess is as good as mine, but I used 1000 m when I did this lab) and determine a free-surface elevation η that will provide the pressure gradients necessary to ensure that the geostrophic flow at the level of no motion is indeed zero (*i.e.,* compute the dynamic topography). Plot the two cross sections of η using the MATLAB® plotting routine.

5. Compute the geostrophic currents implied by the combination of the density structure and the above-computed dynamic topography. Export your results to SPYGLASS® and image or contour the results.

6. Discuss the circulation structure you produce above in terms of the North Atlantic gyre (*e.g.,* do you see evidence for a gyre?) and the Antarctic circumpolar current.

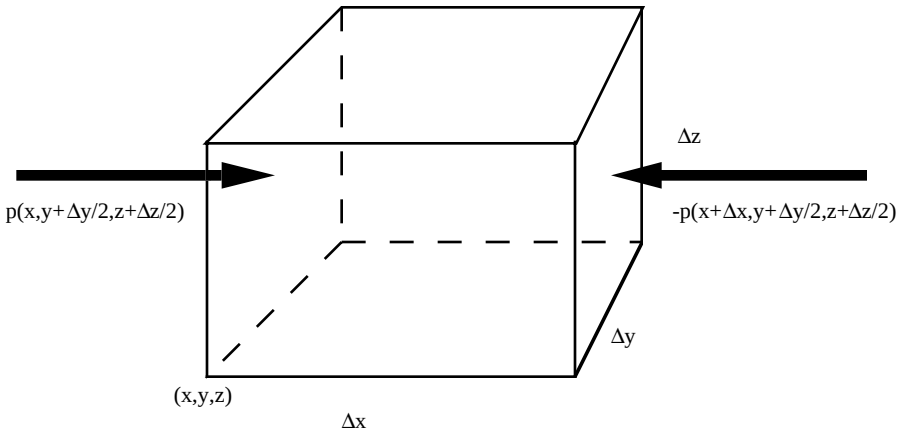

Figure 6.1: Fluid element used to describe balance of forces in the horizontal.

Chapter 7

Ekman Pump

The purpose of this chapter is to begin the task of understanding the pattern of geostrophic currents in the ocean. Here we investigate the effect of atmospheric winds on the ocean surface. We will find that wind stress affects only a very "thin skin" of the upper ocean. This skin is called the surface Ekman layer, and is named after the Norwegian oceanographer V. Walfrid Ekman who first explained the unusual effects of wind on the ocean as a result of analyzing the ship-drift data generated by Frijtoft Nansen's *Fram* expedition (1893-1896). The effects Ekman discovered are important because they determine the wind-driven component of the ocean circulation and the important phenomena called coastal upwelling.

7.1 Ekman Layer: Conceptual View

Consider the effect of a wind stress $\mathbf{T} = (\mathbf{T_x}, \mathbf{0})$ (units of force per square meter of ocean surface area) directed along the x axis that acts on an ocean of uniform density and viscosity, and of infinite extent, as shown in Fig. (7.1). As will be argued in the next section, this wind stress affects only a thin skin of the ocean near the surface because of the fact that ocean water is nearly inviscid. Let h_E be the thickness of this layer (the Ekman layer); let u_E and

v_E be the vertically averaged currents in the layer in the x and y directions, respectively. The net transport $\mathbf{Q_E}$ of fluid caused by the wind stress is thus $u_E h_E$ and $v_E h_E$ in the x and y directions, respectively. Under steady, time-independent conditions, the Coriolis force acting on the net transport must balance the wind stress, thus

$$0 = \rho f v_E h_E + T_x \tag{7.1}$$
$$0 = -\rho f u_E h_E + 0 \tag{7.2}$$

This implies that $\mathbf{Q_E}$ is directed in the negative y direction as shown in Fig. (7.1)

$$v_E h_E = \frac{-T_x}{\rho f} \tag{7.3}$$
$$u_E h_E = 0 \tag{7.4}$$

In general, for an arbitrary pattern of wind stress, the Ekman transport $\mathbf{Q_E}$ is given by

$$v_E h_E = \frac{-T_x}{\rho f} \tag{7.5}$$
$$u_E h_E = \frac{T_y}{\rho f} \tag{7.6}$$

Ekman's discovery that the net transport in the upper skin of the ocean (the thin region effected by wind stress) is directed at right angles to the direction of the wind was made through Ekman's analysis of the drift of the great Norwegian ship *Fram* in the Arctic Ocean. Frijtoft Nansen (a famous polar explorer) had his *Fram* beset in the Arctic ice on purpose so that he could drift with the ice for a year and reach the North Pole. The drift of his beset vessel tended to be directed to the right of the prevailing winds.

7.2 Ekman Pumping

What is the significance of the Ekman transport derived above? It can cause water to be "pumped" into (or sucked out of) the deep, inviscid ocean that

lies below the Ekman layer. Incompressibility of water gives us a means to determine the vertical velocity w_E at the base of the Ekman layer. In cartesian coordinates, the incompressibility condition can be integrated to give

$$w_E = \frac{\partial(u_E h_E)}{\partial x} + \frac{\partial(v_E h_E)}{\partial y} \tag{7.7}$$

Using Eqns. (7.5) and (7.6),

$$w_E = \frac{1}{\rho f}\left(\frac{\partial T_y}{\partial x} - \frac{\partial T_x}{\partial y}\right) + \frac{T_x}{\rho f^2}\frac{df}{dy} \tag{7.8}$$

$$= \frac{1}{\rho f}\nabla \times \mathbf{T} + \frac{\mathbf{T_x}}{\rho \mathbf{f^2}}\beta \tag{7.9}$$

where β is the y-derivative of the Coriolis parameter (we identify y with the meridional direction over which the Coriolis parameter varies with the sin of the latitude). Under most circumstances, the term involving the "β-effect" can be ignored because it is much smaller than the other term. Thus, we will use the following relation:

$$w_E = \frac{1}{\rho f}\nabla \times \mathbf{T} \tag{7.10}$$

To understand wind-driven ocean circulation, we must explore the consequences of "Ekman pumping" (the generation of w_E). There are two areas to explore. The first concerns the effect of abrupt changes in wind stress (such as along a coast), or shifts in the sign of the Coriolis parameter f. The pumping associated with this first effect produces strong, locally intense upwelling that is of prime importance to biological oceanographers in determining the recycling of nutrients in the ocean. The second area to explore concerns the more gentle gradients of wind stress which exist because of the pole to equator shifts in atmospheric circulation. The pumping associated with this second effect gives us the "gyre" circulations so clearly evident in the density structure of the ocean.

7.3 Ekman Pumping in Geographic Coordinates

To determine w_E in geographic coordinates (λ, ϕ), we consider the box depicted in Fig. (7.2). For positive (arbitrary) velocities u_E, v_E, and w_E, the fluid entering the box is made up of three contributions:

$$u_E(\lambda, \phi + \frac{\Delta\phi}{2}) h_E R \Delta\phi \tag{7.11}$$

$$v_E(\lambda + \frac{\Delta\lambda}{2}, \phi) h_E R \cos\phi \Delta\lambda \tag{7.12}$$

and

$$w_E(\lambda + \frac{\Delta\lambda}{2}, \phi + \frac{\Delta\phi}{2}) R^2 \cos\left(\phi + \frac{\Delta\phi}{2}\right) \Delta\lambda\Delta\phi \tag{7.13}$$

The fluid leaving the box is made up of two contributions (we disallow the possibility of fluid leaving the box via evaporation at the ocean surface, but this could also be taken into account):

$$u_E(\lambda + \Delta\lambda, \phi + \frac{\Delta\phi}{2}) h_E R \Delta\phi \tag{7.14}$$

$$v_E(\lambda + \frac{\Delta\lambda}{2}, \phi + \Delta\phi) h_E R \cos(\phi + \Delta\phi) \Delta\lambda \tag{7.15}$$

We make use of the following trigonometric identity to deal with the term $\cos(\phi + \Delta\phi)$:

$$\cos(\phi + \Delta\phi) = \cos\phi\cos\Delta\phi - \sin\phi\sin\Delta\phi \tag{7.16}$$

Making use of the small size of $\Delta\phi$ and the small-angle approximations for cos and sin functions, we obtain:

$$\cos(\phi + \Delta\phi) \approx \cos\phi - \Delta\phi\sin\phi \tag{7.17}$$

With the above approximation, the sum of output fluxes minus the sum of input fluxes gives the following expression, which is equated to zero to conserve mass:

$$\frac{h_E}{R}\left[\frac{u_E(\lambda + \Delta\lambda) - u_E(\lambda)}{\cos\phi\Delta\lambda} + \frac{v_E(\phi + \Delta\phi) - v_E(\phi)}{\Delta\phi} - v_E\tan\phi\right] - w_E = 0 \tag{7.18}$$

When the limits $\Delta\phi \to 0$ and $\Delta\lambda \to 0$ are considered, we obtain the following differential equation:

$$\frac{h_E}{R}\left[\frac{1}{\cos\phi}\frac{\partial u_E}{\partial\lambda} + \frac{\partial v_E}{\partial\phi} - v_E\tan\phi\right] = w_E \tag{7.19}$$

7.4 Upwelling

Consider the equatorial region near the West coast of South America shown in Fig. (7.3). The trade winds blow along the Equator. Ekman transport just North of the Equator is to the North, and just South of the Equator is to the South. The net transport of mass in the Ekman layer along the Equator is thus divergent. To balance this divergence, there must be a narrow band of upwelling (positive w_E) along the Equator. Reference to the surface temperature and salinity maps made in prior labs suggests that, indeed, upwelling along the Equator has an important influence on the hydrographic structure of the ocean.

At the coast of South America in the Southern Hemisphere, the trade winds blow the Ekman transport South. The coast of South America in this region trends NW to SE, thus a Southerly Ekman transport implies that a component of the Ekman transport will be offshore. Upwelling must occur along the coast to balance the offshore transport of fluid in the Ekman layer. This upwelling is responsible for recycling nutrients from the deep ocean into the surface zone. Enhanced biological productivity which results from this nutrient recycling is responsible for the unusual fisheries off the coast of Peru and Equador.

7.5 The Ekman Spiral

A detailed account of the effect of surface wind on the mass transport of the ocean is provided using the equations of motion which balance viscous

frictional forces against the Coriolis force as follows. The momentum balance below the surface of the ocean shown in Fig. (7.1), $-\infty < z < 0$, is represented by

$$0 = fv + \nu u_{zz} \tag{7.20}$$

$$0 = -fu + \nu v_{zz} \tag{7.21}$$

where ν is the kinematic viscosity of seawater (this is usually much larger than the molecular viscosity owing to the turbulence which exists near the ocean surface). The second terms on the right-hand sides of Eqns. (7.20) and (7.21) represent the *diffusion* of momentum downward in the water column as a result of the viscosity (internal friction) of the water. Boundary conditions to be applied at the ocean surface are designed to account for a wind stress $\mathbf{T} = (\mathbf{T_x}, \mathbf{0})$ that is directed along the x-axis

$$u_z = \frac{T_x}{\rho\nu} \tag{7.22}$$

$$v_z = 0 \tag{7.23}$$

Boundary conditions as $z \to -\infty$ (*e.g.,* at the bottom of the ocean far removed from the application of wind stress) are

$$u, v \to 0 \tag{7.24}$$

Following the usual practice, we combine Eqns. (7.20) and (7.21) to obtain a single equation for the single unknown u:

$$\nu^2 u_{zzzz} + f^2 u = 0 \tag{7.25}$$

The solution of this equation is of the form

$$u = Ue^{kz} \tag{7.26}$$

where

$$k = \sqrt[4]{\frac{f^2}{\nu^2}}\sqrt[4]{-1} \tag{7.27}$$

Reference to the complex plane (as a means of evaluating the fourth-root of -1) gives us the four possible values of the exponential decay factor k:

$$k = \pm\sqrt{\frac{f}{2\nu}}(1 \pm i) \tag{7.28}$$

Four values of k are possible according to Eqn. (7.28). Two values have negative real parts, and thus grow exponentially as $z \to -\infty$. The solution must be composed of the other values of k to satisfy the boundary conditions at $z \to -\infty$. Using the trigonometric identities, we may write the acceptable form of the solution as

$$u = U_s e^{z\sqrt{\frac{f}{2\nu}}} \sin z\sqrt{\frac{f}{2\nu}} + U_c e^{z\sqrt{\frac{f}{2\nu}}} \cos z\sqrt{\frac{f}{2\nu}} \tag{7.29}$$

where U_s and U_c are undetermined constants which will be evalutated using the boundary conditions at $z = 0$. Use of Eqn. (7.20) gives

$$v = U_s e^{z\sqrt{\frac{f}{2\nu}}} \cos z\sqrt{\frac{f}{2\nu}} + U_c e^{z\sqrt{\frac{f}{2\nu}}} \sin z\sqrt{\frac{f}{2\nu}} \tag{7.30}$$

The unknown constants U_c and U_s are determined by insisting that the solution in Eqns. (7.29) and (7.30) satisfy the boundary conditions at $z = 0$ given by Eqns. (7.22) and (7.23). This gives two linear equations in two unknowns:

$$U_s + U_c = \sqrt{\frac{2\nu}{f}} \frac{1}{\rho\nu} T_x \tag{7.31}$$

$$-U_s + U_c = 0 \tag{7.32}$$

The solution to the above equations is

$$U_s = U_c = \sqrt{\frac{1}{2f\nu}} \frac{T_x}{\rho} \tag{7.33}$$

Substitution of the above result into Eqns. (7.29) and (7.30) give the Ekman layer flow:

$$u = \sqrt{\frac{1}{2f\nu}} \frac{T_x}{\rho} e^{z\sqrt{\frac{f}{2\nu}}} \left(\sin z\sqrt{\frac{f}{2\nu}} + \cos z\sqrt{\frac{f}{2\nu}} \right) \tag{7.34}$$

$$v = \sqrt{\frac{1}{2f\nu}} \frac{T_x}{\rho} e^{z\sqrt{\frac{f}{2\nu}}} \left(\sin z\sqrt{\frac{f}{2\nu}} - \cos z\sqrt{\frac{f}{2\nu}} \right) \tag{7.35}$$

As $z \to -\infty$, the direction of the flow (*i.e.,* the direction of $\mathbf{u} = (\mathbf{u}, \mathbf{v})$) slowly turns to the right and the magnitude of the flow decays. The velocity vectors in the Ekman layer thus *spiral* downward as shown in Fig. (7.4). At the surface, $z = 0$, the velocity of the ocean is directed at 45 degrees to the right of the direction of the wind stress. The e-fold vertical decay scale of the Ekman currents is $\sqrt{\frac{f}{2\nu}}$, and is about 1 - 10 meters. The small size of this vertical decay scale assures us that we were correct previously in thinking that wind stress would only influence the upper skin of the ocean.

7.6 Ekman Transport

Having described the vertical structure of the Ekman layer flow, we now wish to verify the net, vertically averaged horizontal transport of the Ekman layer deduced previously (Eqns. 7.5 and 7.6). To compute the net transport, we integrate the expressions in Eqns. (7.34) and (7.35) over the interval $-\infty < z < 0$. This necessitates the evaluation of the following integral:

$$\int_{-\infty}^{0} \exp\left(\sqrt{\frac{f}{2\nu}}z\right) \cos\left(\sqrt{\frac{f}{2\nu}}z\right) dz \tag{7.36}$$

$$= \int_{-\infty}^{0} \sqrt{\frac{2\nu}{f}} \frac{d}{dz} \left(\exp\left(\sqrt{\frac{f}{2\nu}}z\right)\right) \cos\left(\sqrt{\frac{f}{2\nu}}z\right) dz \tag{7.37}$$

This integral is evaluated using integration by parts as follows:

$$\int_{-\infty}^{0} \sqrt{\frac{2\nu}{f}} \frac{d}{dz} \left(\exp\left(\sqrt{\frac{f}{2\nu}}z\right)\right) \cos\left(\sqrt{\frac{f}{2\nu}}z\right) dz$$

$$= \sqrt{\tfrac{2\nu}{f}} \left\{ e^{\sqrt{\frac{f}{2\nu}}z} \cos\sqrt{\tfrac{f}{2\nu}}z \Big|_{-\infty}^{0} + \int_{-\infty}^{0} \sqrt{\frac{f}{2\nu}} e^{\sqrt{\frac{f}{2\nu}}z} \sin\sqrt{\frac{f}{2\nu}}z dz \right\}$$

$$= \sqrt{\tfrac{2\nu}{f}} \left\{ 1 + \int_{-\infty}^{0} \frac{d}{dz} \left(e^{\sqrt{\frac{f}{2\nu}} z} \right) \sin \sqrt{\tfrac{f}{2\nu}} z \, dz \right\}$$

$$= \sqrt{\tfrac{2\nu}{f}} \left\{ 1 + \left[e^{\sqrt{\frac{f}{2\nu}} z} \sin \sqrt{\tfrac{f}{2\nu}} z \Big|_{-\infty}^{0} - \int_{-\infty}^{0} e^{\sqrt{\frac{f}{2\nu}} z} \sqrt{\frac{f}{2\nu}} \cos \sqrt{\frac{f}{2\nu}} z dz \right] \right\}$$

$$= \sqrt{\tfrac{2\nu}{f}} - \textstyle\int_{-\infty}^{0} e^{\sqrt{\frac{f}{2\nu}} z} \sqrt{\tfrac{f}{2\nu}} \cos \sqrt{\tfrac{f}{2\nu}} z dz \tag{7.38}$$

The last term on the right-hand side of the above equation is the same as the original integral. We can thus shift it over to the left-hand side, and divide the remainder of the left-hand side by two to get the result:

$$\int_{-\infty}^{0} \exp \left(\sqrt{\frac{f}{2\nu}} z \right) \cos \left(\sqrt{\frac{f}{2\nu}} z \right) dz = \sqrt{\frac{\nu}{2f}} \tag{7.39}$$

Likewise,

$$\int_{-\infty}^{0} \exp \left(\sqrt{\frac{f}{2\nu}} z \right) \sin \left(\sqrt{\frac{f}{2\nu}} z \right) dz = -\sqrt{\frac{\nu}{2f}} \tag{7.40}$$

The net, vertically averaged transport in the Ekman layer can now be evaluated using the above integrals. The result is

$$(Q_E)_x = 0 \tag{7.41}$$

$$(Q_E)_y = -\frac{T_x}{f\rho} \tag{7.42}$$

which is the same as derived previously (see Eqns. 7.3 and 7.4.

7.7 Assignment

In the future, the assignment for this chapter will involve computing the Ekman layer transport and pumping velocity in the world ocean using the annual-average wind stress around the world.

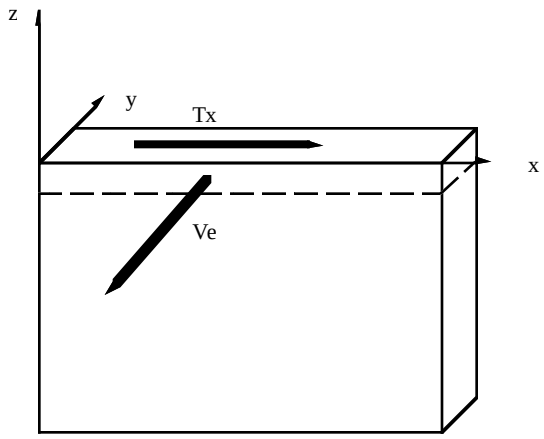

Figure 7.1: The Ekman layer.

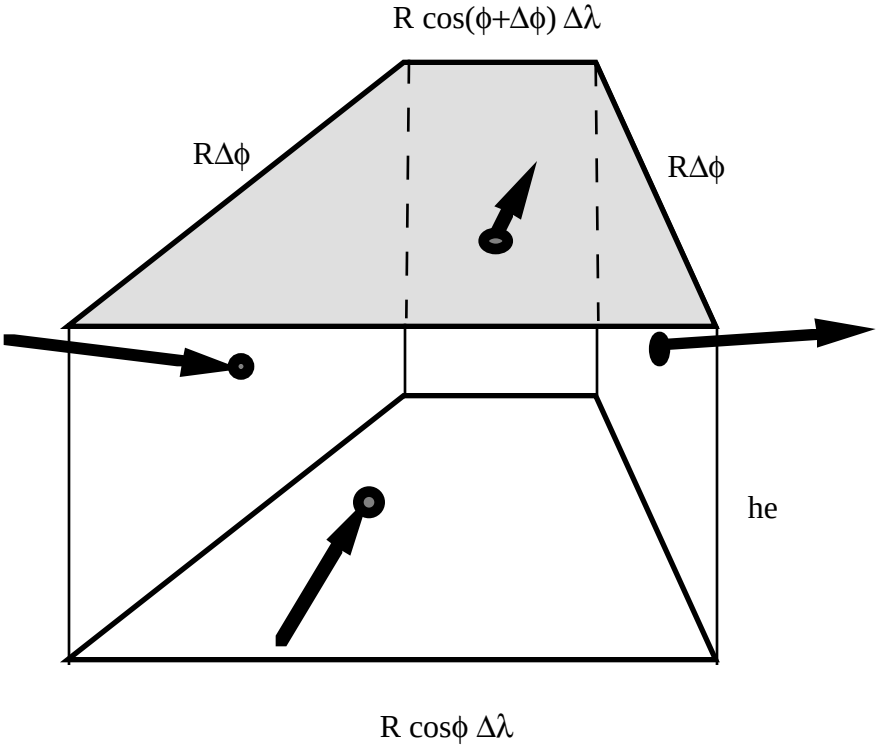

Figure 7.2: To correctly compute the divergence of the flux in the surface-ocean Ekman layer, we must account for the pinching-out with increasing latitude of the sides of the control volume which face north or south.

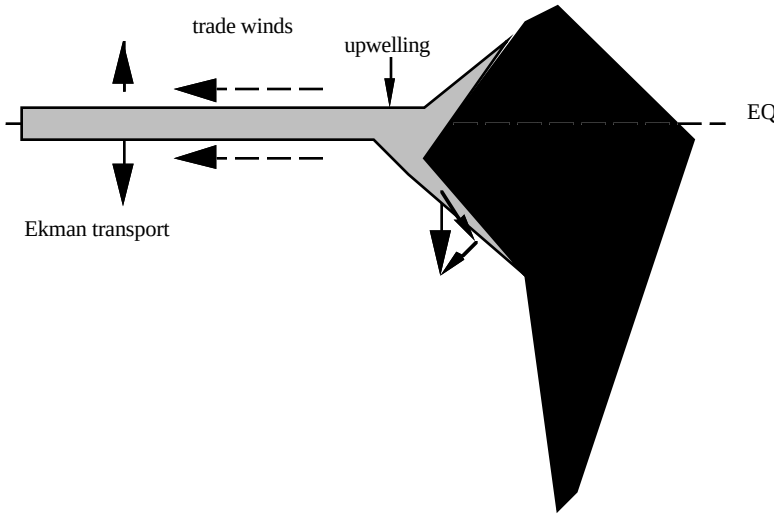

Figure 7.3: Equatorial and coastal upwelling near South America due to the net surface water transport by the Ekman layer.

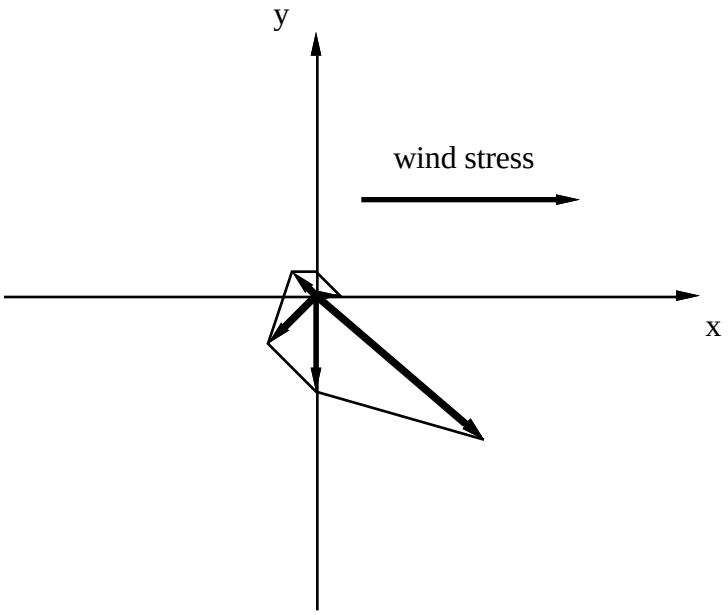

Figure 7.4: The Ekman spiral.

Chapter 8

Wind-Driven Ocean Circulation

In the previous chapter, we came to the realization that the wind stress at the ocean surface direclty affects the vast bulk of the ocean very little. Only the thin skin at the surface of the ocean, or Ekman layer, is able to "feel" the force transmitted by the wind through the ocean surface. The deep ocean below the Ekman layer is only "aware" of the wind forcing through the action of the Ekman pump, the very gentle upwelling and downwelling caused by the convergence (or divergence) of flow in the Ekman layer.

Here we consider how the deep, "interior" ocean deals with the action of the Ekman pump.

8.1 Two Possible Balances

We recall that the vertical velocity at the base of the Ekman layer, w_E, is given by the divergence of the Ekman transport:

$$w_E = \frac{h_E}{R}\left[\frac{1}{\cos\phi}\frac{\partial u_E}{\partial \lambda} + \frac{\partial v_E}{\partial \phi} - v_E \tan\phi\right] \tag{8.1}$$

What happens to the water that is pumped into the portion of the ocean which lies below the Ekman layer? The ocean depth, as we observe it over

long time periods, does not change with time; thus, we anticipate that the flux ejected from the surface Ekman layer is carried away by either the interior geostrophic flow of the ocean (the wind-driven circulation that most interests us), or by an Ekman layer at the bottom of the ocean (due to friction). In what follows, we shall consider both possibilities and learn that both are necessary to yield an interior geostrophic circulation that is consistent with observations discussed in previous chapters.

8.2 Basal Ekman Layer Only

Is it possible that this water is "taken up" by the action of another Ekman layer located at the bottom of the ocean where we expect frictional effects to be as influential as at the surface? Let's pursue this idea. Consider the depiction of a bottom Ekman layer shown in Fig. (8.1). We expect two forces to balance each other in this bottom layer: the force due to the pressure gradient, and the force due to the effects of bottom friction (which we simplify to be expressible in terms of a friction coefficient k). Looking at the balance of forces in the zonal direction first, we have

$$\begin{aligned} p(\lambda,\phi,-d)h_E R\Delta\phi \quad & -p(\lambda+\Delta\lambda,\phi,-d)h_E R\Delta\phi \\ & -ku_b R^2\cos\phi\Delta\lambda\Delta\phi \qquad = 0 \end{aligned} \tag{8.2}$$

where R is the radius of the earth, $\Delta\lambda$ and $\Delta\phi$ are the longitudinal and latitudinal spans of the sides of the box considered in Fig. (8.1), u_b is the zonal component of the z-averaged flow in the bottom Ekman layer, h_E is the thickness of the bottom Ekman layer (assumed to be the same as that of the surface Ekman layer), and k is the bottom friction coefficient (taken here to be ≈ 2 kg m^{-3} s^{-1}). Taking the limit as $\Delta\lambda \to 0$ gives the following relation:

$$\frac{k}{\rho h_E}u_b = \frac{-1}{\rho\cos\phi R}\frac{\partial p}{\partial\lambda} \tag{8.3}$$

where ρ is the density of seawater. A similar consideration of forces acting in the meridional direction gives

$$\frac{k}{\rho h_E}v_b = \frac{-1}{\rho R}\frac{\partial p}{\partial\phi} \tag{8.4}$$

where v_b is the meridional component of the z-averaged flow in the bottom Ekman layer.

If we ignore density variation of ρ in the ocean, then $p = \rho g(\eta(\lambda, \phi) - z)$. This relation allows us to express u_b and v_b in terms of the dynamic topography η:

$$u_b = \frac{-\rho g h_E}{kR\cos\phi}\frac{\partial \eta}{\partial \lambda} \tag{8.5}$$

$$v_b = \frac{-\rho g h_E}{kR}\frac{\partial \eta}{\partial \phi} \tag{8.6}$$

Following the same consideration as used in the last chapter to derive the expression for w_E, the pumping velocity w_b out of the bottom Ekman layer at a level h_E above the the seabed is found to be:

$$w_b = \frac{-h_E}{R}\left[\frac{1}{\cos\phi}\frac{\partial u_b}{\partial \lambda} + \frac{\partial v_b}{\partial \phi} - v_b \tan\phi\right] \tag{8.7}$$

Substituting the above expressions for u_b and v_b, we obtain the relation

$$w_b = \frac{\rho g h_E^2}{kR^2}\left[\nabla^2\eta - \tan\phi\frac{\partial \eta}{\partial \phi}\right] \tag{8.8}$$

where

$$\nabla^2\eta = \left[\frac{1}{\cos^2\phi}\frac{\partial^2\eta}{\partial\lambda^2} + \frac{\partial^2\eta}{\partial\phi^2}\right] \tag{8.9}$$

If we equate w_b with w_E, *i.e.,* we ask the bottom Ekman layer to exactly counterbalance the pumping velocity of the wind-driven surface Ekman layer, we achieve an expression that predicts a dynamic topography of the wind-driven ocean circulation. (Recall that the geostrophic balance tells us that once η is known, the oceanic flow between the two Ekman layers is completely determined.) This expression is written as follows:

$$\frac{\rho g h_E^2}{kR^2}\left[\nabla^2\eta - \tan\phi\frac{\partial \eta}{\partial \phi}\right] = \frac{h_E}{R}\left[\frac{1}{\cos\phi}\frac{\partial u_E}{\partial \lambda} + \frac{\partial v_E}{\partial \phi} - v_E\tan\phi\right] = w_E \tag{8.10}$$

We shall soon examine the consequences of the above prediction, and find that it differs strongly (in magnitude and geometry) from what we expect

from observation. The inadequacy of this method of predicting the dynamic topography of the ocean will force us to consider the other means by which the flux ejected from the surface Ekman layer can be carried away.

8.2.1 Exercise: An Wind-Driven Circulation Predicted by Incomplete Physics

The above reasoning turns out to be flawed in a serious way. To see the consequences of this flaw, you are asked to construct the dynamic topography of the North Atlantic region studied in class using the above formula for η. The result should look something like that shown in Fig. (8.2). How does the dynamic topography so constructed compare with the dynamic topography deduced from the observations and shown in Fig. (8.3)?

8.3 Basal Ekman Layer Plus Divergence of Geostrophic Flow (Sverdrup Balance)

If you did the above exercise, you appreciate the problems with balancing the vertical Ekman pump at the sea surface with an "equal but opposite" Ekman pump (due to friction) at the sea bed. (You should have noticed that the dynamic topography $\eta(\lambda, \phi)$ computed in the above exercise is both too large in magnitude and lacks the western intensification (gulf stream) that is so strongly evident in the observed dynamic topography.)

How next to proceed? One possibility is left open to us: some of what is pumped into the interior ocean by the wind-driven surface Ekman layer may be balanced by a divergence of the geostrophic flow (in addition to the divergence of a basal Ekman layer).

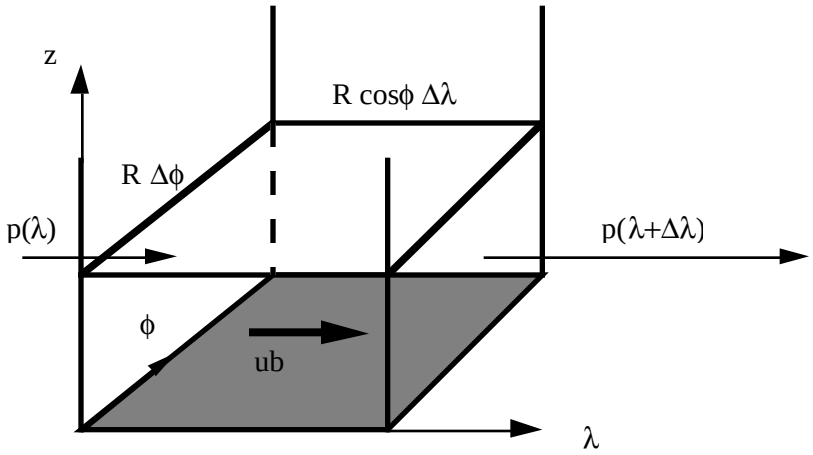

Figure 8.1: Force balance within the basal Ekman layer.

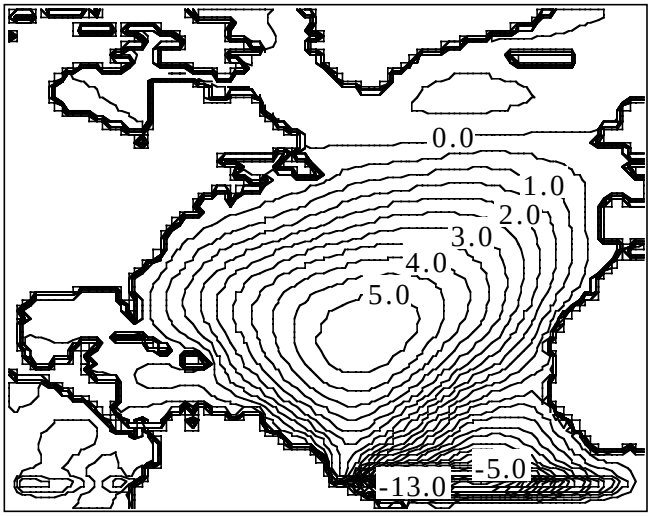

Figure 8.2: Dynamic topography $\eta(\lambda, \phi)$ (in meters) assuming that the Ekman pump at the ocean surface (due to wind forcing) is balanced by an Ekman pump at the ocean base (due to basal friction).

Divergence of a Geostrophic Flow

Denoting the zonal and meridional geostrophic velocities by u_I and v_I, respectively, we can write the geostrophic balance (neglecting density variation in the vertical) as follows:

$$u_I = \frac{-g}{2R\Omega \sin\phi} \frac{\partial \eta}{\partial \phi} \tag{8.11}$$

and

$$v_I = \frac{g}{2R\Omega \sin\phi \cos\phi} \frac{\partial \eta}{\partial \lambda} = \frac{g}{R\Omega \sin 2\phi} \frac{\partial \eta}{\partial \lambda} \tag{8.12}$$

Following the same consideration as used previously to derive the expressions for w_E and w_b (*i.e.,* relating the divergence of the horizontal flow to the vertical change in vertical velocity), we arrive at the expression

$$\frac{-H}{R}\left[\frac{1}{\cos\phi}\frac{\partial u_I}{\partial \lambda} + \frac{\partial v_I}{\partial \phi} - v_I \tan\phi\right] + w_b = w_E \tag{8.13}$$

where H is the depth of the ocean (minus the thickness of the two relatively insignificant Ekman layers at its surface and base). Using the geostrophic relation derived above, and making note of cancellations of terms, we derive

$$\frac{gH}{2R^2\Omega \sin^2\phi} \frac{\partial \eta}{\partial \lambda} + w_b = w_E \tag{8.14}$$

Making use of the expression for w_b derived in the previous section, we obtain

$$\frac{gH}{2R^2\Omega \sin^2\phi} \frac{\partial \eta}{\partial \lambda} + \frac{\rho g h_E^2}{kR^2}\left[\nabla^2 \eta - \tan\phi \frac{\partial \eta}{\partial \phi}\right] = w_E \tag{8.15}$$

A quick comparison with Eqn. (8.8) shows that a single term involving $\frac{\partial \eta}{\partial \lambda}$ is added to the relation between η and w_E when we consider divergence of the internal ocean's geostrophic flow. The fact that this additional term involves a λ-derivative of η gives us our first hint of the origin of the zonal asymmetry that gives rise to strong currents like the Gulf Stream.

Sverdrup Balance

A quick check of the coefficients multiplying the two η-dependent terms on the left-hand side of Eqn. (8.15) suggests that in most circumstances (over most of the ocean) the first term will dominate the second term. (The coefficient of the first term is about a factor of 10 larger than the coefficient of the second term if we take $H \approx 100$ m.) In this circumstance, we have what is known as the Sverdrup balance (named after the Norwegian oceanographer H. U. Sverdrup, who worked at the Scripps Institute of Oceanography for much of his professional life):

$$\frac{gH}{2R^2\Omega \sin^2 \phi} \frac{\partial \eta_{sv}}{\partial \lambda} = w_E \tag{8.16}$$

where the subscript sv on η denotes the portion of the total dynamic topography due to the Sverdrup balance. Using the expression for the meridional component of the geostrophic flow, we obtain

$$\frac{H}{R \tan \phi} v_{sv} = w_E \tag{8.17}$$

Thus, for $w_E < 0$ as is the case over much of the Sargasso sea, $v_{sv} < 0$; or, in other words, there is a southward directed meridional flow over much of the North Atlantic due to the effect of the Ekman pump.

Gulf Stream

The Sverdrup balance presents us with a question: where does v_I reverse its sign and flow back to the north (assuming a point-of-view located in the Sargasso sea)? Another way of realizing the significance of this question is to see what happens when we integrate the Sverdrup balance along a line of constant latitude over an interval $\lambda \in [\lambda_W, \lambda_E]$, where λ_W and λ_E are the longitudes of the western and eastern boundaries, respectively.

$$\frac{gH}{2R^2\Omega \sin^2 \phi} \int_{\lambda_E}^{\lambda_W} \frac{\partial \eta_{sv}}{\partial \lambda} d\lambda = \int_{\lambda_E}^{\lambda_W} w_E d\lambda \tag{8.18}$$

Noting the integrand on the left-hand side is a derivative, and denoting the average value of w_E along the line of integration with $\bar{w}_E$, we obtain

$$\frac{gH}{2R^2\Omega \sin^2\phi\,(\lambda_E - \lambda_W)}\,(\eta_E^{sv} - \eta_W^{sv}) = \bar{w}_E \tag{8.19}$$

Over much of the North Atlantic, $\bar{w}_E < 0$, thus, the above expression gives $\eta_W^{sv} > \eta_E^{sv}$, where η_W^{sv} and η_E^{sv} are the values of η_{sv} at the western and eastern boundaries of the ocean, respectively. For the net southward flow to be balanced (for conservation of mass) by a corresponding northward flow, we must have $\eta_W = \eta_E$, where η_W and η_E are the net dynamic topography values at the two boundaries.

Stommel Boundary Layer Solution

The resolution of the problem of $\eta_W^{sv} > \eta_E^{sv}$ was originally proposed by Henry Stommel, a famous Woods Hole Oceanographic Institution oceanographer. The result is somewhat suprising. Northward flow in a very thin boundary layer (a Gulf Stream) is possible at the western boundary of the ocean if the currents are sufficiently strong as to invoke a balance between the two terms on the left-hand side of Eqn. (8.15):

$$\frac{gH}{2R^2\Omega \sin^2\phi}\frac{\partial \eta_{gs}}{\partial \lambda} + \frac{\rho g h_E^2}{kR^2}\left[\nabla^2 \eta_{gs} - \tan\phi \frac{\partial \eta_{gs}}{\partial \phi}\right] = 0 \tag{8.20}$$

Disregarding non-essential terms for the time being, we have

$$\frac{gH}{2R^2\Omega \sin^2\phi}\frac{\partial \eta_{gs}}{\partial \lambda} + \frac{\rho g h_E^2}{kR^2}\frac{\partial^2 \eta_{gs}}{\partial \lambda^2} = 0 \tag{8.21}$$

where we have used the variable η_{gs} to denote the additive correction to $\eta = \eta_{sv} + \eta gs$ that is necessary to allow $\eta_W = \eta_E$.

If we integrate the above expression once with respect to λ, we obtain an expression which relates η_{gs} to $\frac{\partial \eta_{gs}}{\partial \lambda}$:

$$\frac{\partial \eta_{gs}}{\partial \lambda} = \frac{-1}{\gamma}\eta_{gs} + C \tag{8.22}$$

where C is a constant of integration (which we deduce to be zero), and

$$\gamma = \frac{2\rho\Omega h_e^2 \sin^2 \phi}{Hk} \tag{8.23}$$

The solution of Eqn. (8.22) is an exponential function:

$$\eta_{gs} = Ae^{\frac{-\lambda}{\gamma}} \tag{8.24}$$

where A is another constant of integration (determined below).

We note the fact that η_{gs} is a decaying function of λ, thus we are forced to deduce that the boundary layer within which the above balance is possible must occur on the *western* side of the ocean basin. (An eastern boundary layer would be nonsensical because η_{gs} would increase toward infinity as one travelled west across the ocean from the eastern boundary.) In addition, we realize that with $A = -\eta_W^{sv}$, the boundary layer will close the Sverdrup balance (provide the necessary return flow to the north).

Having deduced the presence of a northward flowing gulf stream (return current to balance the Sverdrup drift) on the western boundary of the ocean, we also can deduce that this current will be relatively narrow. The constant γ (latitude dependent) gives us the angular width of the e-folding decay scale of η_{gs}. A quick check of the numbers suggests that this width should be on the order of several degrees of longitude, or several hundred kilometers at mid latitudes.

In actuality, the real gulf stream is much more narrow. There are several reasons for this associated with the nature of friction and inertia, which are too advanced to go into here.

8.4 Exercise: A Predicted Wind-Driven Circulation That Satisfies Our Preconceptions

Construct the dynamic topography of the North Atlantic region studied in class using the formula for η given in Eqn. (8.15). The result should look something like that shown in Fig. (8.4). How does the dynamic topography so constructed compare with the dynamic topography deduced from the observations and shown in Fig. (8.3)? What features deemed missing from the dynamic topography constructed assuming only a balance between the two Ekman layers are now present?

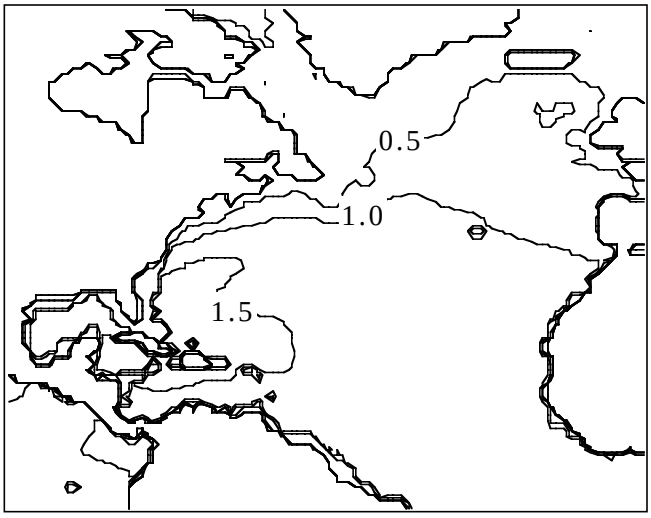

Figure 8.3: Observed dynamic topography $\eta(\lambda, \phi)$ (in meters) assuming a level of no motion at 1000 m (this field was computed in an exercise associated with a previous chapter).

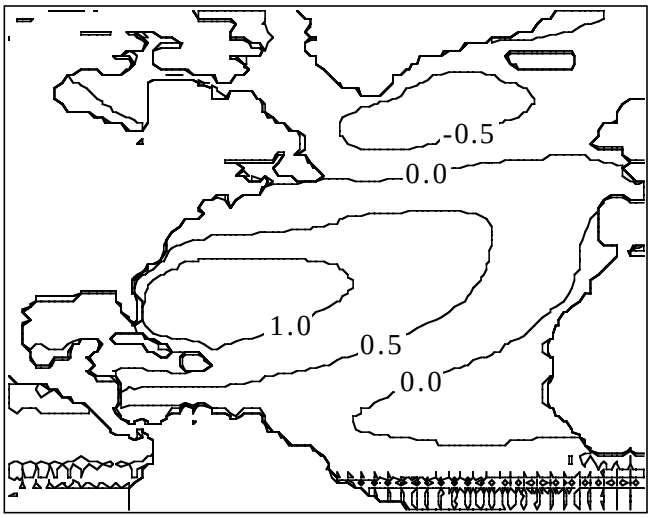

Figure 8.4: Dynamic topography $\eta(\lambda, \phi)$ (in meters) assuming that the Ekman pump at the ocean surface (due to wind forcing) is balanced by the combination of an Ekman pump at the ocean base (due to basal friction) and a Sverdrup balance.

Chapter 9

Shallow Water Gravity Waves

9.1 Overview

The goal of this chapter is to begin the process of describing the three most important fluid dynamical balances in oceanography: the hydrostatic pressure balance (gravity and pressure), the geostrophic balance (pressure gradient and Coriolis force), and the Ekman balance (viscous forces and Coriolis force). We make a long, round-about journey to the geostrophic balance in this chapter by touching on various subjects of importance in a series of long digressions.

We begin with the description of the hydrostatic balance. Following this, we examine the *shallow water* equations (equations which describe fluid motions of the ocean) and search for wave-like solutions. On finding Poincare waves and Kelvin waves, we touch on various phenomena involving those waves, including tsunamis, storm surges, El Niño, and tides. After completing the digression, we proceed to understand the *geostrophic adjustment* problem. In this important problem, we find that no matter how we force the ocean (at least the shallow water version of the ocean) some sort of geostrophic currents are formed in the process. Geostrophic currents are steady in time and reflect the balance between the pressure gradient force

and the Coriolis force. Finally, we derive the description of geostrophic motion in a *stratified* ocean as a preparation for the next chapter.

9.2 Hydrostatic Balance

The hydrostatic balance is perhaps the easiest of all the three important balances in oceanography to be explained. In simple terms, the hydrostatic balance says that the pressure in the ocean is that which is neccessary to support the gravitational weight of the water above. Thus,

$$p(x,y,z,t) = \int_z^{\eta(x,y,t)} \rho(x,y,z,t) g dz \tag{9.1}$$

where p is the pressure, x, y and z form a local Cartesian reference frame, t is time, $\rho(x,y,z,t)$ is density, g is the gravitational acceleration, and $\eta(x,y,t)$ is the elevation of the free surface of the ocean (*i.e.,* the deviation of the free surface from the position $z = 0$ when the ocean is at rest).

The reason the term *balance* applies to the hydrostatic balance of the above equation is that the vertical component of the pressure gradient force $\frac{\partial p}{\partial z}$ exactly balances the gravitational body force ρg. In other words,

$$\frac{\partial p}{\partial z} = -\rho g \tag{9.2}$$

In this chapter, we are not concerned with the stratification of the ocean. (This will come later.) We thus consider the circumstances associated with an ocean of constant density $\rho(x,y,z,t) = \rho_o$. In this situation we may relate horizontal pressure gradients at any level z in the ocean to the slope of the free surface $\nabla\eta$:

$$\begin{aligned} \frac{\partial p}{\partial x} &= \frac{\partial}{\partial x}\left(\int_z^{\eta(x,y,t)} \rho_o g dz\right) \\ &= g\frac{\partial \eta(x,y,t)}{\partial x} = g\eta_x \end{aligned}$$

$$\begin{aligned}\frac{\partial p}{\partial y} &= \frac{\partial}{\partial y}\left(\int_z^{\eta(x,y,t)} \rho_o g dz\right) \\ &= g\frac{\partial \eta(x,y,t)}{\partial y} = g\eta_y\end{aligned}$$

These relations allow us to describe the way fluid motions (horizontal and vertical currents) in the ocean couple with the "topography" of the ocean surface.

9.3 Shallow Water Equations

The study of oceanography is full of approximations designed to focus attention on specific phenomena. In the previous chapter, for example, we described the propagation of internal gravity waves in a stratified ocean. In describing that motion, we disregarded the compressibility of seawater to restrict our analysis to a sound-free environment. Here, we again disregard certain important aspects of ocean dynamics to better capture the phenomena of interest which, in this case, is the propagation of long wavelength and small amplitude waves on the ocean surface.

The equations which describe shallow-water gravity waves are written as follows

$$\begin{aligned}u_t &= -g\eta_x + fv \\ v_t &= -g\eta_y - fu \\ \eta_t &= -H(u_x + v_y)\end{aligned} \tag{9.3}$$

where u and v are the x and y horizontal velocities, respectively, H is the depth of the ocean the terms involving the gradients of η express the horizontal gradients of the hydrostatic pressure (as described in the previous section), and the terms involving $f = 2\Omega \sin\phi$ describe the Coriolis force on the horizontal flow. Equations (9.3) and (9.3) describe the horizontal momentum balance. The vertical momentum balance is simply the hydrostatic balance described in the previous section. This vertical balance has been worked into Eqns. (9.3) and (9.3) by replacing the horizontal pressure gradients with the gradients of surface elevation η. Equation (9.3) expresses the

continuity of mass. If there is a divergence or convergence in the horizontal flow, the free surface elevation η must go down or up, respectively, to compensate. The horizontal velocities are assumed to be independent of depth (z-independent). The vertical velocity in this circumstance is simply a linear function of z because of the incompressibility condition

$$w_z = -(u_x + v_y) = constant \tag{9.4}$$

These are the equations which describe the surface-wave motions associated with long-period seiches, tides, storm surges (destructive waves generated by hurricanes and storms), and tsunamis (destructive waves generated by earthquakes).

9.4 Shallow-Water Gravity Waves

To derive the dispersion relation for shallow-water gravity waves (recall: the dispersion relation tells us what the wavelength is for a given frequency), we manipulate Eqns. (9.3) - (9.3) to obtain a single equation in a single unknown. We begin by taking the time-derivative of Eqn. (9.3)

$$\eta_{tt} = -H(u_{xt} + v_{yt}) \tag{9.5}$$

The x-derivative of Eqn. (9.3) and the y-derivative of Eqn. (9.3) can be used to substitute for u_{xt} and v_{yt} to give

$$\eta_{tt} = -H(-g\eta_{xx} + fv_x - g\eta_{yy} - fu_y) \tag{9.6}$$

or,

$$\eta_{tt} - gH\nabla^2\eta = -fH(v_x - u_y) \tag{9.7}$$

The last factor of the term on the right-hand side of the above equation is known as the relative vorticity (more precisely, the z-component of the relative vorticity). Our next task is to express this relative vorticity in terms of η. To do so, we take the x-derivative of Eqn. (9.3), and subtract from it the y-derivative of Eqn. (9.3), the result is

$$(v_x - u_y)_t = -g\eta_{yx} - fu_x + g\eta_{xy} - fv_y = -f(u_x + v_y) \tag{9.8}$$

We make use of Eqn. (9.3) to express the divergence appearing in the term on the right-hand side in terms of the time-derivative of η,

$$(v_x - u_y)_t = \frac{f}{H}\eta_t \tag{9.9}$$

Substitution of this result into the time-derivative of Eqn. (9.7) gives the single equation in the single unknown that we originally sought

$$\eta_{ttt} - gH^2\nabla^2\eta_t + f^2\eta_t = 0 \tag{9.10}$$

The dispersion relation is found by substituting a plane-wave solution into Eqn. (9.10). In other words, if

$$\eta = Ae^{i(\omega t - kx - ly)} \tag{9.11}$$

is substituded into Eqn. (9.10), and cancellations are made, the result is

$$\omega^2 = f^2 + gH(k^2 + l^2) \tag{9.12}$$

A graph of this dispersion relation is shown in Fig. (9.1). The features to note in Fig. (9.1) are: (1) the graph of ω asymptotes to straight lines when the wavelength is small (large magnitude of k or l), (2) the asymptotic slope of ω for small wavelength large ($\sqrt{k^2 + l^2} \gg 1$) is $\sqrt{gH}$, the phase velocity of shallow-water waves in the absense of rotation, (3) there are no waves that can propagate freely with frequencies smaller than $f = 2\Omega \sin\phi$, and (4) the group velocity $c_g = \nabla_{k,l}\omega$ vanishes at $\omega = f$ (this says that waves at the inertial frequency f do not propagate energy anywhere). The frequency f (also known as the Coriolis parameter) is referred to as the *inertial frequency*. (Recall that in the previous chapter inertial oscillations are simple circular motions of objects in motion in a frictionless rotating reference frame.)

9.5 Particle Motions

To diagnose the fluid motions associated with shallow-water gravity waves, we must step backwards through the proceedure of the previous section to

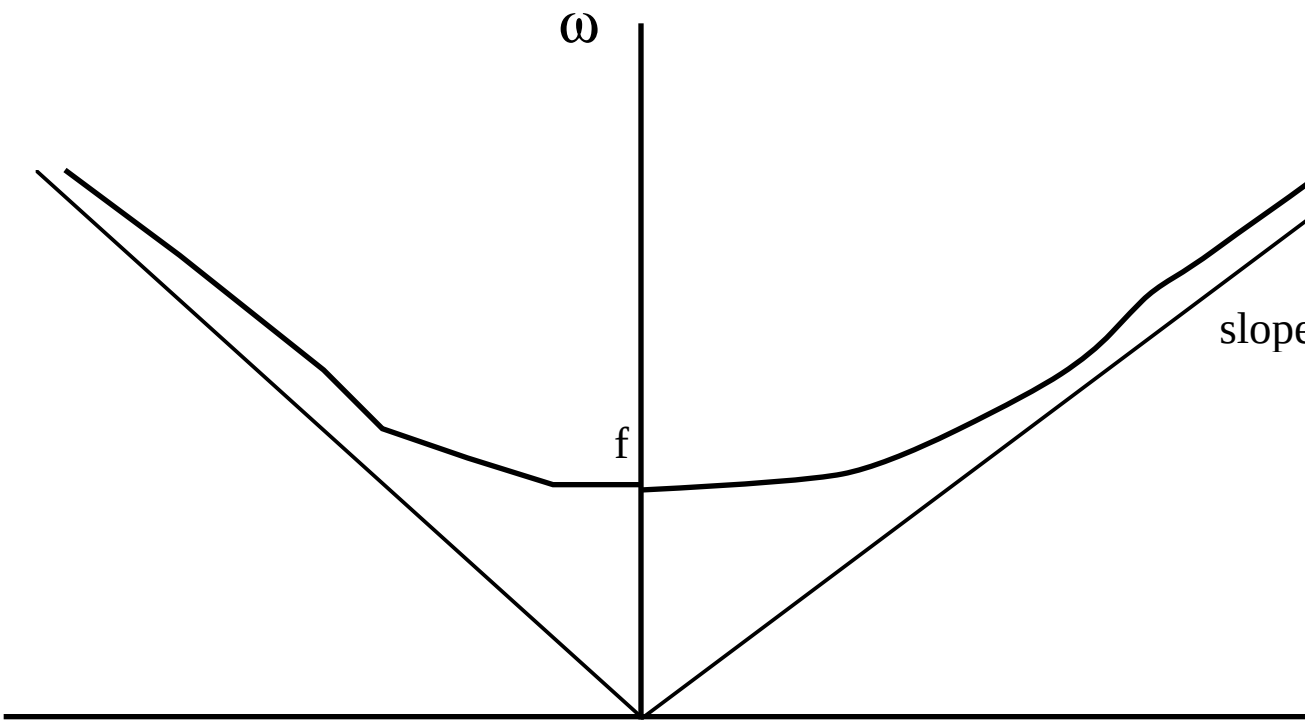

Figure 9.1: Dispersion diagram for shallow water gravity waves on an f-plane.

relate the velocities u and v to the known, wave-like solution for η. If we take the t-derivative of Eqn. (9.3) and use Eqn. (9.3) to replace the time derivative of the Coriolis term, we obtain

$$u_{tt} + f^2 u = -g\eta_{xt} - fg\eta_y \tag{9.13}$$

We can choose the coordinate system in a manner which aligns the direction of wave propagation with the x-axis. In this circumstance, the expression for η is

$$\eta = Ae^{i(\omega t - kx)} \tag{9.14}$$

where A is a real-valued amplitude (*i.e.,* $\eta = A\cos(\omega t - kx)$). We write u as a wave-like field which has an amplitude of arbitrary magnitude and arbitrary phase (*i.e.,* the amplitude for the velocity at this point is a complex number we wish to evaluate)

$$u = Be^{i\gamma}e^{i(\omega t - kx)} \tag{9.15}$$

where B is a real number and γ is an unknown phase shift. Substitution into Eqn. (9.13) gives

$$Be^{i\gamma} = \frac{-gA\omega k}{f^2 - \omega^2} \tag{9.16}$$

Taking note of the dispersion relation derived in the previous section ($f^2 - \omega^2 = -gHk^2$), we obtain the following relation

$$Be^{i\gamma} = \frac{A\omega}{Hk} \tag{9.17}$$

The only way for this equation to be satisfied is to require the factor $e^{i\gamma}$ to be real. This is accomplished by setting

$$\begin{aligned} \gamma &= \frac{\pi}{2} \\ B &= \frac{A\omega}{Hk} \end{aligned} \tag{9.18}$$

We have thus found that the u velocity, the velocity aligned with the direction of propagation is *in phase* with the perturbations of the free-surface elevation η. Maximum positive x-velocity will occur under the crests of the wave, and maximum negative x-velocity will occur under the troughs of the wave. The horizontal velocity in the x-direction thus converges at a point half-way

ahead of the traveling crest. This means that the free-surface will have a rising tendency ($\eta_t > 0$) half-way ahead of the traveling crest; precisely what is needed to advance the crest forward down the x-axis.

The transverse velocity, v, is obtained by substituting the expression for u derived above into Eqn. (9.3) and solving for an unknown amplitude and phase shift, as before. The result is

$$v = \frac{-fA}{Hk} e^{i\left(\omega t - kx + \frac{\pi}{2}\right)} \tag{9.19}$$

The transverse velocity v is thus $\frac{\pi}{2}$ (quarter wave period) out of phase with the longitudinal velocity u. This indicates that the water parcels are undergoing elliptical motions. The ratio of the principal axes of the ellipses is $\frac{f}{\omega}$. Thus, waves of very short period (high ω) have very narrow ellipses (almost rectilinear motions, as in the case of an ocean on an unrotating planet); when $\omega \to f$, the ellipses become circular, as we have seen before in our discussion of inertial oscillations.

sectionKelvin Waves One of the interesting features of the shallow-water gravity waves derived above is that they cannot freely propagate when the frequency of the wave ω is less than the inertial frequency f. There are many wave motions, most notably storm surges and tides, in which the frequency of forcing is indeed less than the intertial frequency. These waves owe their existance to the presence of coastlines (and the equator) which act as *wave guides* along which the waves can propagate.

These waves were studied by Lord Kelvin, and thus have been named "Kelvin Waves". To illustrate the notion of a Kelvin wave, we consider the situation shown in Fig. () in which a coast at $y = 0$ imposes a *no flux* boundary condition on the ocean. We assume that the ocean is semi-infinite in extent (*e.g.,* it extends from $y = 0$ to $y = \infty$ and is unbounded in x). One possible class of motions that satisfies the no-flux condition at the coast is that class in which $v = 0$ everywhere. We examine the properties of this class of motions and find that it contains only Kelvin waves.

The governing equations for $v = 0$ motions are derived from Eqns. (9.3) - (9.3) and are written:

$$u_t \quad = -g\eta_x$$

$$\begin{aligned} 0 &= -g\eta_y - fu \\ \eta_t &= -Hu_x \end{aligned} \tag{9.20}$$

The most general solution to these equations is written

$$\eta = Ae^{i(\omega t - kx)}e^{l_- y} + Be^{i(\omega t + kx)}e^{l_+ y} \tag{9.21}$$

where it is understood that $\omega > 0$ and $k > 0$. The first term on the right-hand side of Eqn. (9.21) represents the wave travelling along the coast to the right, the second term is the wave travelling along the coast to the left. The off-coastal structure of the wave is yet to be determined because l_+ and l_- are not defined.

Following the equation-manipulation techniques we developed previously, we derive a dispersion relation for the Kelvin wave. The time derivative of Eqn. (9.20) and the x-derivative of Eqn. (9.20) are combined to give

$$\eta_{tt} = gH\eta_{xx} \tag{9.22}$$

Substituting η given by Eqn. (9.21) into the above equation gives a dispersion relation

$$\omega = \sqrt{gH}k \tag{9.23}$$

The two unknowns l_+ and l_- are determined by manipulation of Eqns. (9.20) and (9.20). The time derivative of Eqn. (9.20) combined with Eqn. (9.20) give

$$0 = -g\eta_{yt} + fg\eta_x \tag{9.24}$$

Substitution of the expression for η give by Eqn. (9.21) into the above equation gives

$$\begin{aligned} l_- &= -\frac{fk}{\omega} \\ l_+ &= \frac{fk}{\omega} \end{aligned} \tag{9.25}$$

Clearly, one of the two parts of the general solution is unacceptable because $e^{l_+ y}$ diverges as $y \to \infty$. We thus insist that $B = 0$, which means that only the wave that propagates to the right (towards increasing x) is physically possible. We make use of the dispersion relation to express $\frac{fk}{\omega}$ as the inverse

of the Rossby radius of deformation $R_D = \frac{\sqrt{gH}}{f}$. This gives the form of the Kelvin wave as follows

$$\eta = Ae^{i(\omega - kx)} e^{\frac{y}{R_D}} \tag{9.26}$$

The amplitude of the Kelvin wave is maximum at the shorline and decays exponentially offshore with a e-folding decay scale equal to the Rossby radius of deformation. A diagram of this structure is provided in Fig. ().

One of the important features of the Kelvin wave is the *geostrophic balance* between the slope of the free surface and the long-shore currents, *i.e.,* Eqn(9.20). The fact that the Kelvin wave can propagate at any frequency (recall that waves which cannot take advantage of a coastal waveguide cannot have $\omega < f$) and, in particular, the frequencies below the inertial frequency tips us off to the fact that some aspect of geostrophy (geostrophic balance) is at play.

Before moving on, it is worth noting the physical meaning of the Rossby radius of deformation. The quantity $\frac{\sqrt{gH}}{f}$ is proportional to the product of the phase velocity of a shallow-water gravity wave ($\sqrt{gH}$) and the time $T = 2\pi/f$ defining the period of the inertial oscillation. The Rossby radius can thus be thought of as the distance a shallow-water gravity wave propagates in an inertial (rotational) period. This is the distance waves can propagate during the time period required to spin up geostrophic motions.

9.6 Geostrophic Adjustment

We begin our venture into geostrophy by considering the manner in which geostrophically balanced ocean currents are created from arbitrary forcings or disturbances applied at the ocean surface. This subject is known as *geostrophic adjustment* because it describes how the ocean adjusts itself (through the propagation of waves) to set-up and maintain a geostrophic balance.

9.6.1 An analytic example

Consider a shallow-water ocean of constant density and infinite extent which, at $t = 0$, is at rest and has a surface-elevation disturbance representing a *step-like* drop of $2\eta_o$ aligned with the y-axis:

$$\eta(t=0) = -\eta_o \; sign(x) = \begin{cases} \eta_o & \text{if } x < 0 \\ -\eta_o & \text{if } x > 0 \end{cases} \tag{9.27}$$

Following the techniques used in Chapter 6 to wrest a single equation in a single unknown from the three shallow-water equations, we again derive the following equation for the time-evolution of the free-surface evolution

$$\eta_{tt} + Hfv_x - gH\eta_{xx} = 0 \tag{9.28}$$

We take note of the fact that the above equation has been simplified by assuming that the y-derivative of all fields remains zero throughout the entire geostrophic adjustment process. This simplification is justified by the fact that the initial condition, Eqn. 9.27), has no y dependence. The relative vorticity, v_x in this case, obeys the following equation, which is again derived by combining two of the original shallow-water equations

$$v_{xt} = \frac{f}{H}\eta_t \tag{9.29}$$

This equation is readily integrated to give, using the initial condition,

$$v_x = \frac{f}{H}\eta - \frac{f}{H}\eta(t=0) \tag{9.30}$$

Combining Eqns. (9.28) and (9.30), we obtain the following single equation in the single unknown η:

$$\eta_{tt} + f^2\eta - gH\eta_{xx} = f^2\eta(t=0) \tag{9.31}$$

The solution to Eqn. (9.31) has two parts, a steady part (which represents the geostrophic balance) and a transient part (which represents the shallow-water gravity waves which are radiated away from the initial disturbance)

$$\eta = \eta_g + \eta_T \tag{9.32}$$

The transient part of the solution, $\eta_T(x,t)$, need not concern us here (see Gill, 1982 for a derivation of this part of the solution). Our interest is in determining the steady, geostrophic part of the solution, $\eta_g(x)$.

The equation satisfied by the geostrophic part of the solution is the same as Eqn. (9.31) except that none of the time-derivatives appear. In other words, the geostrophic portion of the free-surface elevation satisfies

$$f^2\eta_g - gH(\eta_g)_{xx} = f^2\eta(x,t=0) = -f^2\eta_o sign(x) \tag{9.33}$$

The solution to Eqn. (9.33) is found (by good guess work) to be

$$\eta_g(x) = \eta_o \begin{cases} 1 - e^{\frac{f}{\sqrt{gH}}x} & \text{if } x < 0 \\ -1 + e^{\frac{-f}{\sqrt{gH}}x} & \text{if } x > 0 \end{cases} \tag{9.34}$$

The free-surface elevation is seen to retain a smooth "dip" centered on $x = 0$ even after all the disturbances (waves) caused by the initial condition have radiated away (by wave propagation). The length scale over which the free-surface topography is organized is $\frac{\sqrt{gH}}{f}$, the Rossby radius of deformation.

To balance the pressure-gradient force produced by the stationary part of the free-surface elevation, η_g, is balanced by a Coriolis force in the $-x$ direction. This requires a geostrophic current v_g that flows in the $-y$ direction as dictated by the steady (time independent) version of the x-momentum equation discussed in Chapter 6:

$$0 = -g(\eta_g)_x + fv_g \tag{9.35}$$

The solution to this equation is, using Eqn. (9.34), is

$$v_g(x) = -\sqrt{\frac{g}{H}}\eta_o \begin{cases} e^{\frac{f}{\sqrt{gH}}x} & \text{if } x < 0 \\ e^{\frac{-f}{\sqrt{gH}}x} & \text{if } x > 0 \end{cases} \tag{9.36}$$

9.7 Applications

At a future time, I will add to this chapter a discussion of various applications of the above treatment of shallow-water gravity waves and Kelvin waves.

Interesting applications include: the propagation of Tsunamis, equatorially trapped Kelvin waves, storm surges, and the Stokes' drift. Lab assignments will include: a sample Tsunami prediction program in MATLAB®, simulation of a storm surge, an "internal" equatorially trapped Kelvin wave, and computation of the Stokes drift in a harbor.

Chapter 10

Tides

10.1 overview

Tides are one of the major features of the ocean and are perhaps most significantly recognized through their effect on the coastal and estuarine environment. Our interest in tides is motivated by the fact that they represent an application of our study of shallow-water waves. Tides are nothing more than the standing waves in the ocean forced by the weak gravitational attraction of the sun and moon on the volume of ocean water. The goal of this chapter is to derive the tide-generating potential, and to examine the consequences of forced shallow-water wave propagation.

10.2 A Conceptual View

Consider the gravitational attraction $\mathbf{F}(\mathbf{P})$ felt by a plumb bob of mass m held at various locations P on the surface of the earth due to a planetary body such as the moon or sun. As shown in Fig. (10.1), this attraction diminishes with increasing distance between the plumb bob and the planetary body. In particular, the attraction is least at the *antipodal* point (the point

on the earth's surface that is farthest away from the planetary body) and greatest at the *nadir* point (the point on the earth's surface that is closest to the planetary body). The gravitational attraction $\mathbf{F(O)}$ felt by the earth is much greater than that acting on the plumb bob due to the greater mass M_e of the earth. The acceleration of the earth induced by this attraction, $\mathbf{F(O)/M_e}$, is comparable to that experienced by the plumb bob, $\mathbf{F(P)/m}$, and is equivalent to the acceleration experienced by the plumb bob if it could be held at point O the center of the earth, $\mathbf{F(O)/m}$.

The tidal force $\mathbf{T(P)}$ is that force which describes the relative acceleration of the plumb bob with respect to the rigid earth. In other words,

$$\mathbf{T(P)} = \mathbf{m}\left(\frac{\mathbf{F(P)}}{\mathbf{m}} - \frac{\mathbf{F(O)}}{\mathbf{M_e}}\right) \tag{10.1}$$

As shown in Fig. (10.1), $\mathbf{T(P)}$ points toward the attracting planetary body in the hemisphere of the earth that faces the planetary body; and points *away* from the attracting planetary body in the hemisphere that faces away.

The ocean is subject to the tidal force and responds in a complex manner. To get a simple idea of how this response is organized, we can consider the ocean surface that would exist on a completely water-covered earth. If we assume that the tidal force is balanced everywhere by the pressure gradient induced by a slope of the ocean surface, then the picture of a distorted, ellipsoidal fluid envelope to the earth emerges as in Fig. (10.2). A tidal bulge is seen at both the nadir point and the antipodal point. Next, consider the fact that the earth's axis of rotation may be tilted with respect to the line that is perpendicular to the line connecting the center of the earth and the center of the planetary body. In this circumstance, a point of fixed latitude and longitude sweeps through each of the two tidal bulges once a day (thus introducing the semidiurnal tide), but one tidal bulge produces a higher tide than the other (thus introducing a diurnal component to the tide).

The asymmetric semidiurnal tidal cycle experienced by a point that rotates with the earth underneath the fluid envelope can be thought of as the superposition of two separate tidal motions. Two sinusoidal tidal oscillations, one with a 12-hour period and the other with a 12-hour period, can be combined to form an asymmetric tidal cycle. This is demonstrated in Fig. (10.3)

where the superposition of the following two sinusoids is demonstrated

$$\eta(t) = 2\sin\left(\frac{2\pi}{24}t\right) + 4\sin\left(\frac{4\pi}{24}t\right) \tag{10.2}$$

The fact that complicated, asymmetric tidal oscillations can be decomposed into the superposition of several sinusoids of varying frequency has led oceanographers to decompose the tidal motions of the ocean into numerous components. Each individual component is assumed to produce a perfectly sinusoidal tide at all points on the earth (the amplitude and phase of this tide can change with the location of the point).

10.3 Tide Generating Potential

The above conceptual view can be formalized using Newton's law of gravitation and the simple use of plane and spherical geometries to derive the potential field which generates the tides in the ocean. Consider the gravitational force per unit mass at two locations, A and O, caused by a planetary body of mass M_i as shown in Fig. (10.4). Newton's law of gravitation says that the these forces can be written (recall that these are the forces for a unit mass)

$$\begin{aligned} \mathbf{F(A)} &= \gamma M_i \left\{ \frac{\cos\zeta'}{R'^2}\mathbf{n_r} + \frac{\sin\zeta'}{\mathbf{R'^2}}\mathbf{n}_\theta \right\} \\ \mathbf{F(O)} &= \gamma M_i \left\{ \frac{\cos\zeta}{R^2}\mathbf{n_r} + \frac{\sin\zeta}{\mathbf{R^2}}\mathbf{n}_\theta \right\} \end{aligned} \tag{10.3}$$

where γ is Newton's gravitational constant. The tidal force per unit mass $\mathbf{T(A)}$ is the difference between these two forces, $\mathbf{F(A)} - \mathbf{F(O)}$,

$$\mathbf{T(A)} = \gamma \mathbf{M_i} \left\{ \left(\frac{\cos\zeta'}{\mathbf{R'^2}} - \frac{\cos\zeta}{\mathbf{R^2}} \right) \mathbf{n_r} + \left(\frac{\sin\zeta'}{\mathbf{R'^2}} - \frac{\sin\zeta}{\mathbf{R^2}} \right) \mathbf{n}_\theta \right\} \tag{10.4}$$

We rewrite the above expression in a manner that lends itself to simplification as follows,

$$\mathbf{T(A)} = \gamma \left(\frac{\mathbf{r}}{\mathbf{R}} \right)^{\mathbf{2}} \frac{\mathbf{M_i}}{\mathbf{r^2}} \left\{ \left(\frac{\mathbf{R^2}}{\mathbf{R'^2}} \cos\zeta' - \cos\zeta \right) \mathbf{n_r} + \left(\frac{\mathbf{R^2}}{\mathbf{R'^2}} \sin\zeta' - \sin\zeta \right) \mathbf{n}_\theta \right\} \tag{10.5}$$

The geometry presented in Fig. (10.4) allows us to recognize the following identities

$$\begin{aligned} R' \sin\zeta' &= R\sin\zeta \\ R' \cos\zeta' &= R\cos\zeta - r \\ R'^2 &= R^2 + r^2 - 2rR\cos\zeta \end{aligned} \tag{10.6}$$

These identities allow us to simplify terms which appear in Eqn. (10.5) as follows. From Eqn. (10.6) we may write

$$\frac{R'^2}{R^2} = 1 + \frac{r^2}{R^2} - 2\frac{r}{R}\cos\zeta \tag{10.7}$$

For the moon, the quantity $\frac{r}{R}$ is approximately $\frac{1}{60} \ll 1$. We may thus disregard the second term in the above equation without serious error,

$$\frac{R'^2}{R^2} \approx 1 - 2\frac{r}{R}\cos\zeta \tag{10.8}$$

Thus,

$$\frac{R}{R'} \approx \frac{1}{\sqrt{1 - 2\frac{r}{R}\cos\zeta}} \tag{10.9}$$

This expression may further be simplified using the following approximation

$$\frac{1}{\sqrt{1-x}} \approx 1 + \frac{x}{2} \tag{10.10}$$

Use of this simplification gives

$$\frac{R}{R'} \approx 1 + \frac{r}{R}\cos\zeta \tag{10.11}$$

and

$$\left(\frac{R}{R'}\right)^2 \approx 1 + 2\frac{r}{R}\cos\zeta \tag{10.12}$$

Further simplifications may be made by combining Eqn. (10.12) with Eqns. (10.6) and (10.6) as follows

$$\sin\zeta' = \frac{R}{R'}\sin\zeta \approx \sin\zeta + \frac{r}{R}\cos\zeta\sin\zeta \tag{10.13}$$

and

$$\begin{aligned}\cos\zeta' &= \frac{R}{R'}\cos\zeta - \frac{r}{R}\frac{R}{R'} \\ &\approx \cos\zeta - \frac{r}{R}(1-\cos^2\zeta) \\ &\approx \cos\zeta - \frac{r}{R}\sin^2\zeta \end{aligned} \tag{10.14}$$

Having developed the above simplifications, we are now ready to apply them toward the simplification of the expression which gives the tidal force, Eqn. (10.5)

$$\begin{aligned}\mathbf{T}(\mathbf{A}) &= \gamma\left(\frac{r}{R}\right)^2\frac{M_i}{r^2}\left[\left(1+2\frac{r}{R}\cos\zeta\right)\left(\cos\zeta - \frac{r}{R}\sin^2\zeta\right) - \cos\zeta\right]\mathbf{n_r} \\ &\quad +[\left(1+2\frac{r}{R}\cos\zeta\right)\left(\sin\zeta + \frac{r}{R}\cos\zeta\right) \\ &\quad \left(\sin\zeta + \frac{r}{R}\cos\zeta\sin\zeta\right) - \sin\zeta]\mathbf{n}_\theta \end{aligned} \tag{10.15}$$

The coefficient for the $\mathbf{n_r}$-term may be simplified as follows

$$\begin{aligned}\cos\zeta + 2\tfrac{r}{R}\cos^2\zeta - \tfrac{r}{R}\sin^2\zeta + \mathcal{O}\left(\tfrac{r^2}{R^2}\right) - \cos\zeta &\approx \\ &= \frac{r}{R}\left(2\cos^2\zeta - \sin^2\zeta\right) \\ &= \frac{r}{R}\left(2\cos^2\zeta - (1-\cos^2\zeta)\right) \\ &= \frac{r}{R}\left(3\cos^2\zeta - 1\right) \end{aligned} \tag{10.16}$$

Likewise, the coefficient for the $\mathbf{n}_\theta$-term becomes

$$\begin{aligned}\sin\zeta + 3\tfrac{r}{R}\cos\zeta\sin\zeta + \mathcal{O}\left(\tfrac{r^2}{R^2}\right) - \sin\zeta &\approx \\ &= 3\frac{r}{R}\cos\zeta\sin\zeta \\ &= \frac{3}{2}\frac{r}{R}\sin 2\zeta \end{aligned} \tag{10.17}$$

The tide generating force may now be expressed as follows

$$\mathbf{T}(\mathbf{A}) \approx \gamma\mathbf{M_i}\frac{\mathbf{r}}{\mathbf{R^3}}\left[\left(\mathbf{3}\cos^{\mathbf{2}}\zeta - \mathbf{1}\right)\mathbf{n_r} + \frac{\mathbf{3}}{\mathbf{2}}\sin\mathbf{2}\zeta\mathbf{n}_\theta\right] \tag{10.18}$$

It is convenient to describe this force using a potential function $W(r, \zeta)$

$$\mathbf{T}(\mathbf{A}) = \nabla \mathbf{W} \tag{10.19}$$

where the gradient operator is defined in terms of polar coordinates (recall that $\zeta = -\theta$, this is seen by moving the point A to a position of greater θ, when this is done ζ is decreased)

$$\nabla = \frac{\partial}{\partial r}\mathbf{n_r} - \frac{\mathbf{1}}{\mathbf{r}}\frac{\partial}{\partial \zeta} \tag{10.20}$$

The potential function W which satisfies Eqn. (10.19) is

$$W(r, \zeta) = \gamma M_i \frac{r^2}{R^2}\left[\frac{1}{2}\left(3\cos^2\zeta - 1\right)\right] \tag{10.21}$$

To know the tidal potential at a given point on the surface of the earth, the angle ζ must be expressed in terms of the geographic location of the point, ϕ and λ, and the declination and hour angle of the planetary body which causes the tide, $\delta(t)$ and $T(t)$. This evaluation is performed using spherical geometry and one of the trigonometric identities for the spherical triangle $\angle AiP$ shown in Fig. (10.5). Using spherical trigonometry, we have

$$\cos\zeta = \sin\phi\sin\delta + \cos\phi\cos\delta\cos(T+\lambda) \tag{10.22}$$

Multiplication by $\cos\zeta$ gives

$$\cos^2\zeta = \sin^2\phi\sin^2\delta + \cos^2\phi\cos^2\delta\cos^2(T+\lambda) + 2\sin\phi\sin\delta\cos\phi\cos\delta\cos(T+\lambda) \tag{10.23}$$

Using this expression, the tide-generating potential becomes

$$\begin{aligned} W(\phi, \lambda, T(t), \delta(t)) &= \gamma M_i \frac{r^2}{R^3}\frac{3}{4}[\cos^2\phi\cos^2\delta(t)\cos 2(T(t)+\lambda) \\ &\quad + \sin 2\phi \sin 2\delta(t)\cos(T+\lambda) \\ &\quad + 3\left(\sin^2\phi - \frac{1}{3}\right)\left(\sin^2\delta(t) - \frac{1}{3}\right)] \\ &= W_{sd} + W_d + W_{lp} \end{aligned} \tag{10.24}$$

The first portion of the tide-generating potential, W_{sd}, is what generates the semidiurnal tide. Its time variation is produced primarily by the term

$\cos 2(T(t) + \lambda)$ which goes through 2 cycles in a day because $T(t)$, the hour angle of the planetary body, goes through one cycle in a day. The other trigonometric factors in W_{sd} indicate that the semidiurnal tide is *sectoral* in nature; that is, it vanishes at the geographic poles, and is largest at the equator. Zones of positive and negative W_{sd} form "orange peel" slices on the surface of the earth as shown in Fig. (10.6).

The second portion of the tide-generating potential in Eqn. (10.24), W_d, generates the diurnal tide because the term $\cos(T(t) + \lambda)$ goes through one cycle a day. The other trigonometric factors in W_{sd} indicate that the diurnal tide is *tesseral* in nature; that is, it vanishes at the geographic poles and at the equator, and changes sign across the equator. Zones of positive and negative W_d form half hemispheric patches on the surface of the earth as shown in Fig. (10.7).

The third portion of the tide-generating potential in Eqn. (10.24), W_{lp}, generates the long-period tides such as the fortnightly tide (14 days), the 27-day tide, the 182-day tide and the 18-year tide. The long-period nature of these tides comes from the fact that the declinations, $\delta(t)$, of the moon and sun change very slowly. These tides have no longitudinal structure, and are thus sometimes referred to as "pole tides". Zones of positive and negative W_{lp} are organized as shown in Fig. (10.8). The latitudes 35N and 35S represent the locations where the potential changes sign, as required by the condition $\sin^2 \phi - \frac{1}{3} = 0$.

10.4 Tidal Response

The tide-generating potential describes the forces which generate waves in the ocean known as tides. Due to the fact that the ocean has a complex geometry, the wave-like response of the ocean to the tidal forcing is quite complex compared to the geometry of the tide-generating potential. The simple sectoral geometry of W_{sd}, for example, produces a system of amphidromic points around which wheel great Kelvin waves that propagate along the coasts of the world ocean (Fig. (10.9)). Amphidromic points are places where the free-surface elevation is undisturbed by the tide (it is motionless) and where

the lines of constant phase (lines describing the crest of the tidal wave at different points during the tidal cycle) converge. The maximum amplitude of the ocean's tidal response typically occurs at the coasts as in the case of an unforced Kelvin wave.

10.5 Assignment

In the future, lab assignments will involve computing the tidal response of long water filled canals. Possibly, one lab problem will involve computing the tide for a water covered earth using spherical harmonics as the means to expand the oceanic response to the tide generating potential.

Figure 10.1: Acceleration induced by gravitational attraction of moon or sun relative to the acceleration of the bulk (rigid) earth due to the same gravitational attraction.

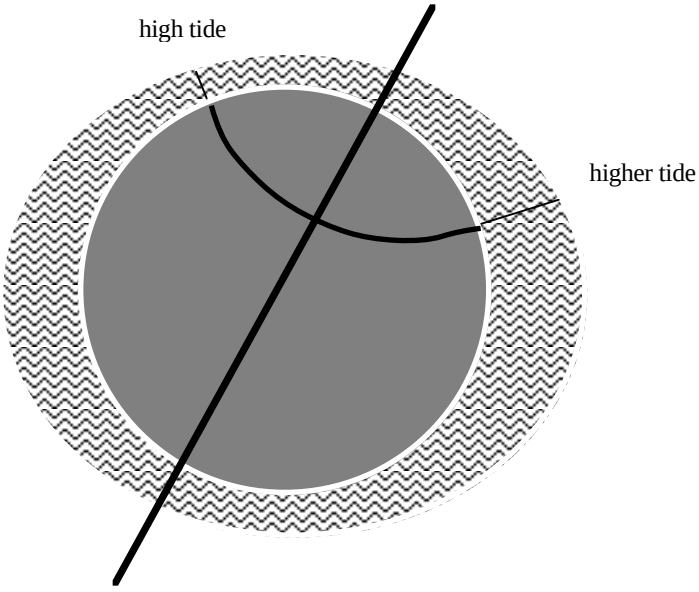

Figure 10.2: The fluid envelope on a purely water-covered earth that would introduce pressure gradients sufficient to balance the tidal force.

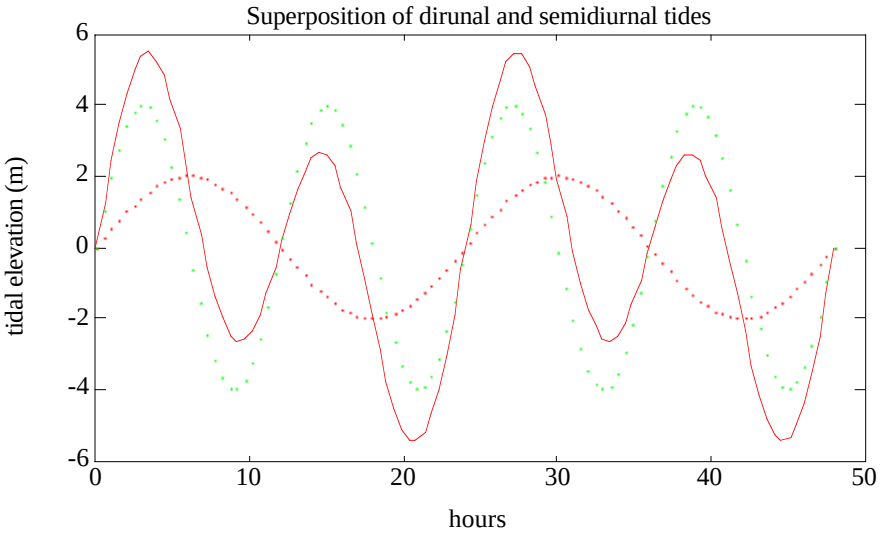

Figure 10.3: The superposition of two sinusoidal tidal motions of different period yield an assymetric tidal oscillation.

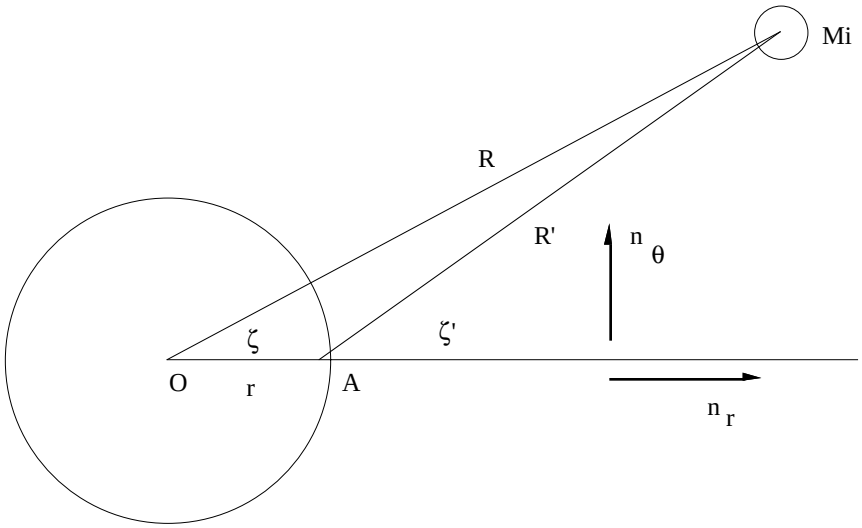

Figure 10.4: The plane geometry of the earth and a gravitating planetary body used to determine the tide-generating potential.

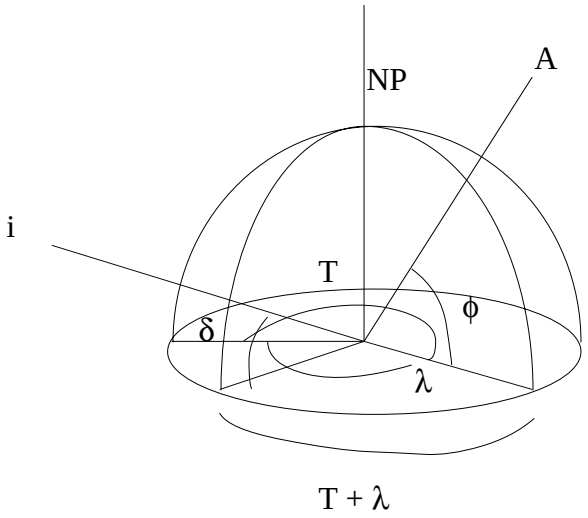

Figure 10.5: The spherical triangle which allows us to determine ζ in terms of the geographic position of point A and the declanation and hour angle of the planetary body (having a nadir at point i).

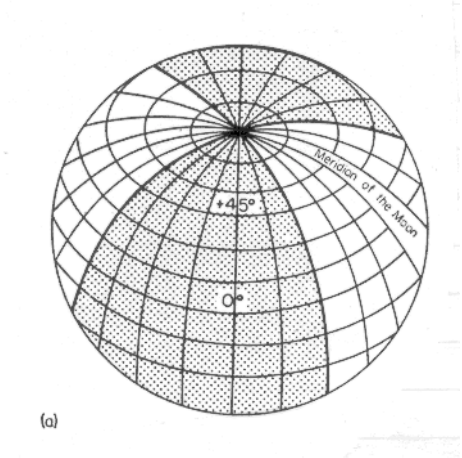

Figure 10.6: The tide-generating potential for the semidirunal tide has the geometry of slices of an orange peel. This is called a *sectoral* geometry.

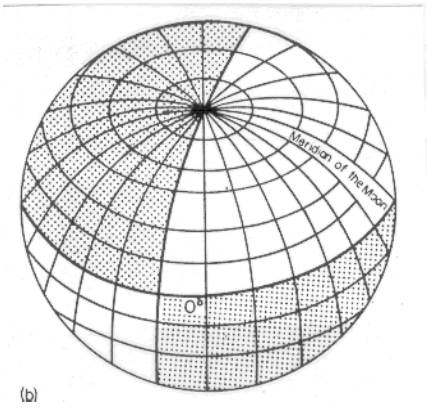

Figure 10.7: The tide-generating potential for the dirunal tide has a *tesseral* geometry.

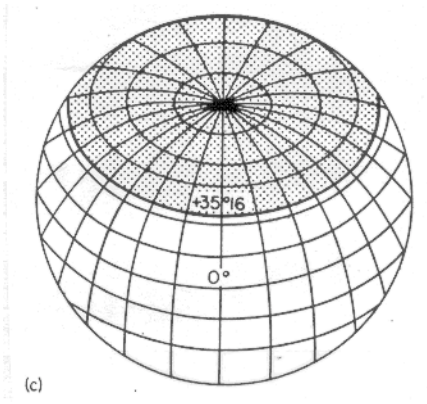

Figure 10.8: The tide-generating potential for the long-period tides which owe their existance only to the fact that the declanation $\delta(t)$ changes very slowly with time (*e.g.,* monthly, yearly, etc.).

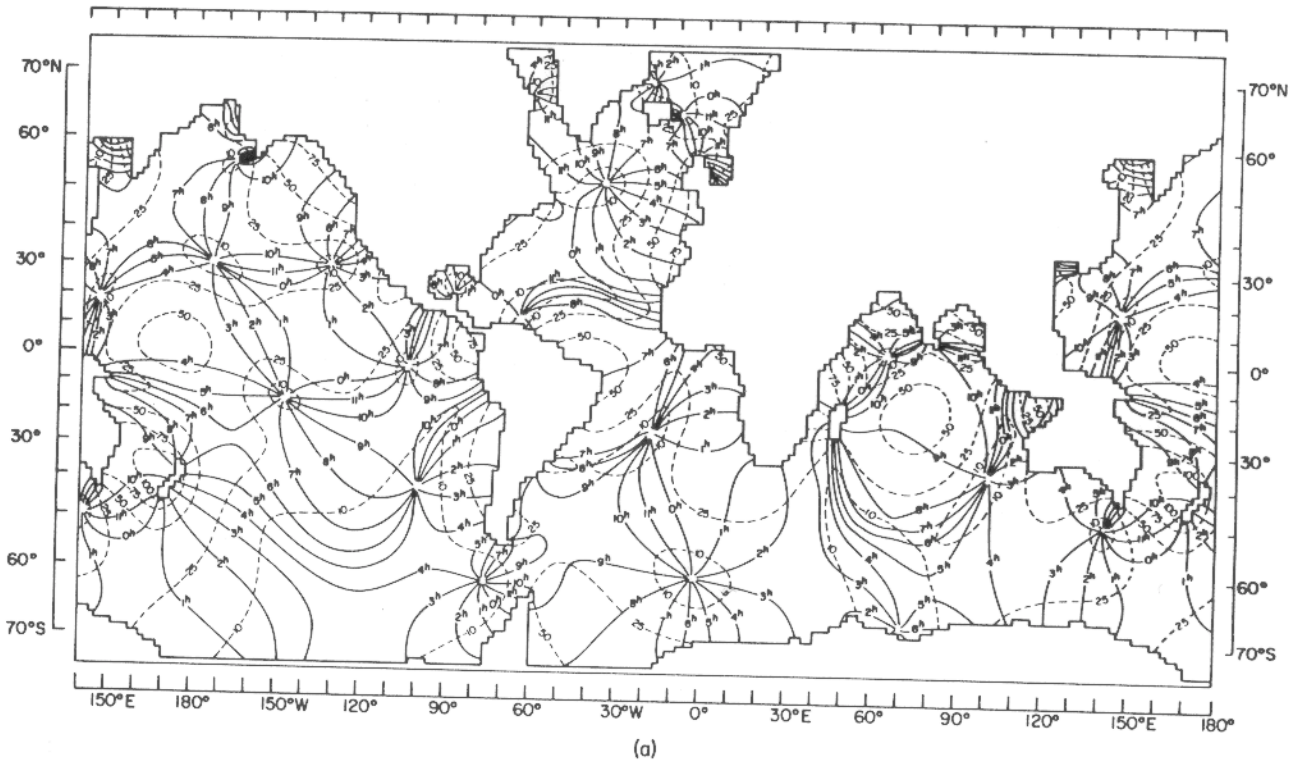

Figure 10.9: The tidal response (phase and amplitude) of the ocean to the semidiurnal tide generated by the Moon (Accad and Pekeris, 1978).